Analytical Approach to Position and Attitude Control of an Underactuated Satellite Using Thrusters

吉村, 康広

https://doi.org/10.15017/1398376

出版情報：九州大学, 2013, 博士（工学）, 課程博士
バージョン：
権利関係：全文ファイル公表済

Doctoral Dissertation

Analytical Approach to Position and Attitude Control of an Underactuated Satellite Using Thrusters

解析的アプローチによるスラスタを用いた劣駆動衛星の位置・姿勢制御

Yasuhiro Yoshimura

Kyushu University

Supervisor: Professor Shinji Hokamoto

September 2013

Contents

List of Figures

List of Tables

Chapter 1

Introduction

1.1 Background and Objective

Space probes require autonomous control to achieve their planetary explorations because of communication lag caused from large distance between the Earth and an asteroid or a planet. For example, the communication delay between a ground-station and the Near Earth Asteroid(NEA), Itokawa, which is located around 300 million kilometers away, is about 40 minutes [1]. Thus, in a proximity operation to an asteroid, a satellite firstly estimates the position and attitude of the satellite using several sensors, and then autonomously controls to a desired state using actuators, e.g., reaction wheels(RWs), control momentum gyros(CMGs), and thrusters. To this end, a large number of sensors and actuators are equipped on the satellite considering some of them as backup. Hayabusa, the first spacecraft achieved an asteroid sample return mission, had three RWs for attitude control and 12 chemical thrusters for both position and attitude control. These many actuators enable to generate translational forces independent from rotational torques and vice versa, and consequently it makes a control procedure much simple. If malfunctions of some actuators occur, however, the state control of the satellite becomes more complicated due to the coupling effect between the translation and the rotation. In such practical situation, the position and attitude control with the remained actuators is required to continue the mission. In other words, underactuated controllers have the possibility to extend satellite mission lifetimes. Furthermore, from the viewpoint of a satellite design, the control method may be able to reduce the number of actuators equipped on the satellite even when considering some of them as backup.

When a nonlinear system has less number of inputs than the number of state variables, the system is called "underactuated" system. Since the number of inputs are limited, such system often includes nonintegrable constraints, i.e. "nonholonomic" constraints. It is known that control systems with nonholonomic constraints, called nonholonomic systems, have the possibility to control their state

variables in spite of the less number of inputs. Brockett [2] provides a necessary condition for symmetric affine systems, equivalently first-order nonholonomic systems, to be controllable. The condition indicates that no continuous state feedback can control the systems, and this negative result has motivated many researchers to derive nonholonomic control laws not to violate the condition. To avoid the Brockett's condition, intensive studies have been conducted and consequently discontinuous controllers and time-varying feedback ones are proposed for symmetric affine systems [3–5]. The proposed methods can be applied to the systems described with a canonical form, whereas control theories for asymmetric affine systems have not been fully established.

This dissertation presents new control approaches for asymmetric affine systems, especially a satellite position and attitude control using a small number of thrusters. The control systems in this paper form a "second-order" nonholonomic system and have not only nonholonomic constraints due to a few thrusters, but also input constraints, i.e. the constant magnitudes of thrusts in one direction. These input constraints thus disable to apply studies proposed on the second-order nonholonomic systems [6–8] to the systems in this dissertation, and even the controllability of the systems is hard to be discussed as shown in the following section. To tackle the problem, the control methods based on analytical solutions are proposed. The proposed methods would contribute to autonomous control of space probes in free-floating condition to continue the missions even when some actuators have failed and be useful to design backup systems of actuator configurations based on the underactuated controllers. Furthermore, the control method is extended to a control of formation flying of a satellite, a key technology for future space missions.

1.2 Literature Review

An attitude control of a satellite with less than three inputs is a nonholonomic system due to the angular momentum conservation. Crouch [9] provides necessary and sufficient conditions for an attitude control of an underactuated satellite considering RWs or pairs of gas-jet thrusters as actuators. The paper claims the pairs of gas-jet thrusters can control when the control torques are applied around two principal axes of the satellite, whereas less than three RWs cannot control the satellite attitude due to the angular momentum conservation of the RWs. The uncontrollability, however, indicates the satellite attitude is controllable if and only if the total angular momentum is zero. Regardless of actuators, it is known that there is no smooth feedback controller which asymptotically control a satellite attitude to a target one [10]. Thus proposed underactuated controllers are designed to be discontinuous or time-varying to avoid the uncontrollability condition. Yamada and Yoshikawa [11] derive a discontinuous and periodic feedback controller using

a holonomy approach. Krishnan et al. [12] show a discontinuous procedure to control the attitude angles of a satellite sequentially. Morin and Samson [13] propose a time-varying control law based on a technique for homogeneous systems. While the proposed control laws are verified with numerical simulations in these works, few studies report in-orbit experiment results of an underactuated control. Terui et al. [14, 15] show in-orbit experiment results for an attitude control of a satellite with two reaction wheels. The experiment results demonstrate that the designed controller essentially works well, but a limit cycle around the target point is arisen. Horri and Palmer [16] also report successful attitude control results with two reaction wheels, and on-orbit experiments are conducted for two control cases: the attitude stabilization without the angular velocity measurements, and reference angular rates tracking. These papers conducted the experiments of the underactuated control with momentum exchange devices, whereas no in-orbit experiments have been conducted using external torquers such as gas-jet thrusters.

In contrast to an underactuated attitude control of a satellite, few studies consider simultaneous control of a satellite's position and attitude. Terui [17] proposes a position and attitude control method using sliding mode control. The satellite attitude is controlled to coincide with the one of a tumbling satellite, and the robustness due to the sliding mode control is also discussed. Senda et al. [18] studies a position and attitude control of a spacecraft in two-dimension experimentally by using an air-table. Curti et al. [19] also propose a position and attitude controller based on Lyapunov stability and show the experiment results for the verification of the proposed method. These papers, however, assume that enough number of actuators are equipped on a satellite so that arbitrary translational forces and rotational torques are generated. Such assumption simplifies the control systems and consequently some control techniques for nonlinear systems are applicable.

Thrust directions of a spacecraft are restricted when the spacecraft equips a small number of thrusters or some thrusters have failed, and the controllability of the system is hard to be discussed. Sussmann [20] shows a theorem on a sufficient condition for local controllability of nonlinear systems. Then the Sussmann's theorem is further extended to controllability of systems with unilateral inputs by Goodwine [21]. This theorem, however, supposes a system which includes both bidirectional and unilateral control inputs. That is, the theorem is not applicable to the systems that have only one-directional inputs. Thus the controllability of such systems needs to be respectively discussed and proved for each system. Lynch [22], for instance, proves the controllability of in-plane motion of a satellite for two cases: a satellite with one thruster whose direction is variable, and another with two fixed thrusters. The study shows the system is controllable even when the magnitude of thruster forces are constant.

A position and attitude control of a satellite is required for not only a proximity operation to an asteroid, but also formation flying. Formation flying is a promising technology for near-future space missions using small satellite clusters.

Two or more small spacecrafts orbiting in a close orbit are controlled to adapt their relative position and attitude to one another. The synchronization enables the cluster to obtain high resolution images of Earth observation such as a Synthetic Aperture Radar (SAR). For instance, TanDEM-X(TerraSAR-X Add-oN for Digital Elevation Measurement), in which two satellites were launched on June 21, 2010 by the German Space Agency, demonstrates new techniques and applications using the formation flying [23]. In a formation flying control, equations of motion of a "follower" satellite is described with linearized equations with respect to a "leader" satellite. The relative motion of the follower in a near-circular orbit is described with the Hill's equations [24], and the one in an elliptical orbit is written with the Tschauner-Hempel (TH) equations [25], respectively. Carter [26] shows state transition matrices for TH equations without the singularity which occurs when the eccentricity becomes zero, and the result is further modified and simplified by Yamanaka and Ankersen [27].

Rendezvous maneuvers and formation reconfigurations are typical control techniques required for formation flying missions. Autonomous rendezvous, for example, is necessary when a satellite autonomously provides supplies to the International Space Station(ISS) or on-orbit repair missions. Carter [28] shows a fuel-optimal rendezvous maneuver with bounded thrusts. Shibata and Ichikawa [29] describe an optimal control method for both a circular and elliptical orbit based on null controllability with vanishing energy. On the other hand, formation reconfiguration is necessary to keep or change the relative distance between a leader and a follower. Palmer [30] shows an analytical solution to relocate a follower satellite to a desired relative orbit using the Fourier series. The method is extended to discuss the reachability of a reconfiguration problem with bounded inputs [31] as well as to derive an optimal reconfiguration method for a formation flying in an elliptic orbit [32]. Xi and Li [33] also show an optimal reconfiguration controller in an elliptic orbit, and both energy and fuel optimality are discussed based on a homotopic approach.

This dissertation describes analytical approaches to a simultaneous control of position and attitude using a small number of thrusters for a free-floating satellite as well as for a formation flying of satellites. The use of a few thrusters as actuators forms second-order nonholonomic systems under input constraints, and most of results and theorems shown in the above papers are not directly applicable to the systems in the current paper. Novel control methods are therefore proposed based on analytical solutions and they enable calculations of proper input timings and durations to steer the satellite to a desired state. The control technique for a free-floating satellite is further extended to the one in formation flying. While many works have addressed formation control without the consideration of attitude change of a satellite, this dissertation explicitly takes into account the dynamics of rotational motion, and it allows us to design a trajectory under practical attitude constraints.

1.3 Dissertation Overview

This dissertation is organized as follows. Chapter 2 firstly discusses the minimum necessary number of thrusters to control an attitude of an underactuated satellite. The necessary number of thrusters and their configuration are shown using Minkowski-Farkas theorem, which describes conditions that an equation has positive solutions, because thrusters generate only positive forces due to their mechanisms. Based on the discussion for the minimum necessary number and the configuration of the thrusters, an attitude controller for the underactuated satellite is derived which is applicable to any satellites regardless of the moment of inertia ratios. Numerical simulation results verify the effectiveness of the proposed controller and the relationship between the thruster configurations and the necessary thruster forces. Chapter 3 deals with a position and attitude control of a free-floating satellite using four thrusters which generate only constant inputs in one direction. To this end, the analytical solutions of both translational and rotational motion with constant inputs are derived to calculate the proper input timings and durations. Based on the analytical solution the proposed control procedure consists of three steps which controls the state variables sequentially, and is verified with a numerical simulation. Chapter 4 considers a position and attitude control for formation flying in which a rendezvous problem and a formation reconfiguration problem using a small number of thrusters are discussed. Both problems assume that a follower satellite equips two thrusters for in-plane motion control, and the less number of inputs similarly form an underactuated system in the formation flying. In the rendezvous control, a relative motion of the satellite is simplified with modal analysis. The modal analysis also shows the controllability and the energy efficiency for the rendezvous maneuver with restricted inputs. Also, an optimal formation reconfiguration of a satellite is studied under attitude constraints with respect to an inertial frame. A tracking method for reference inputs is firstly derived to control the satellite's relative attitude and position with a few thrusters. The optimal reference inputs are obtained using the Fourier series and are designed to satisfy the attitude constraints in the inertial frame. Chapter 5 concludes this dissertation and further developments are addressed.

Chapter 2

Three Dimensional Attitude Control of an Underactuated Satellite with Thrusters

This chapter deals with a three-dimensional attitude control of an underactuated satellite with a small number of thrusters. Though an attitude control with less than three inputs have been studied by many researchers in recent decades [34–37], these works control only angular rates or have assumptions on the moment of inertia, e.g. an axisymmetric or near-axisymmetric inertia. This chapter thus derives a novel attitude controller of an underactuated satellite which is effective for any satellites regardless the moment of inertia. Also the minimum necessary number of thrusters to control a satellite attitude is specified from the viewpoint of nonholonomic control. Several studies claim four thrusters are necessary to control a satellite attitude [38–41]. This chapter, however, provides new results for the necessary number of thrusters considering the nonholonomic attitude control under positive input constraints. The conditions to generate arbitrary control torques around two principal axes are addressed because the controllability of an underactuated satellite's attitude with two control torques is proved by Crouch [9], and the derived condition shows the necessary number of thrusters and their configuration. Furthermore the graphical interpretation of the thruster configuration provides proper one to require less thruster forces than the other allocations. Numerical simulation results verify the effectiveness of the proposed controller and discuss the relationship between the necessary thrust forces and the thruster configurations.

2.1 Dynamic equations of motion

This chapter assumes a satellite's body-fixed frame coincides with the principal axes of inertia and expresses them as $\{\boldsymbol{x}_b, \boldsymbol{y}_b, \boldsymbol{z}_b\}$. This assumption is introduced to discuss the minimum necessary number of thrusters based on the result in [9] and to derive a nonholonomic control law. The dynamic equation of motion of a satellite with two control torques about x_b- and y_b axes is expressed with the Euler equation as

$$J_x\dot{\omega}_x = (J_y - J_z)\omega_y\omega_z + T_x, \tag{2.1}$$
$$J_y\dot{\omega}_y = (J_z - J_x)\omega_x\omega_z + T_y, \tag{2.2}$$
$$J_z\dot{\omega}_z = (J_x - J_y)\omega_x\omega_y, \tag{2.3}$$

where ω_j, J_j $(j = x, y, z)$, and T_k $(k = x, y)$ denote the satellite's angular velocity, the moment of inertia, and control torques, respectively. The dot on a parameter means the time derivative of the parameter. Let the moment of inertia ratios be denoted as

$$\sigma_x := \frac{J_y - J_z}{J_x}, \tag{2.4}$$
$$\sigma_y := \frac{J_z - J_x}{J_y}, \tag{2.5}$$
$$\sigma_z := \frac{J_x - J_y}{J_z}. \tag{2.6}$$

The moment inertia ratios simplify the equations of motion as follows.

$$\dot{\omega}_x = \sigma_x\omega_y\omega_z + T_x/J_x, \tag{2.7}$$
$$\dot{\omega}_y = \sigma_y\omega_x\omega_z + T_y/J_y, \tag{2.8}$$
$$\dot{\omega}_z = \sigma_z\omega_x\omega_y. \tag{2.9}$$

Here, we assume that $\sigma_z \neq 0$, i.e. $J_x \neq J_y$, otherwise $\sigma_z = 0$ in Eq. (2.6) and Eq. (2.9) becomes $\dot{\omega}_z = 0$. This indicates that the rotational motion around the z_b-axis is uncontrollable.

2.2 Necessary Number of Thrusters and Configuration

Let $\boldsymbol{r}_i \in \mathbb{R}^3$ and $\boldsymbol{d}_i \in \mathbb{R}^3$ denote the i-th thruster's attachment position vector and the normalized directional vector, respectively. The magnitudes of the thrust forces are assumed to be continuously changeable from zero to a specified positive

value. The control torque $\boldsymbol{T}_i \in \mathbb{R}^3$ generated by the i-th thruster can be expressed as follows.

$$\boldsymbol{T}_i = \boldsymbol{r}_i \times \boldsymbol{d}_i f_i, \tag{2.10}$$

where $f_i(\geq 0)$ is the magnitude of the thruster force. When the satellite equips n thrusters, the total control torques generated by the thrusters are described as

$$\begin{aligned} \boldsymbol{T} = \sum_{i=1}^{n} \boldsymbol{T}_i &= \begin{bmatrix} a_{1x} & a_{2x} & \cdots & a_{nx} \\ a_{1y} & a_{2y} & \cdots & a_{ny} \\ a_{1z} & a_{2z} & \cdots & a_{nz} \end{bmatrix} \begin{bmatrix} f_1 \\ f_2 \\ \vdots \\ f_n \end{bmatrix} && (2.11) \\ &= \begin{bmatrix} \boldsymbol{a}_1 & \boldsymbol{a}_2 & \cdots & \boldsymbol{a}_n \end{bmatrix} \boldsymbol{f} && (2.12) \\ &\Rightarrow \quad \boldsymbol{T} = A\boldsymbol{f}, && (2.13) \end{aligned}$$

where each column vector of the matrix $A \in \mathbb{R}^{3\times n}$ is written as $\boldsymbol{a}_i = \boldsymbol{r}_i \times \boldsymbol{d}_i$ $(i = 1, \ldots, n)$.

2.2.1 Parallel Thruster Configuration

First a thruster configuration that all thrusters are oriented parallel to the satellite's z_b-axis is considered for the sake of simplicity. These thrusters generate no control torque about the z_b-axis, and thus Eq. (2.13) is simplified as

$$\begin{aligned} \boldsymbol{T} &= \begin{bmatrix} a'_{1x} & a'_{2x} & \cdots & a'_{nx} \\ a'_{1y} & a'_{2y} & \cdots & a'_{ny} \\ 0 & 0 & \cdots & 0 \end{bmatrix} \begin{bmatrix} f_1 \\ f_2 \\ \vdots \\ f_n \end{bmatrix} && (2.14) \\ &= \begin{bmatrix} \boldsymbol{a}'_1 & \boldsymbol{a}'_2 & \cdots & \boldsymbol{a}'_n \end{bmatrix} \boldsymbol{f} && (2.15) \\ &\Rightarrow \quad \boldsymbol{T} = A'\boldsymbol{f}, && (2.16) \end{aligned}$$

Several studies [12,13,37,42,43] show that arbitrary magnitudes of control torques around x_b- and y_b-axes can control the satellite's three-dimensional attitude. Thus, to clarify the necessary number of thrusters, we discuss the condition that the vector $\boldsymbol{T}$ is generated in arbitrary directions of the x_b-y_b plane with the thrusters.

Since every thruster force must be positive or zero, we use the Minkowski-Farkas theorem. (For the proof of the theorem, see Broyden [44].) Note that this dissertation describes a vector as positive when all of components are positive or zero.

Theorem 1 (Minkowski-Farkas) *Given a matrix $B \in \mathbb{R}^{m\times n}$ and a vector $\boldsymbol{u} \in \mathbb{R}^m$, the following conditions are equivalent.*

1. $(\forall \boldsymbol{b} \in R^m)\ \boldsymbol{b}^T B \geq \boldsymbol{0}^T \Rightarrow \boldsymbol{b}^T \boldsymbol{u} \geq 0.$

2. $(\exists \boldsymbol{g} \geq 0\ )\ B\boldsymbol{g} = \boldsymbol{u}.$

The second condition of the above theorem indicates that Eq. (2.16) has positive solutions $\boldsymbol{f} \geq 0$, and the existence condition of the positive solutions is equivalent to the following one.

$$(\forall \boldsymbol{b} \in R^n)\boldsymbol{b}^T A'^T \geq \boldsymbol{0}^T \Rightarrow \boldsymbol{b}^T \boldsymbol{T} \geq 0. \tag{2.17}$$

For the sake of simplicity, we firstly consider the case when $n = 2$. The first relation in Eq. (2.17) means that the angle between the vector $\boldsymbol{b}$ and each column vector of A' must be less than or equal to 90 degrees since the scalar products between them should be positive or zero. Thus, the area in which the vector $\boldsymbol{b}$ exists can be drawn by the shadowed area in Fig. 2.1. Similarly, the area of the vector $\boldsymbol{T}$ satisfying the second relation of Eq. (2.17) can be shown with the shadow in Fig. 2.2. For the torque vector $\boldsymbol{T}$ in arbitrary directions of the x_b-y_b plane, the

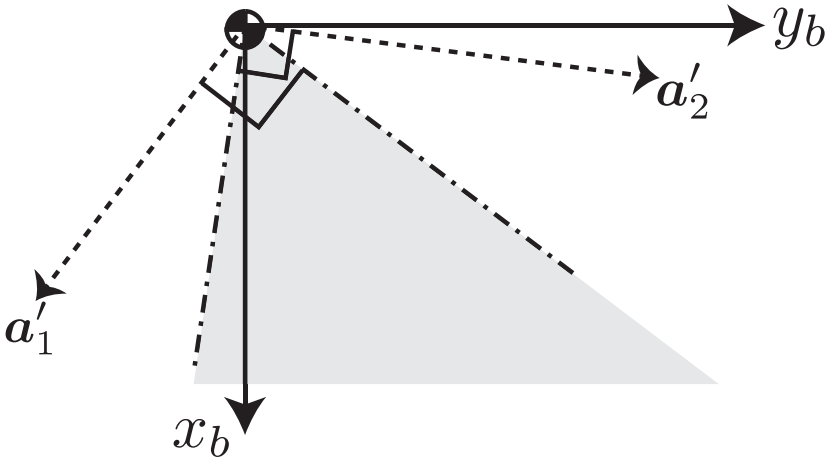

Figure 2.1: The existence region of the vector $\boldsymbol{b}$.

third thruster is thus necessary and it must be oriented in a direction opposite to the shadowed region in Fig. 2.2 as shown in Fig. 2.3. Then the combination of the thrusters 1 and 3 can produce a torque vector $\boldsymbol{T}$ in arbitrary directions between the vectors $\boldsymbol{a}'_1$ and $\boldsymbol{a}'_3$, and the combination of the thrusters 2 and 3 covers the region between the vectors $\boldsymbol{a}'_2$ and $\boldsymbol{a}'_3$. Thus, the three thrusters consequently can generate control torques in arbitrary directions of the x_b-y_b plane and can control the satellite's three-dimensional attitude motion. Note that this thruster number is less than the result shown by Sidi [38].

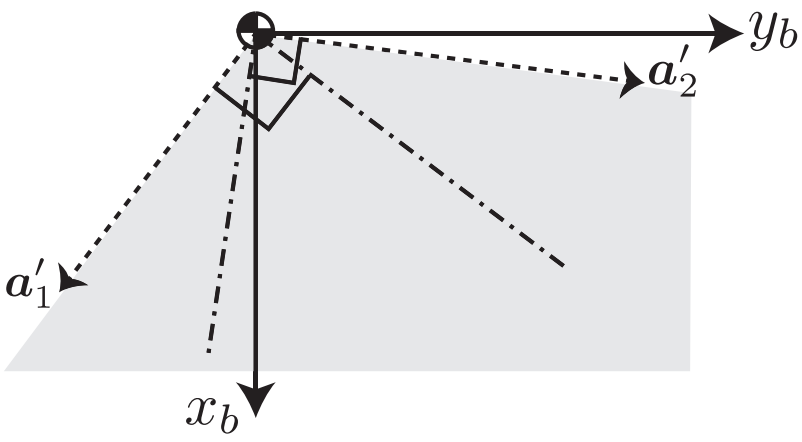

Figure 2.2: The existence region of the vector $\boldsymbol{T}$.

2.2.2 Arbitrary Thruster Configuration

This subsection extends the result for three thrusters in parallel configuration to an arbitrary configuration. In the arbitrary thruster allocation, each thruster generates control torques around all three axes as written in Eq. (2.13). From the similar discussion of the previous subsection, the combination of the three thrusters can generate control torques in any directions included in the triangular pyramid formed with $\boldsymbol{a}_1, \boldsymbol{a}_2$, and $\boldsymbol{a}_3$ as shown in Fig. 2.4. In the x_b-y_b plane, however, the direction of the control torques is limited to an intersection between the triangular pyramid and the x_b-y_b plane. This intersection is illustrated in a hatched triangle in the figure. Note that the satellite's center of mass is the origin of this frame and is placed on a vertex of the triangular pyramid. Three thrusters thus cannot generate arbitrary directional torques in the x_b-y_b plane.

The preceding discussion shows that at least four thrusters are necessary to control the satellite's three-dimensional attitude. Furthermore, the fourth thruster must be placed in the opposite direction to a point inside the triangular pyramid in Fig. 2.4. Then, these four thrusters give us four choices to select three thrusters and consequently formulate one large triangular pyramid containing the origin inside it as shown in Fig. 2.5. Thus, this four-thruster configuration can generate control torques to arbitrary directions in the x_b-y_b plane. (From a different point of view, these four thrusters can generate any directional control torque in three-dimension, and therefore this result indicates the same result derived by Sidi [38].)

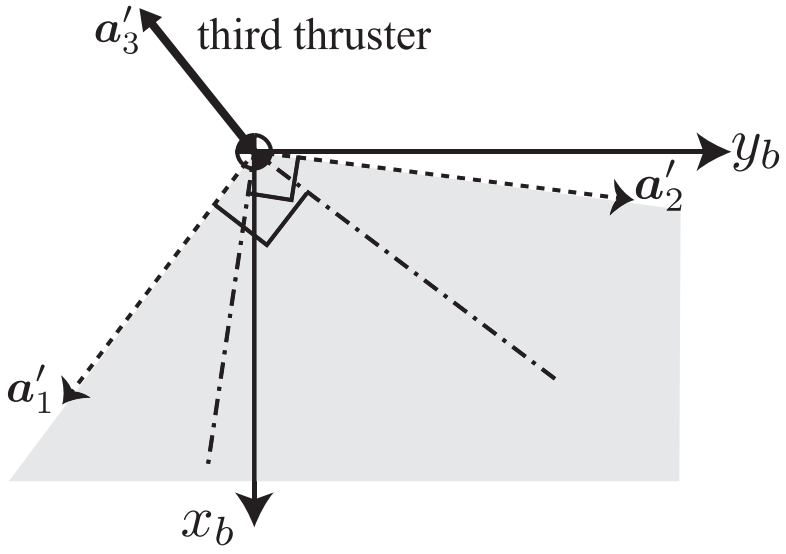

Figure 2.3: Third thruster allocation required for controllability.

2.3 Kinematic equations of motion

There are several sets of attitude parameters to describe kinematic equations of a spacecraft. Although Euler angles, quaternion, and Rodrigues parameters are most frequently used, this chapter uses the wz-parameters proposed by Tsiotras and Longuski [45] to represent the satellite attitude. The attitude representation with wz-parameters decouple the parameter z from the parameters w_1 and w_2, and the resulting equations are further simplified by combining the parameters w_1 and w_2 into a complex form as $w = w_1 + iw_2$, where i is an imaginary number. The kinematic equations with wz-parameters are obtained with two successive rotations, whereas Euler angles take three rotations and quaternions and Rodrigues parameters use one rotation. In the wz-parameters, an inertial frame is rotated to coincide with the satellite-fixed frame through the following two rotations. The first rotation is defined about the z_b-axis, and the second one is about an axis in the x_b-y_b plane and denoted by w_1 and w_2. The kinematic equations of the satellite can be expressed with the following two differential equations [45].

$$\dot{w} = -i\omega_z w + \frac{\omega}{2} + \frac{\bar{\omega}}{2} w^2, \tag{2.18}$$

$$\dot{z} = \omega_z + \frac{i}{2}(\bar{\omega} w - \omega \bar{w}), \tag{2.19}$$

where angular velocities of the satellite are also written as a complex variable, i.e., $\omega = \omega_x + i\omega_y$, and $\bar{*}$ indicates its complex conjugation.

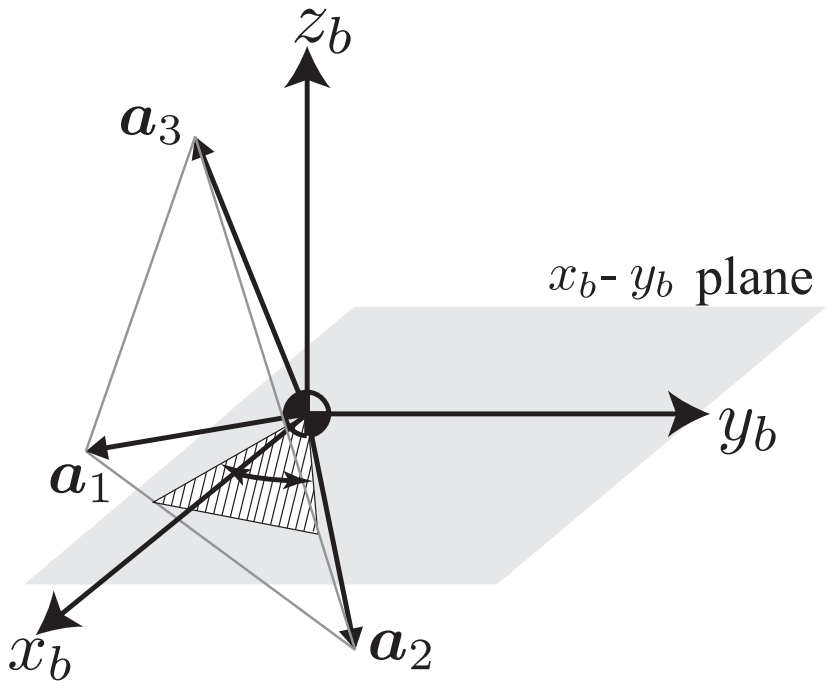

Figure 2.4: The control torques formulated with three thrusters.

2.4 Control Law

As seen in the dynamic and kinematic equations, the attitude parameters and the control torques are decoupled. That is, no input torques appear in the kinematic equations. Thus, we consider the angular velocities around the x_b- and y_b-axes in the kinematic equations as virtual inputs.

Substituting Eq. (2.18) into the relation

$$\frac{\mathrm{d}}{\mathrm{d}t}|w|^2 = 2\mathrm{Re}(\dot{w}\bar{w}), \tag{2.20}$$

we obtain

$$\frac{\mathrm{d}}{\mathrm{d}t}|w|^2 = (1+|w|^2)\mathrm{Re}(\omega\bar{w}). \tag{2.21}$$

Equation (2.19) corresponds to the following equation.

$$\dot{z} = \mathrm{Im}(\omega\bar{w} + \omega_z). \tag{2.22}$$

It should be noted that the real part of $\omega\bar{w}$ appears only in Eq. (2.21), whereas the imaginary part of $\omega\bar{w}$ is only in Eq. (2.22). Thus, we design the virtual input

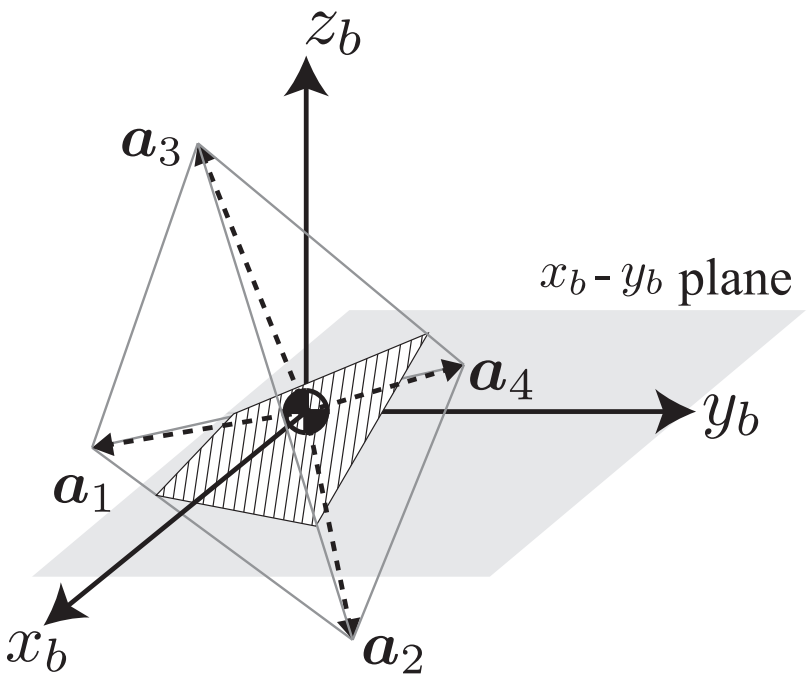

Figure 2.5: The control torque formulated with four thrusters

ω_d as the following form:

$$\omega_d = -\kappa w - i\frac{\mu z - \lambda\omega_z/\sigma_z}{\bar{w}}, \tag{2.23}$$

where κ, μ, and λ are positive constant gains. In the controller, $\lambda\omega_z/\sigma_z$ is the additional term modified from the controller shown in [46] and behaves to change the control gain depending on the moment of inertia ratio σ_z. That is, when the satellite has a near-axisymmetric moment of inertia, the value of σ_z becomes small, and consequently it makes the control gain large.

Using the virtual inputs, we can obtain the following equation.

$$\frac{\mathrm{d}}{\mathrm{d}t}|w|^2 = -\kappa(1+|w|^2)|w|^2, \tag{2.24}$$

$$\dot{z} = -\mu z + (1+\lambda/\sigma_z)\omega_z. \tag{2.25}$$

The integrals of these equations are given as follows

$$|w|^2 = \frac{1}{ce^{\kappa t}-1}, \tag{2.26}$$

$$z = e^{-\mu t}\left\{z(0) + \int e^{\mu t}(1+\lambda/\sigma_z)\omega_z \mathrm{d}t\right\}. \tag{2.27}$$

Thus both w- and z-parameters exponentially converge to zero at the rate specified by the control gains κ and μ. Furthermore, from the second term of the right-hand side in Eq. (2.23), the z- parameter must converge to zero faster than the w-parameter does. Thus, considering the degree of the w-parameter in Eq. (2.26), we should design the gains as $\mu > \kappa/2$.

The virtual inputs are realized using actual input torques through the dynamic equations. To simplify the expression, we combine the control torques T_x and T_y in the following complex form

$$T = T'_x + iT'_y, \tag{2.28}$$

where $T'_x := T_x/J_x$ and $T'_y := T_y/J_y$. The error of the angular velocity is defined as

$$e = \omega - \omega_d. \tag{2.29}$$

Then substituting Eq. (2.23) into Eq. (2.29) and differentiating it with respect to time, we obtain the following equation.

$$\begin{aligned}\dot{e} = \sigma_x\omega_y\omega_z + T'_x + i(\sigma_y + \omega_x\omega_z + T'_y) + \kappa\left(-i\omega_z w + \frac{\omega}{2} + \frac{\bar{\omega}}{2}w^2\right) \\ + i\mu\left\{\frac{\mathrm{Im}(\omega\bar{w} + \omega_z)}{\bar{w}} - \frac{z}{\bar{w}^2}\left(i\omega_z\bar{w} + \frac{\bar{\omega}}{2} + \frac{\omega}{2}\bar{w}^2\right)\right\}.\end{aligned} \tag{2.30}$$

Thus, we design the following control law.

$$\begin{aligned}T = -B(\omega, \omega_z) - \kappa\left(-i\omega_z w + \frac{\omega}{2} + \frac{\bar{\omega}}{2}w^2\right) \\ - iC(w, z, \omega, \omega_z) - \alpha\left(\omega + \kappa w + i\frac{\mu z - \lambda\omega_z/\sigma_z}{\bar{w}}\right),\end{aligned} \tag{2.31}$$

where

$$B(\omega, \omega_z) = \sigma_x\omega_y\omega_z + i\sigma_y\omega_z\omega_x, \tag{2.32}$$

$$C(w, z, \omega, \omega_z) = \frac{\mu\mathrm{Im}(\omega\bar{w} + \omega_z) - \lambda\omega_x\omega_y}{\bar{w}} + \frac{\mu z - \lambda\omega_z/\sigma_z}{\bar{w}^2}\left(i\omega_z\bar{w} + \frac{\bar{\omega}}{2} + \frac{\omega}{2}\bar{w}^2\right), \tag{2.33}$$

and α is a positive control gain. Consequently, the angular rate error has the following expression.

$$\dot{e} = -\alpha e. \tag{2.34}$$

This indicates that the error parameter exponentially converges to zero at the convergence rate determined by the control gain α. Thus, the control torques shown in Eq. (2.31) can implement the designed virtual inputs.

The thruster forces to generate the control torques shown in Eq. (2.31) can be calculated through Eq. (2.16) as

$$\boldsymbol{f} = A'^{+}\boldsymbol{T}. \tag{2.35}$$

Note that the matrix A' is not full rank for any parallel thruster configuration. Thus the inverse matrix of A' should be calculated using a pseudo inverse matrix A'^{+} to minimize the norm of $\boldsymbol{f}$.

2.5 Numerical Simulations

This section shows some simulation results to demonstrate the validity of the derived control law. From the above discussion, we deal with a satellite that equips three thrusters oriented parallel to the satellite's z_b-axis.

Since each column vector of the matrix A' in Eq. (2.16) expresses the torques when $f_i = 1$ $(i = 1, 2, 3)$, a thruster configuration graph gives us a clue for better thruster configurations. For example, a thruster configuration whose geometric center coincides with the satellite's mass center can equally distribute the load of the control torques to each thruster. This feature is exploited to determine the thrusters' attachment positions in the following simulations. When the thrusters' magnitude ranges are different, divide the distances from the mass center to the thrusters by the maximum magnitudes. Then, that result helps us to find a better thruster configuration to distribute the control torques.

Here we assume that three thrusters have the same magnitude range. Since the regular triangle configuration should be efficient for three thrusters, we firstly deal with the thruster configuration depicted in Fig. 2.6. In this configuration, all distances from the mass center to the thrusters are equal, and the geometric center of the triangle coincides with the mass center. The following matrix shows the thruster configuration.

$$A_a = \begin{bmatrix} 0.50 & -1.00 & 0.50 \\ 0.87 & 0.00 & -0.87 \\ 0.00 & 0.00 & 0.00 \end{bmatrix}. \tag{2.36}$$

Table 2.1 summarizes the simulation parameters and the initial condition: the satellite's moment of inertia, the angular rate, the attitude angle, and the control gains used in the simulations. The initial attitude angles are expressed with the ZYX Euler angles for better understandings. Since the inertial frame can be set arbitrarily, without loss of generality, the target state is defined as zero-attitude angles in the simulations. Note that the controller in [46] cannot be applied to the asymmetric moment of inertia case, and that Morin's time-varying feedback controller [13] suffers from a slow convergence rate.

Table 2.1: Simulation parameters

Moment of inertia J_x, J_y, J_z[kgm^2]	
Asymmetric case:	15.0, 10.0, 6.0
Near-axisymmetric case:	15.0,14.0,6.0
Initial angular rate $\omega_x(0), \omega_y(0), \omega_z(0)$[rad/s]	1.0, 1.0, 1.0
Initial attitude angle $\phi(0), \theta(0), \psi(0)$[deg]	0.0, 45.0, 45.0
Control gains $\alpha, \kappa, \mu, \lambda$	10.0, 0.2, 5.0, 2.0

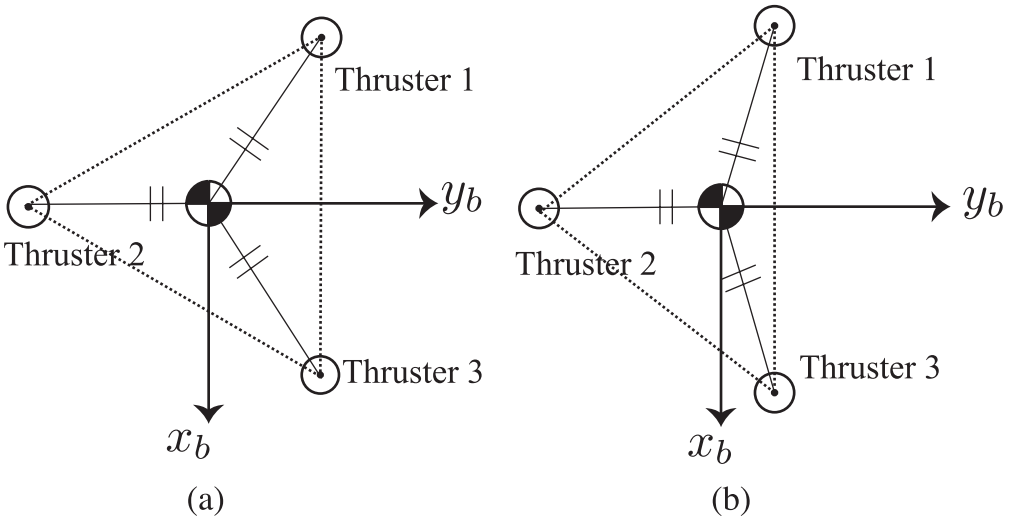

Figure 2.6: Three-thruster configurations view from the positive z_b-direction

The simulation results for the asymmetric moment of inertia in Table 2.1 are shown in Figs. 2.7, 2.8, and 2.9. Figures 2.7 and 2.8 indicate the time profiles of the angular velocities and the wz-parameters, respectively. Figure 2.9 is the time profile of the Euler angles and is added for better understanding of the attitude motion. For the near-axisymmetric case, the time profiles of the angular velocities, the wz-parameters, and the Euler angle expressions are shown in Figs. 2.10, 2.11, and 2.12, respectively. The convergence of the three attitude parameters to zero means that the satellite's attitude has been controlled to the target attitude successfully. Figure 2.13 describes the time profiles of the thruster forces for the symmetric moment of inertia model, and it is shown that the required forces are kept positive or zero during the attitude maneuver. These results indicate that the proposed controller is valid and effective, because it is applicable for any satellites regardless of its moment of inertia, and because the convergence rate is not slow

for both moment of inertia cases.

Next, we examine the different thruster configuration depicted in Fig. 2.6b. In this configuration, though the distances to the three thrusters are equal, the geometric center of the triangle coincides with the mass center. The configuration matrix is expressed as follows.

$$A_b = \begin{bmatrix} 0.28 & -1.00 & 0.28 \\ 0.96 & 0.0 & -0.96 \\ 0.00 & 0.00 & 0.00 \end{bmatrix}. \tag{2.37}$$

Figure 2.14 shows the time profiles of the thruster forces for the symmetric moment of inertia case. Thus, comparing Fig. 2.13 with Fig. 2.14, it is verified that the regular triangle configuration shown in Fig. 2.6a requires lower thruster magnitudes than the ones for the thruster configuration shown in Fig. 2.6b. It indicates that proper thruster configuration can reduce the required forces.

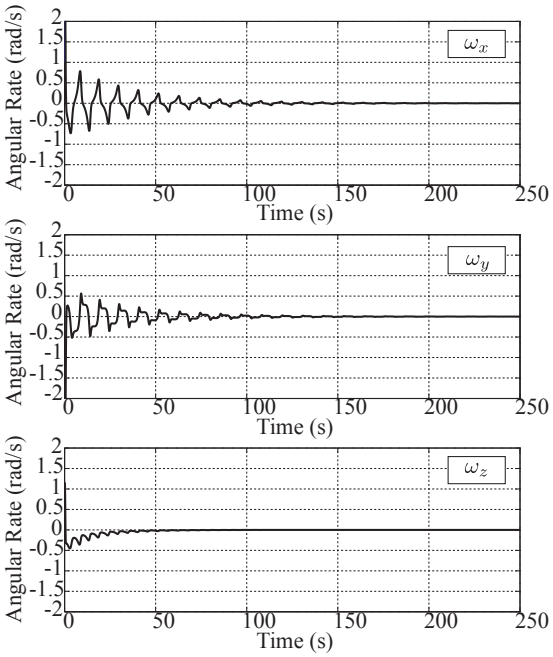

Figure 2.7: The time histories of the angular velocity(asymmetric)

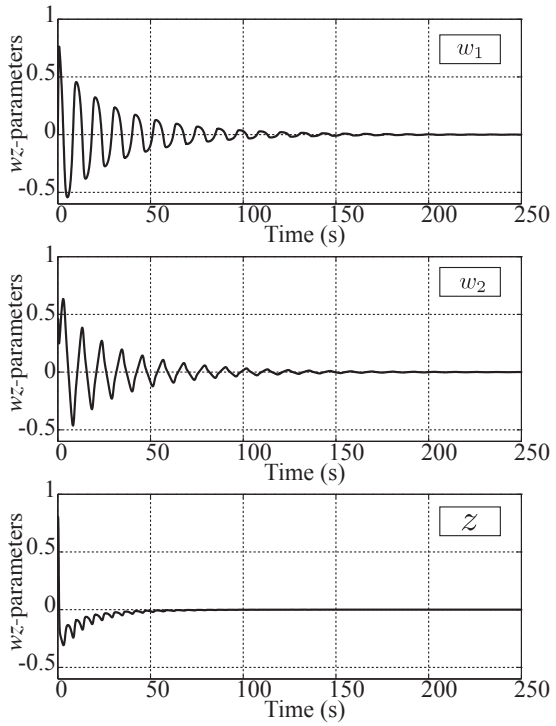

Figure 2.8: The time histories of the wz-parameters(asymmetric)

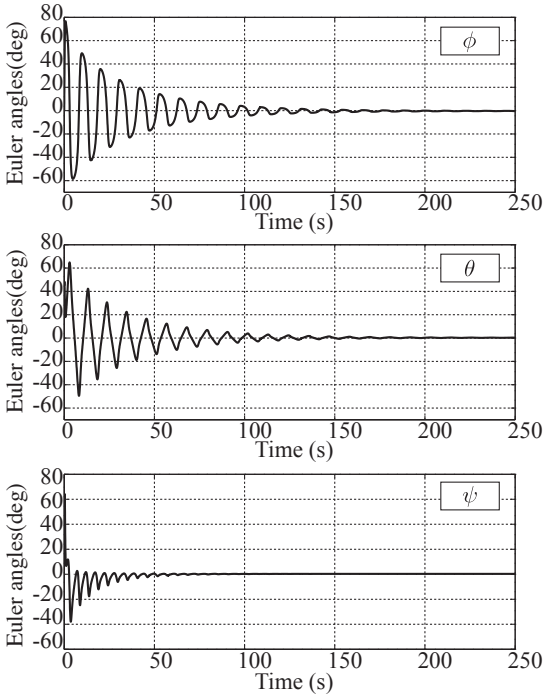

Figure 2.9: The time histories of the ZYX Euler angles(asymmetric)

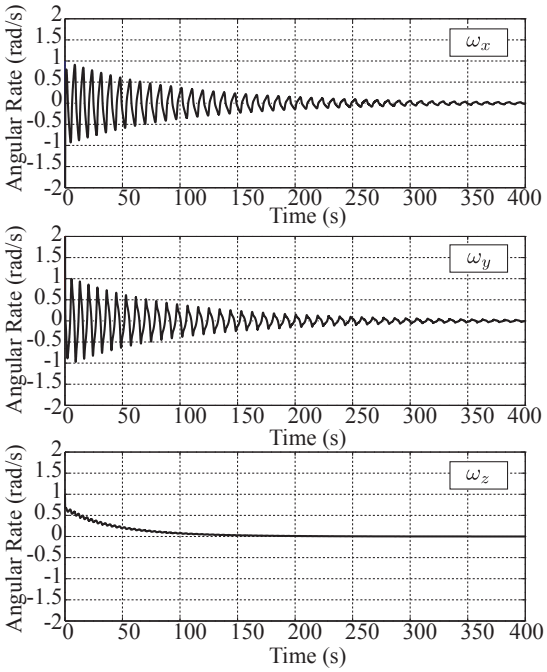

Figure 2.10: The time histories of the angular velocity(near-axisymmetric)

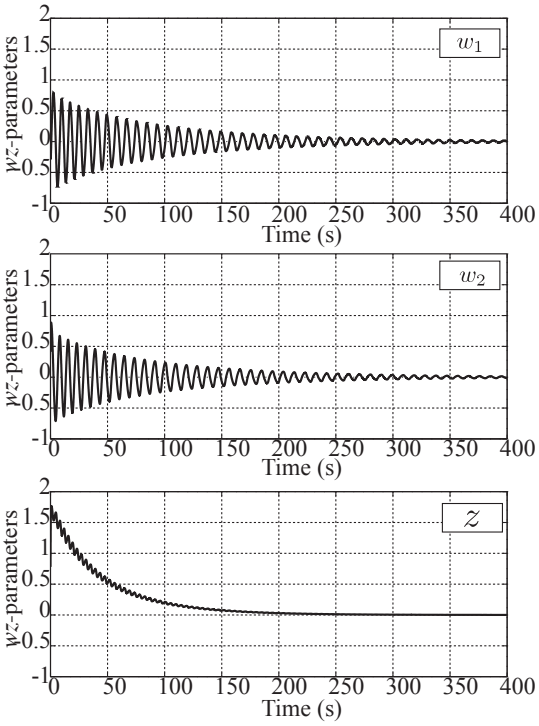

Figure 2.11: The time histories of the wz-parameters(near-axisymmetric)

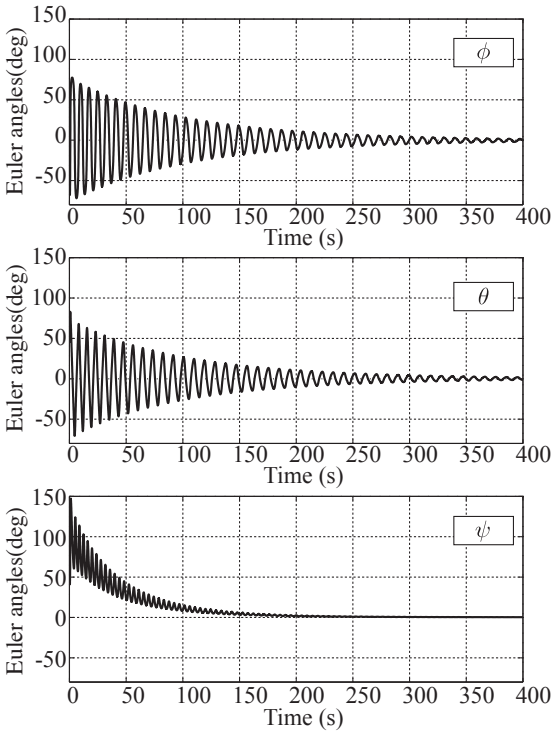

Figure 2.12: The time histories of the ZYX Euler angles(near-axisymmetric)

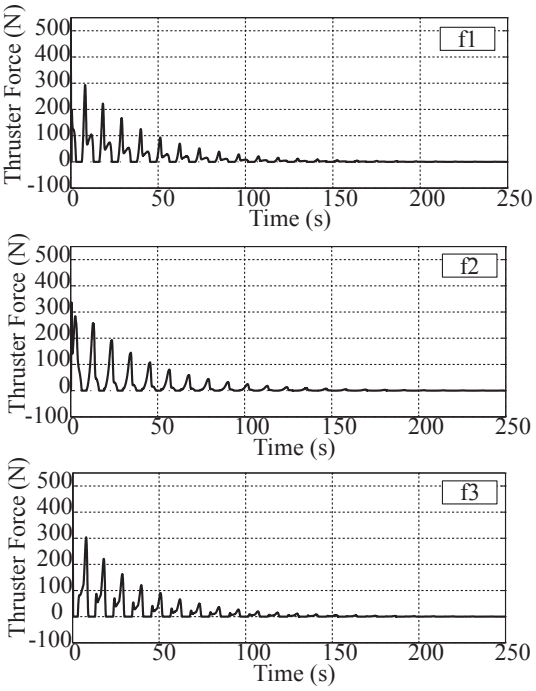

Figure 2.13: The time histories of the thruster forces in Fig. 2.6(a)

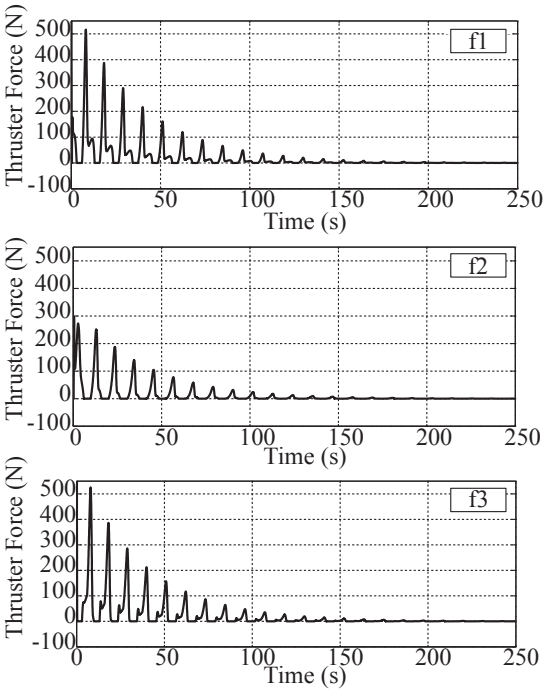

Figure 2.14: The time histories of the thruster forces in Fig. 2.6(b)

2.6 Summary of Chapter 2

This chapter has discussed the minimum necessary number of thrusters required for a satellite's three-dimensional attitude control. Considering the satellite's nonholonomic constraint and applying the Minkowski-Farkas theorem, we have analytically shown that three thrusters placed in parallel to the satellite's one principal axis can control the satellite attitude motion. Furthermore, a nonholonomic controller is obtained using the wz-parameters fore the attitude representation. The controller is effective for any satellite regardless of its moment of inertia. Numerical simulations have demonstrated the effectiveness of the proposed control law, and the efficiency of a properly placed thruster configuration has been numerically verified.

Chapter 3

Position and Attitude Control of an Underactuated Satellite with Constant Inputs

This chapter discusses a position and attitude control of an underactuated satellite which uses only on-off thruster mechanisms. Though several studies deal with a position and attitude control of a satellite, they assume enough number of actuators, i.e. translational forces are independent from rotational torques and vice versa. On the other hand, this chapter assumes only four on-off thrusters are equipped on a satellite, and thus they cause a coupled motion between the translation and the rotation. The control system becomes a second-order nonholonomic system with input constraints, and the input constraints disable us to apply most of existing control theories. The purpose of this chapter is to show that a satellite's position and attitude can be simultaneously controlled with a small number of thrusters. First, considering the input constraints, we obtain a three-step control procedure of a satellite attitude. The control procedure is then extended to the control of the satellite's translational and rotational motion in three-dimensions based on analytic solutions. In section 3.7, the proposed control technique is applied to a practical example of a lunar landing mission. For the lunar landing, a powered descending phase is studied considering the satellite mass change due to the fuel consumption of thrusters. In spite of the mass change of the satellite, the proposed analytical solution can accurately approximate the position and attitude of the satellite, and consequently enable the pinpoint landing. Numerical simulation results demonstrate the validity of the proposed controller for both the free-floating satellite and the lunar lander.

3.1 Equations of motion

This chapter considers the Cartesian coordinates $\{\boldsymbol{X}, \boldsymbol{Y}, \boldsymbol{Z}\}$ as an inertial reference system and denotes the principal axes of a satellite as $\{\boldsymbol{x}_b, \boldsymbol{y}_b, \boldsymbol{z}_b\}$. The origin of the body-fixed frame is placed to the satellite's mass center.

3.1.1 Thruster Configuration

The minimum thruster configuration to control both position and attitude of a satellite is difficult to be determined because of the nonholonomic and input constraints. As mentioned in Chapter 1 and Chapter 2, Sidi [38] claims that the minimum number of thrusters to control a satellite's attitude is four from a discussion on generating arbitrary control torques around three axes. The paper, however, does not consider nonholonomic constraints of the satellite's rotational motion. The minimum number of thrusters thus has not been discussed considering the nonholonomic constraints, and a new result would be obtained. Also, some theorems to prove controllability of nonlinear systems, e.g. Sussmann [20] or Goodwine [21], are not applicable because of unilateral and constant inputs. This paper therefore deals with a thruster configuration which can generate two independent control torques around the principal axes. Although this thruster configuration has not been analytically proved to be the minimum number of thrusters because there is no control theories to discuss the controllability with constant inputs, we predict this thruster configuration enables the position and attitude control of a satellite from the viewpoint of nonholonomic attitude control shown in Chapter 2.

This chapter, for simplicity, places four thrusters to be parallel to the satellite's principal axis y_b as shown in Fig. 3.1, and assumes that all thrusters generate the same magnitude of constant force $\mathrm{F_c}$ and have the same length of moment arm about the x_b- and z_b-axes. Then, in spite of the constant and unilateral inputs, this thruster allocation can generate a pure rotational torque, i.e. without the influence about the other two axes, around the x_b- and z_b-axes, respectively.

The thruster combinations below are employed to control the attitude of the satellite:

$$T_x^+ : f_3 = f_4 = \mathrm{F_c}, f_1 = f_2 = 0, \tag{3.1}$$
$$T_x^- : f_1 = f_2 = \mathrm{F_c}, f_3 = f_4 = 0, \tag{3.2}$$
$$T_z^+ : f_1 = f_4 = \mathrm{F_c}, f_2 = f_3 = 0, \tag{3.3}$$
$$T_z^- : f_2 = f_3 = \mathrm{F_c}, f_1 = f_2 = 0, \tag{3.4}$$

where T_j^+ and T_j^- $(j = x, z)$ denote positive and negative directional control torques around the x_b- and z_b-axes, respectively. Note that, the thrusters cannot attenuate the translational velocity without an attitude change due to the unilateral constraint on the thrust forces. Thus, both the satellite's translational and rotational motion must be controlled simultaneously.

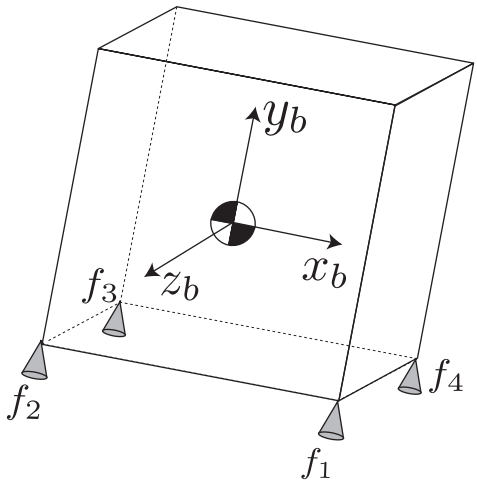

Figure 3.1: Thruster configuration.

3.1.2 Rotational Equations of Motion

The dynamics of an underactuated spacecraft with two control torques, are written as

$$\dot{\omega}_x = \sigma_x \omega_y \omega_z + T_x/J_x, \tag{3.5}$$
$$\dot{\omega}_y = \sigma_y \omega_z \omega_x, \tag{3.6}$$
$$\dot{\omega}_z = \sigma_z \omega_x \omega_y + T_z/J_z, \tag{3.7}$$

where ω_k and J_k $(k = x, y, z)$ denote an angular velocity and the principal moment of inertia, respectively, and σ_k $(k = x, y, z)$ are the moment of inertia ratios defined in Eqs. (2.4), (2.5), and (2.6). Similarly to Chapter 2, but for different axes, we assume that $\sigma_y \neq 0$, i.e. $J_x \neq J_z$, otherwise Eq. (3.6) indicates that the rotational velocity around the y_b-axis becomes uncontrollable.

Let R_{bi} denote a direction cosine matrix (DCM) from the inertial frame to the body-fixed frame. The relation between the DCM and the angular velocities satisfies the following equation [47].

$$\dot{R}_{bi} = Q(\boldsymbol{\omega}) R_{bi}, \tag{3.8}$$

where $Q(\boldsymbol{\omega})$ expresses the skew-symmetric matrix which consists of the angular velocity vector $\boldsymbol{\omega}$, and is written as

$$Q(\boldsymbol{\omega}) = \begin{bmatrix} 0 & \omega_z & -\omega_y \\ -\omega_z & 0 & \omega_x \\ \omega_y & -\omega_x & 0 \end{bmatrix}. \tag{3.9}$$

This chapter also represents the satellite attitude angles using the wz-parameters, and the parameters make it possible to foresee a proper control procedure and control the satellite attitude to a desired target with fewer number of maneuvers as shown in the later section.

The DCM using the wz-parameters is described as

$$R_{bi} = \frac{1}{1+w_1^2+w_2^2} \cdot \begin{bmatrix} (1+w_1^2+w_2^2)c - 2w_1w_2s & (1+w_1^2-w_2^2)s + 2w_1w_2c & -2w_2 \\ 2w_1w_2c - (1-w_1^2+{w^2}_2)s & 2w_1w_2s + (1-w_1^2+{w_2}^2)c & 2w_1 \\ 2w_2c + 2w_1s & 2w_2s - 2w_1c & 1-w_1^2-w_2^2 \end{bmatrix}, \tag{3.10}$$

where $c := \cos z$ and $s := \sin z$, respectively. The kinematic equations of the satellite are again written as follows:

$$\dot{w}_1 = \omega_z w_2 + \omega_y w_1 w_2 + \frac{\omega_x}{2}(1+{w_1}^2-w_2^2), \tag{3.11}$$

$$\dot{w}_2 = -\omega_z w_1 + \omega_x w_1 w_2 + \frac{\omega_y}{2}(1+{w_2}^2-w_1^2), \tag{3.12}$$

$$\dot{z} = \omega_z - \omega_x + \omega_y w_1. \tag{3.13}$$

3.1.3 Translational Equations of Motion

A satellite's translational motion in an inertial frame is expressed with a DCM from the inertial frame to the body-fixed frame. Since the DCM is an orthonormal matrix, the DCM from the body-fixed frame to the inertial frame has the relationship $R_{ib} = R_{bi}^T$. Thus, the translational equations in the Cartesian coordinate are written as

$$m\dot{\boldsymbol{V}} = R_{ib}\boldsymbol{F}, \tag{3.14}$$

where m, $\boldsymbol{V}$, and $\boldsymbol{F}$ denote the mass of the satellite, a translational velocity vector in the inertial frame, and an external force vector in the body-fixed frame, respectively. Also, the kinematic equations for the translational motion are described as

$$\dot{\boldsymbol{X}} = \boldsymbol{V}, \tag{3.15}$$

where $\boldsymbol{X}$ indicates the satellite's position vector in the inertial reference frame. When the thrusters are allocated parallel to the y_b-axis, the components of Eq.

(3.14) are simplified as follows.

$$m\dot{V}_X = \frac{F_y}{1+w_1^2+w_2^2}\left(2w_1w_2\cos z - (1--w_1^2+w_2^2)\sin z\right), \tag{3.16}$$

$$m\dot{V}_Y = \frac{F_y}{1+w_1^2+w_2^2}\left(2w_1w_2\sin z + (1-w_1^2+w_2^2)\cos z\right), \tag{3.17}$$

$$m\dot{V}_Z = \frac{2F_y}{1+w_1^2+w_2^2}w_1. \tag{3.18}$$

3.2 Attitude Control Method

Since the thruster forces are constrained to be constant, the constraints make it difficult to design a feedback controller, and control theories for nonlinear systems are not directly applicable to the system in this chapter. This section thus shows a new attitude control method using the wz-parameters. Although quaternions or Euler angles can be used for the satellite's attitude control, we have shown that the wz-parameters enable control of the satellite's attitude with only three steps [48].

In the following discussion in this chapter, the satellite is assumed to have no initial angular velocity because Kojima [49] shows that two constant torques around two principal axes of a satellite can stabilize the satellite's angular velocities to zero based on the manifolds discussed by Livneh [50].

The attitude control method proposed in this chapter consists of three steps as summarized in Table 3.1. Because the control inputs are constrained to be constant, analytic solutions for a single spin motion are derived for each maneuver and they provide proper input timings to control the attitude parameters to zero sequentially. In maneuver 1, for instance, after w_2 is converged to zero, the next step controls $w_1 \to 0$ while w_2 is kept invariant, i.e. $\dot{w}_2 = 0$. Each maneuver in Table 3.1 is explained through the following discussion.

Table 3.1: Attitude control procedure.

Maneuvers	Target state	Input timing
1	$(w_1, 0, z)$ w_1,z:arbitrary	$\phi_d = \frac{T_z^-}{2J_z}(\Delta t^-)^2 + \omega_{z0}^-\Delta t^-$
2	$(0, 0, z)z$:arbitrary	$w_{1d} = \tan\left(-\frac{T_x^-}{4J_x}(\Delta t^-)^2 - \frac{\omega_{x0}^-}{2}\Delta t^-\right)$
3	$(0, 0, 0)$	$z_d = -\frac{T_z^-}{2J_z}(\Delta t^-)^2 - \omega_{z0}^-\Delta t^-$

In maneuver 1, a positive control torque about the z_b-axis is applied during a finite time Δt^+ to generate a single spin motion, where the superscript "+" denotes a parameter when a positive directional torque is applied. Since the single spin motion avoids the coupling effect of the angular velocity, the dynamic equations

are described as follows:

$$\dot{\omega}_x = \dot{\omega}_y = 0, \tag{3.19}$$

$$\dot{\omega}_z = \frac{T_z^+}{J_z}. \tag{3.20}$$

Equation (3.20) is integrable and thus the analytic solution is obtained as

$$\omega_z = \frac{T_z^+}{J_z} t + \omega_{z0}^+. \tag{3.21}$$

The subscript "0" henceforth means the initial value when a single spin motion is generated or attenuated for each maneuver. On the other hand, the kinematic equations are expressed as follows:

$$\dot{w}_1 = \omega_z w_2, \tag{3.22}$$

$$\dot{w}_2 = -\omega_z w_1, \tag{3.23}$$

$$\dot{z} = \omega_z. \tag{3.24}$$

The norm of the w-parameter is defined as W, that is,

$$W^2 = w_1^2 + w_2^2. \tag{3.25}$$

Then, differentiating Eq. (3.25) with respect to time and using Eqs. (3.22) and (3.23), we obtain

$$\begin{aligned} 2W\dot{W} &= 2\dot{w}_1 w_1 + 2\dot{w}_2 w_2 \\ &= 0. \end{aligned} \tag{3.26}$$

This equation indicates that the norm of w_1 and w_2 is invariant in the duration. Thus, they circulate in the w_1-w_2 plane and their analytic solutions are described as follows:

$$w_1 = A\cos\phi, \tag{3.27}$$

$$w_2 = A\sin\phi, \tag{3.28}$$

where

$$A^2 := w_{1,0}^2 + w_{2,0}^2, \tag{3.29}$$

$$\phi := \arctan\left(w_2/w_1\right). \tag{3.30}$$

Equations (3.27) and (3.28), however, also mean that w_1 and w_2 cannot be controlled to zero simultaneously, and we firstly control w_2 to zero.

Because the motion of the parameter w_2 is expressed with the phase angle ϕ, and $w_2 = 0$ is achieved for $\phi = 0$, the phase angle is controlled to zero. The time derivative of ϕ is obtained from Eqs. (3.22), (3.23), and (3.77):

$$\begin{aligned} \dot{\phi} &= \frac{1}{1+(w_1/w_2)^2}\frac{\dot{w}_2 w_1 - \dot{w}_1 \dot{w}_2}{w_1^2} \\ &= -\omega_z. \end{aligned} \tag{3.31}$$

Then, the substitution of Eq. (3.20) into Eq. (3.31) yields

$$\phi(t) = -\frac{T_z^+}{2J_z}t^2 - \omega_{z,0}^+ t + \phi_0^+. \tag{3.32}$$

This analytic solution provides a desired input timing ϕ_d to control ϕ and ω_z to zero at the same time. Since this chapter assumes $|T_z^+| = |T_z^-|$, the input duration Δt^- to despin the single spin motion is determined, i.e. $\Delta t^- = \Delta t^+$. Thus, the desired input timing to converge the angular rate and the attitude angle to zero is specified as

$$\phi_d = \frac{T_z^-}{2J_z}(\Delta t^-)^2 + \omega_{z0}^- \Delta t^-. \tag{3.33}$$

In maneuver 2, a control torque about the x_b-axis is applied to generate a single spin motion. Since $\omega_z = 0$ is kept during this maneuver, the time derivative of w_2, z, and w_1 are expressed as

$$\dot{w}_2 = \dot{z} = 0, \tag{3.34}$$

$$\dot{w}_1 = \frac{\omega_x}{2}(1 + w_1^2). \tag{3.35}$$

Equations (3.34) and (3.35) show that w_1 can be controlled independently, and Eq. (3.35) is integrated as follows:

$$\begin{aligned} \frac{\mathrm{d}w_1}{1+w_1^2} &= \frac{\omega_x}{2}\mathrm{d}t \\ &= \frac{1}{2}\left(\frac{T_x^+}{J_x}t + \omega_{x0}^+\right)\mathrm{d}t \end{aligned} \tag{3.36}$$

$$\Rightarrow \quad \arctan w_1 = \frac{T_x^+}{4J_x}t^2 + \frac{\omega_{x0}^+}{2}t + \arctan w_{1,0}^+. \tag{3.37}$$

Similarly, this analytical solution presents the input timing w_{1d} which controls w_1 to an arbitrary value.

Finally, the attitude parameter z is controlled using a torque about the z_b-axis in maneuver 3. Since $\dot{w}_1 = \dot{w}_2 = 0$, the equation around the z_b-axis is written as

$$\dot{z} = \omega_z. \tag{3.38}$$

It is obvious that Eq. (3.38) is integrable and z is controlled to a target value. Note that the above discussion is for a case when a positive control torque is applied to generate a single spin motion, and a similar discussion can be obtained for a negative control torque.

3.3 Analytical Solution for Translational Motion

The analytic solutions of the satellite's translational motion during maneuvers 2 and 3 are derived in this section. As discussed later, the translational motion in three-dimension can be controlled in these maneuvers. When the attitude control torques are applied in each maneuver, the corresponding translational equations are described from Eqs. (3.16), (3.17), and (3.18) as follows:

Maneuver 2

$$m\dot{V}_X = -F_y \frac{1-w_1^2}{1+w_1^2}\sin z, \tag{3.39}$$

$$m\dot{V}_Y = F_y \frac{1-w_1^2}{1+w_1^2}\cos z, \tag{3.40}$$

$$m\dot{V}_Z = F_y \frac{2w_1}{1+w_1^2}. \tag{3.41}$$

Maneuver 3

$$m\dot{V}_X = -F_y \sin z, \tag{3.42}$$

$$m\dot{V}_Y = F_y \cos z, \tag{3.43}$$

$$m\dot{V}_Z = 0. \tag{3.44}$$

In maneuver 3, the translational velocity along the Z-axis is uncontrollable. Thus the satellite's position along the Z-axis should be controlled to the target value before maneuver 3 is applied. In the following discussion, first the analytic solutions for maneuver 3 is found, and then the analytic solutions for maneuver 2 is derived.

As shown in Eq. (3.38), the orientation angle for a single spin can be described analytically for maneuver 3. Thus, the analytic solution of the translational equations is derived. Equations (3.42) and (3.43) are rewritten as follows:

$$m\dot{V}_X = -F_y \sin\left(\frac{T_z^+}{2J_z}(\Delta t^+)^2 + \omega_{z0}^+ \Delta t^+ + z_0^+\right), \tag{3.45}$$

$$m\dot{V}_Y = F_y \cos\left(\frac{T_z^+}{2J_z}(\Delta t^+)^2 + \omega_{z0}^+ \Delta t^+ + z_0^+\right). \tag{3.46}$$

Equation (3.45) can be transformed as

$$\begin{aligned} m\dot{V}_X &= -F_y \sin\left(\frac{T_z^+}{2J_z}(\Delta t^+)^2 + \omega_{z0}^+ \Delta t^+ + z_0^+\right) \\ &= -F_y \sin\left(\frac{1}{2}\beta^+(\tau^+)^2 + B^+\right), \end{aligned} \tag{3.47}$$

where

$$\beta^+ := \frac{T_z^+}{J_z}, \tag{3.48}$$

$$B^+ := {z^+}_0 - \frac{\left(\omega_{z0}^+\right)^2}{2\beta^+}, \tag{3.49}$$

$$\tau^+ := \Delta t^+ + \frac{\omega_{z0}^+}{\beta^+}. \tag{3.50}$$

Similarly Eq. (3.46) is simplified as

$$m\dot{V}_Y = F_y \cos\left(\frac{1}{2}\beta^+(\tau^+)^2 + B^+\right). \tag{3.51}$$

Equations (3.47) and (3.51) cannot be integrated nor expressed with elementary functions. Using Fresnel integrals, however, makes it possible to obtain the analytic solutions for the translational motion. It is known that the normalized Fresnel integrals are defined as

$$S(x) := \int_0^x \sin\left(\frac{\pi}{2}t^2\right)\mathrm{d}t, \tag{3.52}$$

$$C(x) := \int_0^x \cos\left(\frac{\pi}{2}t^2\right)\mathrm{d}t. \tag{3.53}$$

Equations (3.47) and (3.51) are transformed as

$$\dot{V}_X = -\frac{F_y}{m}\left\{\sin\left(\frac{1}{2}\beta^+(\tau^+)^2\right)\cos B^+ + \cos\left(\frac{1}{2}\beta^+(\tau^+)^2\right)\sin B^+\right\}, \tag{3.54}$$

$$\dot{V}_Y = -\frac{F_y}{m}\left(\cos\frac{1}{2}\beta^+(\tau^+)^2\cos B^+ - \sin\frac{1}{2}\beta^+(\tau^+)^2\sin B^+\right). \tag{3.55}$$

Note that the replacement of by τ^+ in Eq. (3.50) changes the integral interval from $(0 \to \Delta t^+))$ to $(\omega_{z0}^+/\beta^+ \to \Delta t^+ + \omega_{z0}^+/\beta^+)$. Fresnel integrals are used to integrate Eqs. (3.54) and (3.55), and consequently the analytic solutions are described as follows:

$$V_X = -\frac{F_y}{m}\left(S_1^+ \cos B^+ + C_1^+ \sin B^+\right) + V_{X0}, \tag{3.56}$$

$$V_Y = \frac{F_y}{m}\left(S_1^+ \sin B^+ - C_1^+ \cos B^+\right) + V_{Y0}, \tag{3.57}$$

where

$$
\begin{aligned}
S_1^+ &:= \int_{\frac{\omega_{z0}^+}{\beta^+}}^{\Delta t^+ + \frac{\omega_{z0}^+}{\beta^+}} \sin\left(\frac{1}{2}\beta^+(\tau^+)^2\right) \mathrm{d}\tau^+ \\
&= \sqrt{\frac{\pi}{\beta^+}} \left(S\left(\sqrt{\frac{\beta^+}{\pi}}\left(\Delta t^+ + \frac{\omega_{z0}^+}{\beta^+}\right)\right) - S\left(\sqrt{\frac{\beta^+}{\pi}}\frac{\omega_{z0}^+}{\beta^+}\right)\right), \qquad (3.58) \\
C_1^+ &:= \int_{\frac{\omega_{z0}^+}{\beta^+}}^{\Delta t^+ + \frac{\omega_{z0}^+}{\beta^+}} \cos\left(\frac{1}{2}\beta^+(\tau^+)^2\right) \mathrm{d}\tau^+ \\
&= \sqrt{\frac{\pi}{\beta^+}} \left\{ C\left(\sqrt{\frac{\beta^+}{\pi}}\left(\Delta t^+ + \frac{\omega_{z0}^+}{\beta^+}\right)\right) - C\left(\sqrt{\frac{\beta^+}{\pi}}\frac{\omega_{z0}^+}{\beta^+}\right)\right\}. \qquad (3.59)
\end{aligned}
$$

Fresnel integrals are further integrated as:

$$
\begin{aligned}
\int_0^x S(x)\mathrm{d}x &= xS(x) + \frac{1}{\pi}\cos\left(\frac{1}{2}\pi x^2\right), \qquad (3.60) \\
\int_0^x C(x)\mathrm{d}x &= xC(x) - \frac{1}{\pi}\sin\left(\frac{1}{2}\pi x^2\right). \qquad (3.61)
\end{aligned}
$$

Hence, the integrations of Eqs. (3.56) and (3.57) provide the analytic solutions for the satellite's position as follows:

$$
\begin{aligned}
X = &-\frac{F_y}{m}\cos B^+ \left\{ S_2^+(\Delta t^+) - \sqrt{\frac{\pi}{\beta^+}} S\left(\sqrt{\frac{\beta^+}{\pi}}\frac{\omega_{z0}^+}{\beta^+}\right)\Delta t^+ \right\} \\
&- \frac{F_y}{m}\sin B^+ \left\{ C_2^+(\Delta t^+) - \sqrt{\frac{\pi}{\beta^+}} C\left(\sqrt{\frac{\beta^+}{\pi}}\frac{\omega_{z0}^+}{\beta^+}\right)\Delta t^+ \right\} \\
&+ \frac{F_y}{m}\left(S_2^+(0)\cos B^+ + C_2^+(0)\sin B^+\right) + V_{X0}\Delta t^+ + X_0, \qquad (3.62)
\end{aligned}
$$

$$
\begin{aligned}
Y = &\frac{F_y}{m}\cos B^+ \left\{ {C_2}^+(\Delta t^+) - \sqrt{\frac{\pi}{\beta^+}} C\left(\sqrt{\frac{\beta^+}{\pi}}\frac{\omega_{z0}^+}{\beta^+}\right)\Delta t^+ \right\} \\
&- \frac{F_y}{m}\sin B^+ \left\{ {S_2}^+(t) - \sqrt{\frac{\pi}{\beta^+}} S\left(\sqrt{\frac{\beta^+}{\pi}}\frac{\omega_{z0}^+}{\beta^+}\right)\Delta t^+ \right\} \\
&+ \frac{F_y}{m}\left(-C_2^+(0)\cos B^+ + S_2^+(0)\sin B^+\right) + V_{Y0}\Delta t^+ + Y_0. \qquad (3.63)
\end{aligned}
$$

where

$$S_2^+(\Delta t^+) = \frac{1}{\beta^+}\cos\left(\frac{\beta^+}{2}\left(\Delta t^+ + \frac{\omega_{z0}^+}{\beta^+}\right)^2\right) + \sqrt{\frac{\pi}{\beta^+}}\left(\Delta t^+ + \frac{\omega_{z0}^+}{\beta^+}\right) S\left(\sqrt{\frac{\beta^+}{\pi}}\left(\Delta t^+ + \frac{\omega_{z0}^+}{\beta^+}\right)\right), \quad (3.64)$$

$$C_2^+(\Delta t^+) = -\frac{1}{\beta^+}\sin\left(\frac{\beta^+}{2}\left(\Delta t^+ + \frac{\omega_{z0}^+}{\beta^+}\right)^2\right) + \sqrt{\frac{\pi}{\beta^+}}\left(\Delta t^+ + \frac{\omega_{z0}^+}{\beta^+}\right) C\left(\sqrt{\frac{\beta^+}{\pi}}\left(\Delta t^+ + \frac{\omega_{z0}^+}{\beta^+}\right)\right). \quad (3.65)$$

In maneuver 2, the translational motion along the Z-axis should be controlled to a target value. To utilize the analytic solution derived above, Eq. (3.41) is transformed as

$$\begin{aligned} m\dot{V}_Z &= 2F_y \frac{w_1}{\sqrt{1+w_1^2}} \frac{1}{\sqrt{1+w_1^2}} \\ &= F_y \sin\left(2\arctan w_1\right). \end{aligned} \quad (3.66)$$

Thus, from Eq. (3.37), Eq. (3.66) can be rewritten as

$$m\dot{V}_Z = F_y \sin\left(\frac{T_x^+}{2J_x}t^2 + \omega_{x0}^+ t + 2\arctan w_{1,0}^+\right) \quad (3.67)$$

Because this equation has the same form as Eq. (3.45), it is clear that the equation of motion along the Z-axis in maneuver 2 can be integrated using Fresnel integrals in the same way. Note that though the Fresnel integrals are transcendental functions, their calculations in practice can be conducted using approximate equations, and the approximation yields $C(x)$ and $S(x)$ to $\pm 3 \times 10^{-6}$ for arbitrary value of x [51].

3.4 Translational Velocity Control

This section shows a control method to drive the satellite's translational velocity and attitude angle to zero in maneuver 3. Since, as shown in Eq. (3.67), the analytic solution in maneuver 2 becomes the same form as that of maneuver 3, the control technique shown in the following discussion is applicable to both maneuvers 2 and 3.

As seen in Eqs. (3.56) and (3.57), the translational velocities are affected by not only the satellite's attitude angle, but also the angular velocity. For one "on"-interval of thruster firing, the attitude angle at which the thrust force should be applied is uniquely specified according to the angular velocity. That is, the translational velocity and the attitude angle cannot be controlled to the target state at the same time. However, for several on-intervals to despin the rotation, the final translational velocity after the despin maneuver can be varied. In the following, n on-intervals are applied for thruster firing satisfying the following relation to despin the rotational motion:

$$\Delta t^{+} = \sum_{i=1}^{n} \Delta t^{i}, \tag{3.68}$$

where the superscript i is used to indicate a variable expressing the i-th on-interaval.

Equations (3.56) and (3.57) are rewritten in matrix form as

$$\begin{bmatrix} V_X \\ V_Y \end{bmatrix} = -\frac{F_y}{m} \begin{bmatrix} \cos B^{+} & -\sin B^{+} \\ \sin B^{+} & \cos B^{+} \end{bmatrix} \begin{bmatrix} S_1^{+} \\ -C_1^{+} \end{bmatrix} + \begin{bmatrix} V_X(0) \\ V_Y(0) \end{bmatrix}$$
$$\Rightarrow \boldsymbol{V} = -\frac{F_y}{m} R_B \boldsymbol{V}_1 + \boldsymbol{V}(0). \tag{3.69}$$

The matrix R_B in this equation takes a rotation matrix form and includes the initial attitude angle z_0^i for each on-interval. Thus, using different firing timings can change the time profile of translational velocity $\boldsymbol{V}$. Equation (3.69) also indicates that the direction of $\boldsymbol{V}$ depicts a circle whose center is $\boldsymbol{V}(0)$ in the V_X-V_Y plane. Furthermore, since the vector $\boldsymbol{V}_1$ is changeable by changing the input interval Δt, the velocity vector $\boldsymbol{V}$ can be changed to any values in the inner area of the circle. That is, it indicates the satellite's velocity can be controlled arbitrarily.

After the n-th on-interval, the translational velocity of the satellite must be zero. As mentioned above, the attitude angle of the n-th thruster firing z_0^n is uniquely determined according to the angular velocity ω_{z0}^n due to the constant inputs. The angular rate ω_{z0}^n is specified by the $(n-1)$-th ω_{z0}^{n-1} and the interval Δt^{n-1} as $\omega_{z0}^n = \omega_{z0}^{n-1} - \beta \Delta t^{n-1}$. Thus, to vanish the translational velocity after the n-th despin maneuver, the following conditions must be satisfied by two proper variables Δt^{n-1} and z_0^{n-1}:

$$V_{X0}^{n-1} + \Delta V_X^{n-1}(z_0^{n-1}, \Delta t^{n-1}) + \Delta V_X^{n}(z_0^{n-1},\ \Delta t^{n-1}) = 0, \tag{3.70}$$

$$V_{Y0}^{n-1} + \Delta V_Y^{n-1}(z_0^{n-1}, \Delta t^{n-1}) + \Delta V_Y^{n}(z_0^{n-1},\ \Delta t^{n-1}) = 0. \tag{3.71}$$

The solutions satisfying the above two conditions can be obtained numerically, because the analytic solutions of the translational velocities are described by using

the Fresnel integrals. Note that Eqs. (3.70) and (3.71) have solutions because the initial velocities can be made relatively small before the $(n-1)$-th maneuver by using the discrete input intervals Δt^i $(i = 1, \ldots, n-2)$. Thus, the satellite's translational velocities and attitude can be converged to zero simultaneously.

3.5 Position Control

From Eqs. (3.42) and (3.43), when the spacecraft has a negative translational velocity $V_Y < 0$ with zero attitude angle, the satellite's position and translational velocity along the Y-axis can be easily controlled. It implies that the positive part of the inertial axis Y can be used as an invariant manifold. That is, the translational motion of the satellite can be converged to the origin, once the satellite reaches the manifold with the following states: ($X = V_X = Z = V_Z = 0$, $V_Y < 0$, $Y > 0$).

Figure 3.2 describes the position and attitude control procedure in maneuver 3. When the satellite has states ($X > 0$, $Y \gg 0$, $V_X < 0$, $V_Y < 0$), using the drift motion of the satellite makes it possible to calculate the input timings to control the attitude angles and the translational velocity in the X-direction. Equation (3.62) then gives the position increments ΔX for such maneuvers. The summation of those increments thus can specify the start position of the thrust firings. Consequently, maneuvering the satellite to the manifold with the target attitude angles can control and stop the satellite at the origin.

The proposed control procedure is described in Fig. 3.3 and is summarized as follows.

Maneuver 1 : The angular rate ω_z and the attitude parameter w_2 are simultaneously controlled to zero with a single spin motion around z_b-axis. The input timing is uniquely determined with Eq. (3.33).

Maneuver 2 : After a single spin motion around x_b-axis is generated, the satellite's translational velocity and position along the Z-axis are controlled to zero with discrete thruster firings. The angular rate ω_x and the attitude parameter w_1 are simultaneously converged to a target state in the maneuver. The thruster firing timings are specified with the analytic solutions obtained from Eq. (3.67).

Maneuver 3 : The satellite state is firstly driven to a preferable state satisfying ($X > 0$, $Y \gg 0$, $V_X < 0$, $V_Y < 0$) with a control of single rotation around z_b-axis. Through the drift motion, the satellite's translational velocity and position along the X-axis are controlled onto a manifold with discontinuous inputs satisfying Eq. (3.70). The satellite then moves along the manifold and stops at the origin of the inertial frame.

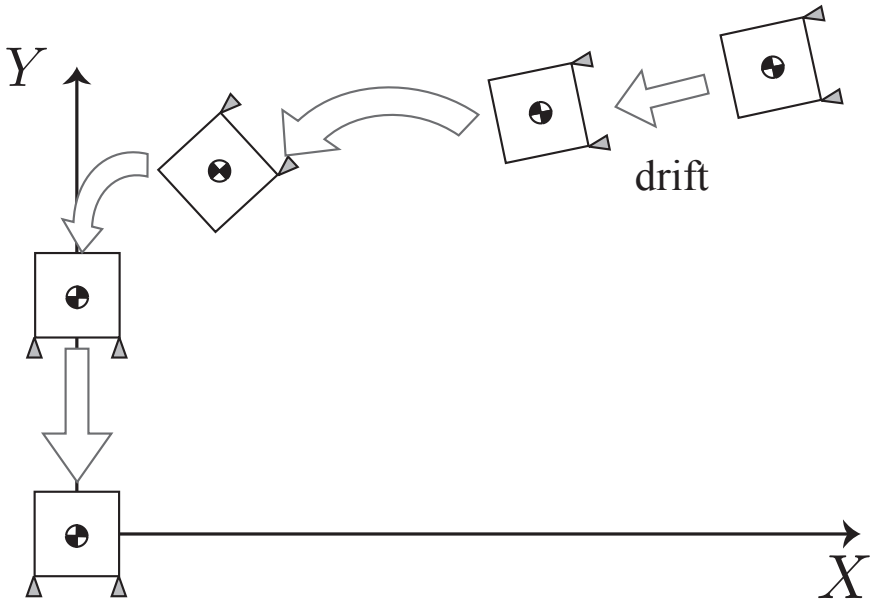

Figure 3.2: Proposed control procedure with the invariant manifold in maneuver 3.

3.6 Numerical Simulations

Numerical simulation results demonstrate the validity of the proposed control algorithm. The simulation parameters and the initial condition are summarized in Tables 3.2 and 3.3, respectively. For better understanding, the initial attitude angles are expressed with ZYX Euler angles. The numbers of thruster firings, n, to despin a rotation are set as two and one in maneuvers 2 and 3, respectively. Although for general cases despin maneuver is completed with multiple thrust firing, the despin maneuver in this simulation has the solution to Eq. (3.70) with one thruster firing. This is because the drift velocity vector and the attitude angle at the beginning of the maneuver happen to be preferable for control.

Table 3.2: Simulation Parameters.

Satellite mass, m	500.0 [kg]
Thruster force, $\mathrm{F_c}$	100.0 [N]
Moment of inertia, (J_x, J_y, J_z)	250.0, 300.0, 350.0 [kgm^2]
Moment arm, a	1.0 [m]

Figures 3.4 and 3.5 describe the time histories of the angular velocities and the attitude angles, respectively, and they show all parameters converge to zero. Since the inertial frame is defined to be coincident with the target attitude and the every

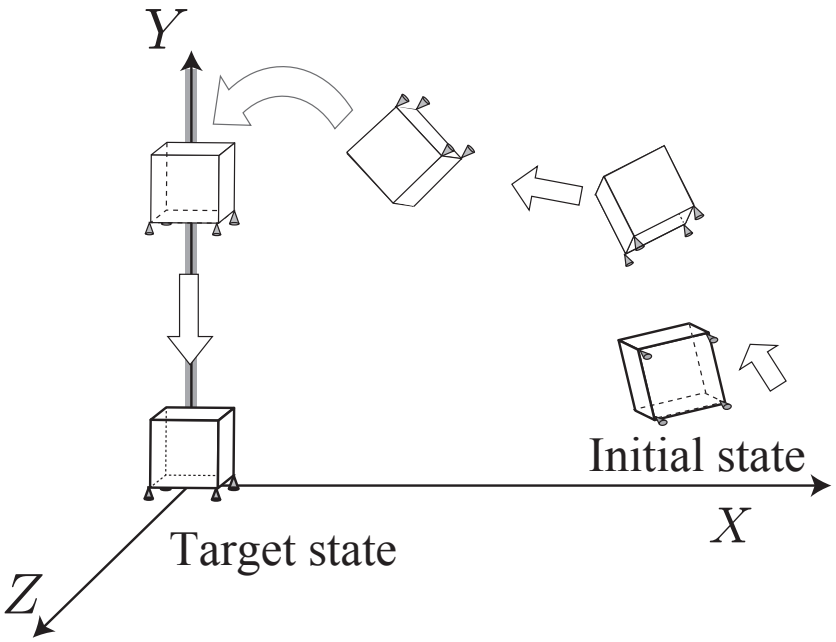

Figure 3.3: The proposed control procedure.

Table 3.3: Initial Conditions.

Angular rate, $(\omega_x, \omega_y, \omega_z)$	0.0, 0.0, 0.0 [rad/s]
ZYX Euler angles, (Φ, Θ, Ψ)	20.0, 30.0, 45.0 [deg]
Translational velocity, (V_X, V_Y, V_Z)	0.0, 0.0, 0.0 [m/s]
Position (X, Y, Z)	-20.0, -20.0, -20.0 [m]

state parameters become zero at the target, these figures mean that the satellite's attitude is controlled successfully. Figures 3.6 and 3.7 show the time histories of the satellite's translational velocities and positions. In maneuver 3, the satellite is initially controlled to the invariant manifold defined by $V_X = X = 0$. Then, the satellite's position and velocity along the Z-axis is converged to the origin. The three-dimensional trajectory of the satellite and the thruster inputs for the control procedure are shown in Figs. 3.8 and 3.9, respectively, and they show the satellite is successfully controlled with constant thrusts in one direction.

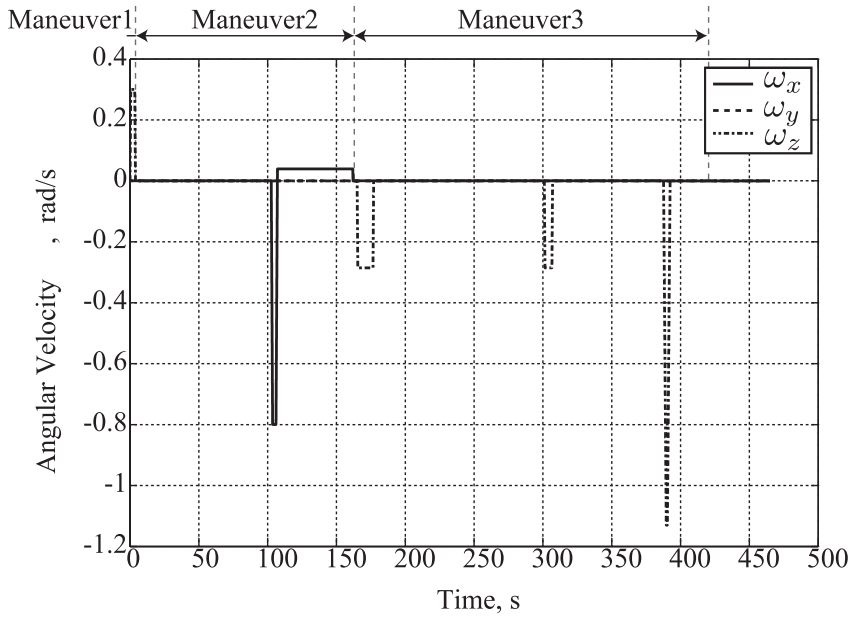

Figure 3.4: The time history of the angular velocity.

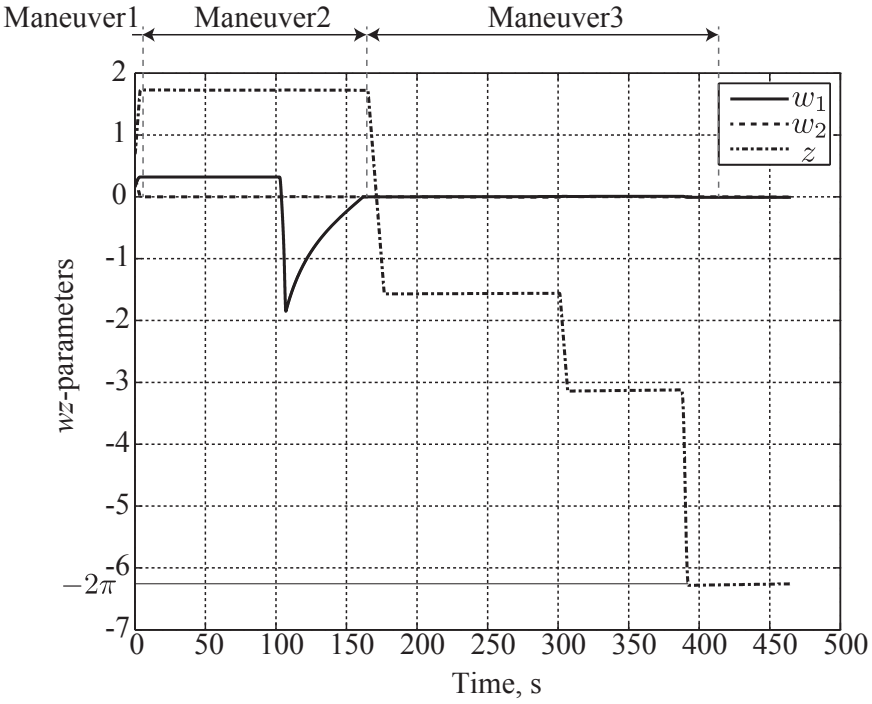

Figure 3.5: The time history of the attitude angle.

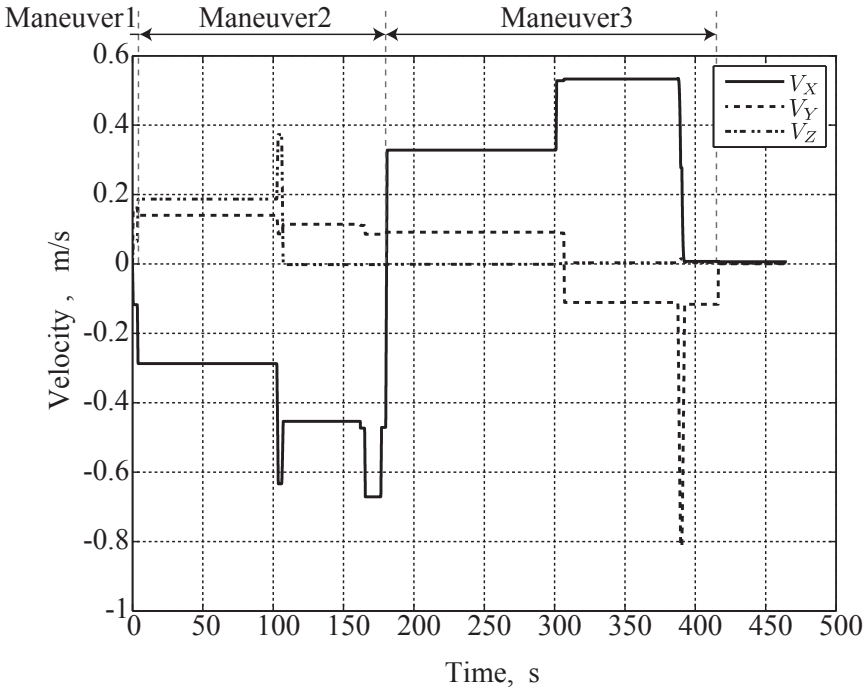

Figure 3.6: The time histories of the translational velocity.

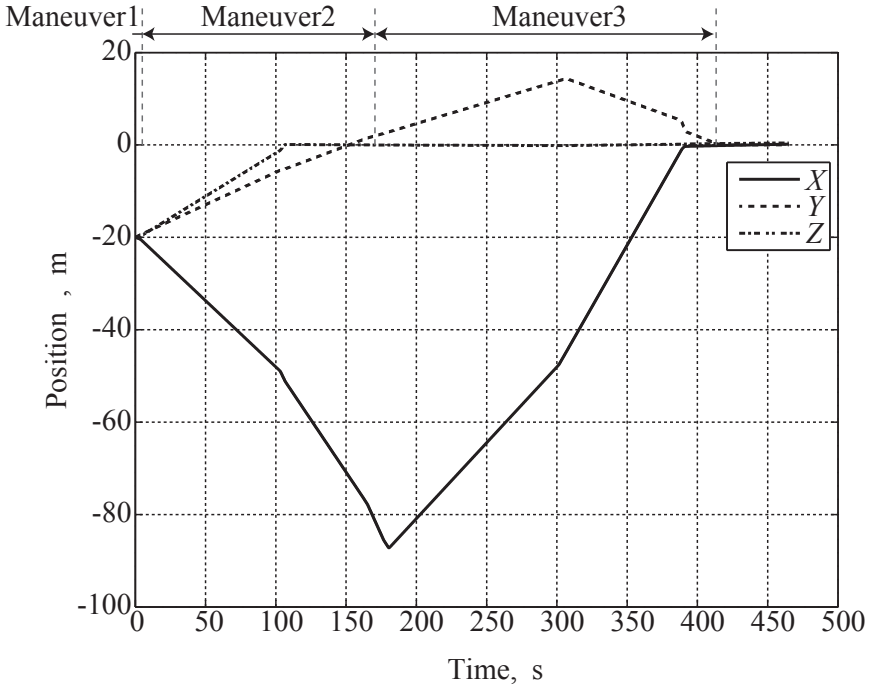

Figure 3.7: The time history of the position.

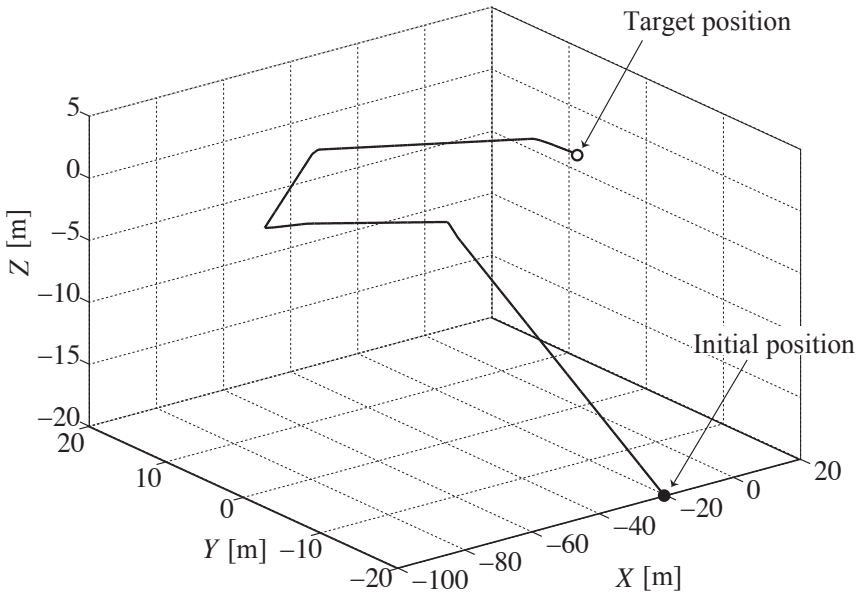

Figure 3.8: Three-dimensional trajectory of the satellite.

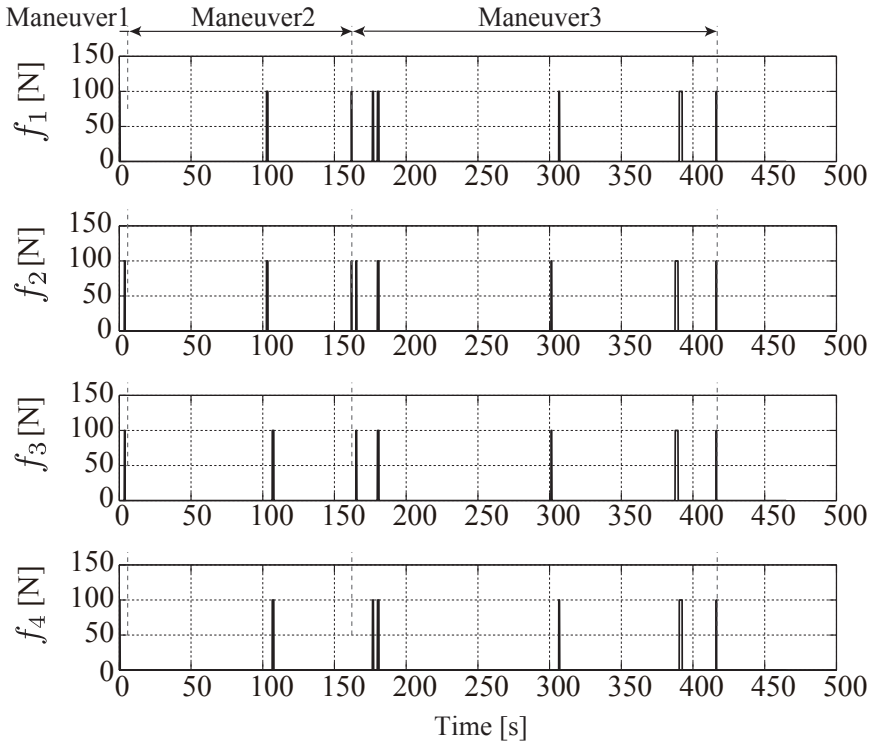

Figure 3.9: The time histories of the thruster inputs.

3.7 Application to Practical Case

This section applies the proposed method to a practical situation considered in a project of Japan Aerospace eXploration Agency (JAXA). In the project, the satellite mass constantly changes due to the fuel consumption of thrusters, and the control strategy must include the influence of the mass change. That is, the satellite mass becomes a time-varying parameter depending on the control inputs. Although the analytical solutions cannot be obtained even if Fresnel integrals are applied, nevertheless, a similar control technique shown in the previous section can derive the approximate analytic solution considering the satellite's mass change to achieve an accurate control of the satellite's position and attitude. The accuracy of the proposed approximate solution is numerically verified by applying it to a condition considered in the project.

JAXA is planning to launch a lunar lander for smart landing demonstration at a specified target point, which is called Smart Lander for Investigating Moon(SLIM) project. In the powered descending phase of the mission, the lander firing its main thruster is guided from the lunar transfer orbit to the region above the target point (see Fig. 3.10). The sub-thrusters change the lander's attitude and controls its horizontal velocity to zero. Because the lander fires the main thruster for most of the powered descending phase, the satellite's mass changes due to the fuel consumption. The mass change affects the satellite's motion, and thus the control strategy must consider the mass change for the accurate landing.

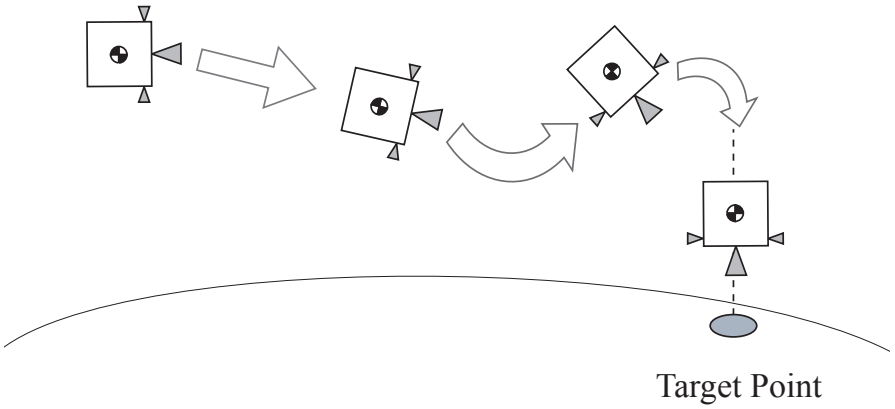

Figure 3.10: Lunar landing mission.

3.7.1 Equations of Motion

In the powered descending phase of the mission, the satellite is controlled from a lunar transfer orbit to a target point, and the satellite motion can be considered

in two-dimensions. The equations of motion for the satellite model shown in Fig. 3.11 are written as:

$$m(t)\ddot{X} = (f_1 + f_2)\cos\alpha\cos\psi - (f_1 - f_2)\sin\alpha\sin\psi, \tag{3.72}$$

$$m(t)\ddot{Y} = (f_1 + f_2)\cos\alpha\sin\psi + (f_1 - f_2)\sin\alpha\cos\psi - m(t)g, \tag{3.73}$$

$$J\ddot{\psi} = \beta(f_1 - f_2), \tag{3.74}$$

where m, ψ, and J are the mass of satellite, an attitude angle and the moment of inertia, respectively. For simplicity, we assume that the two thrusters generate the same magnitude of thrusts, i.e. $f_1 = f$ or 0, $f_2 = f$ or 0, and they are attached at the angle of α to the satellite body. The distance β illustrated in Fig. 3.11 denotes the moment arm of control torques generated by the thrusters. Note that the β is defined as a negative value when the thruster f_1 generates a clockwise directional control torque. Also, the satellite mass is assumed to change at a constant rate c due to the fuel consumption.

$$\dot{m} = -c. \tag{3.75}$$

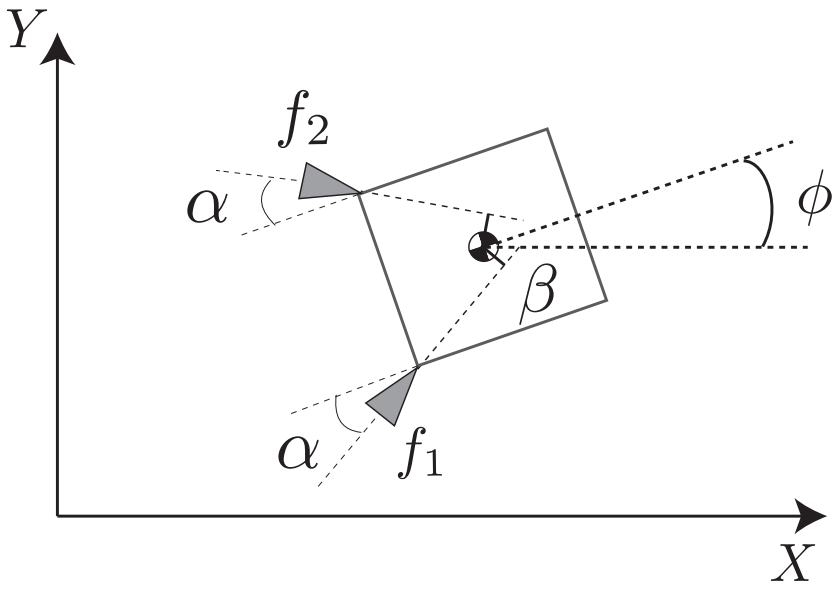

Figure 3.11: Satellite model

3.7.2 Approximate Solution

Considering the constant magnitude of thruster force, we obtain an approximate analytical solution. When the thruster f_1 is fired, Eqs. (3.74) and (3.75) are

integrated as

$$\dot{\psi} = \frac{\beta}{J} f t + \dot{\psi}_0, \tag{3.76}$$

$$\psi = \frac{\beta f}{2J} t^2 + \dot{\psi}_0 t + \psi_0, \tag{3.77}$$

$$m = m_0 - ct. \tag{3.78}$$

As shown in Eqs. (3.76) and (3.77), the satellite's rotational motion is integrable. Thus, Eq. (3.72) is rewritten as follows.

$$\ddot{X} = \frac{1}{m_0 - ct} \cdot \left\{ f \cos\alpha \cos\left(\frac{\beta f}{2J} t^2 + \dot{\psi}_0 t + \psi_0 \right) - f \sin\alpha \sin\left(\frac{\beta f}{2J} t^2 + \dot{\psi}_0 t + \psi_0 \right) \right\}. \tag{3.79}$$

In this equation, since the denominator varies with time due to the mass change, this equation cannot be integrated nor expressed with any elementary functions of mathematics. Thus, this subsection derives the approximated expression for the analytic solution of the translational motion utilizing Fresnel integrals and the partial integration.

Since the two terms of the right-hand in Eq. (3.79) have similar form,here, we deal with only the first term. The first term can be transformed as

$$\begin{aligned} &\frac{f\cos\alpha}{m_0 - ct} \cos\left(\frac{\beta f}{2J} t^2 + \dot{\psi}_0 t + \psi_0 \right) \\ &= \frac{f\cos\alpha}{m_0 - c(\tau - t_1)} \cos\left(\frac{\pi}{2} A^2 \tau^2 + B \right), \\ &= \frac{f\cos\alpha}{m_0 - c\{\tau - t_1)} \left(\cos\left(\frac{\pi}{2} A^2 \tau^2 \right) \cos B - \sin\left(\frac{\pi}{2} A^2 \tau^2 \right) \sin B \right\}, \end{aligned} \tag{3.80}$$

where A, B, and τ are redefined as follows.

$$A = \sqrt{\frac{\beta f}{\pi J}}, \tag{3.81}$$

$$B = \phi_0 - \frac{J\dot{\psi}_0^2}{2\beta f}, \tag{3.82}$$

$$t_1 = \frac{J\dot{\psi}_0}{\beta f}, \tag{3.83}$$

$$\tau = t + t_1. \tag{3.84}$$

Note that if $\beta < 0$, A is defined as,

$$A = \sqrt{\frac{-\beta f}{\pi J}}. \tag{3.85}$$

Using the partial integration repeatedly, we can integrate Eq. (3.80) and describe the approximate solution as:

$$
\begin{aligned}
&\int_0^t \frac{f\cos\alpha}{m_0 - ct}\cos\left(\frac{\beta f}{2J}t^2 + \dot{\psi}_0 t + \psi_0\right)\mathrm{d}t \\
&\quad= \int_{t_1}^{t+t_1} \frac{f\cos\alpha}{m_0 - c\left(\tau - t_1\right)}\left(\cos\left(\frac{\pi}{2}A^2\tau^2\right)\cos B - \sin\left(\frac{\pi}{2}A^2\tau^2\right)\sin B\right)\mathrm{d}\tau, \\
&\quad= \left[\frac{f\cos\alpha}{m_0 - c(\tau - t_1)}\left(\cos B\frac{C(A\tau)}{A} - \sin B\frac{S(A\tau)}{A}\right)\right]_{t_1}^{t+t_1} \\
&\qquad- \int_{t_1}^{t+t_1} \frac{fc\cos\alpha}{\left(m_0 - c(\tau - t_1)\right)^2}\left(\cos B\frac{C(A\tau)}{A} - \sin B\frac{S(A\tau)}{A}\right)\mathrm{d}\tau, \\
&\quad= \left[\frac{f\cos\alpha}{m_0 - c(\tau - t_1)}\left(\cos B\frac{C(A\tau)}{A} - \sin B\frac{S(A\tau)}{A}\right)\right]_{t_1}^{t+t_1} \\
&\qquad- \left[\frac{fc\cos\alpha}{\left(m_0 - c(\tau - t_1)\right)^2}\left(\cos B\int_0^\tau \frac{C(A\tau)}{A}d\tau - \sin B\int_0^\tau \frac{S(A\tau)}{A}\mathrm{d}\tau\right)\right]_{t_1}^{t+t_1} \\
&\qquad+ \int_{t_1}^{t+t_1}\left\{\frac{2fc^2\cos\alpha}{\left(m_0 - c(\tau - t_1)\right)^3}\left(\cos B\int_0^\tau \frac{C(A\tau)}{A}\mathrm{d}\tau - \sin B\int_0^\tau \frac{S(A\tau)}{A}\mathrm{d}\tau\right)\right\}\mathrm{d}\tau, \\
&\quad= \cdots, \\
&\quad= \sum_{n=0}^{\infty}\left[\frac{(-1)^n n! c^n f\cos\alpha}{\left(m_0 - c\left(\tau - t_1\right)\right)^{n+1}}\left(\cos B\iint\cdots\int\frac{C(A\tau)}{A}\mathrm{d}\tau\mathrm{d}\tau\cdots\mathrm{d}\tau\right.\right. \\
&\qquad\left.\left.- \sin B\iint\cdots\int\frac{S(A\tau)}{A}\mathrm{d}\tau\mathrm{d}\tau\cdots\mathrm{d}\tau\right)\right]_{t_1}^{t+t_1},
\end{aligned}
$$

where $C(\cdot)$ and $S(\cdot)$ are Fresnel integrals defined in Eqs. (3.53), (3.52), respectively. Here, we define the degree n for Fresnel integrals to denote the number of partial integrations. In realistic systems, the satellite mass is obviously much larger than the total fuel consumption, i.e. $m_0 \gg ct$. Therefore we can consider that the remained integral term becomes small enough to ignore as the degree n increases.

The approximated analytical solution of translational velocities are consequently

described as:

$$
\begin{aligned}
V_X &= \dot{X} \\
&= \sum_{n=0}^{\infty}\Bigg[\frac{(-1)^n n! c^n f\cos\alpha}{\left(m_0 - c\left(\tau - t_1\right)\right)^{n+1}}\Bigg(\cos B\iint\cdots\int\frac{C(A\tau)}{A}\mathrm{d}\tau\mathrm{d}\tau\cdots\mathrm{d}\tau \\
&\quad - \sin B\iint\cdots\int\frac{S(A\tau)}{A}\mathrm{d}\tau\mathrm{d}\tau\cdots\mathrm{d}\tau\Bigg)\Bigg]_{t_1}^{t+t_1} \\
&\quad - \sum_{n=0}^{\infty}\Bigg[\frac{(-1)^n n! c^n f\sin\alpha}{\left(m_0 - c\left(\tau - t_1\right)\right)^{n+1}}\Bigg(\cos B\iint\cdots\int\frac{S(A\tau)}{A}\mathrm{d}\tau\mathrm{d}\tau\cdots\mathrm{d}\tau \\
&\quad \sin B\iint\cdots\int\frac{C(A\tau)}{A}\mathrm{d}\tau\mathrm{d}\tau\cdots\mathrm{d}\tau\Bigg)\Bigg]_{t_1}^{t+t_1} \\
&\quad + V_{X0},
\end{aligned}
\tag{3.86}
$$

$$
\begin{aligned}
V_Y &= \dot{Y} \\
&= \sum_{n=0}^{\infty}\Bigg[\frac{(-1)^n n! c^n f\cos\alpha}{\left(m_0 - c\left(\tau - t_1\right)\right)^{n+1}}\Bigg(\cos B\iint\cdots\int\frac{S(A\tau)}{A}\mathrm{d}\tau\mathrm{d}\tau\cdots\mathrm{d}\tau \\
&\quad + \sin B\iint\cdots\int\frac{C(A\tau)}{A}\mathrm{d}\tau\mathrm{d}\tau\cdots\mathrm{d}\tau\Bigg)\Bigg]_{t_1}^{t+t_1} \\
&\quad + \sum_{n=0}^{\infty}\Bigg[\frac{(-1)^n n! c^n f\sin\alpha}{\left(m_0 - c\left(\tau - t_1\right)\right)^{n+1}}\Bigg(\cos B\iint\cdots\int\frac{C(A\tau)}{A}\mathrm{d}\tau\mathrm{d}\tau\cdots\mathrm{d}\tau \\
&\quad - \sin B\iint\cdots\int\frac{S(A\tau)}{A}\mathrm{d}\tau\mathrm{d}\tau\cdots\mathrm{d}\tau\Bigg)\Bigg]_{t_1}^{t+t_1} \\
&\quad - gt + V_{Y0}.
\end{aligned}
\tag{3.87}
$$

Equations. (3.86) and (3.87) can be further integrated, and the approximate so-

lutions of the position are shown as:

$$
\begin{aligned}
X = &\sum_{n=0}^{\infty}\left[\frac{(-1)^n n! c^n f\cos\alpha}{(m_0-ct)^{n+1}}\left(\cos B\iint\cdots\int C_1\left(A\left(t+t_1\right)\right)\mathrm{d}t\mathrm{d}t\cdots\mathrm{d}t\right.\right.\\
&\left.\left.-\sin B\iint\cdots\int S_1\left(A\left(t+t_1\right)\right)\mathrm{d}t\mathrm{d}t\cdots\mathrm{d}t\right)\right]_0^t\\
&-\sum_{n=0}^{\infty}\left(\frac{(-1)^n n! c^n f\cos\alpha}{m_0^{n+1}}t\left(\cos\left(B\right)C_1(At_1)-\sin\left(B\right)S_1(At_1)\right)\right)\\
&-\sum_{n=0}^{\infty}\left[\frac{(-1)^n n! c^n f\sin\alpha}{(m_0-ct)^{n+1}}\left(\cos B\iint\cdots\int S_1\left(A\left(t+t_1\right)\right)\mathrm{d}t\mathrm{d}t\cdots\mathrm{d}t\right.\right.\\
&\left.\left.+\sin B\iint\cdots\int C_1\left(A\left(t+t_1\right)\right)\mathrm{d}t\mathrm{d}t\cdots\mathrm{d}t\right)\right]_0^t\\
&+\sum_{n=0}^{\infty}\left(\frac{(-1)^n n! c^n f\sin\alpha}{m_0^{n+1}}t\left(\cos\left(B\right)S_1(At_1)+\sin BC_1(At_1)\right)\right)\\
&+V_{X0}t+X_0,
\end{aligned}
\tag{3.88}
$$

$$
\begin{aligned}
Y = &\sum_{n=0}^{\infty}\left[\frac{(-1)^n n! c^n f\cos\alpha}{(m_0-ct)^{n+1}}\left(\cos B\iint\cdots\int S_1\left(A\left(t+t_1\right)\right)\mathrm{d}t\mathrm{d}t\cdots\mathrm{d}t\right.\right.\\
&\left.\left.+\sin B\iint\cdots\int C_1\left(A\left(t+t_1\right)\right)\mathrm{d}t\mathrm{d}t\cdots\mathrm{d}t\right)\right]_0^t\\
&-\sum_{n=0}^{\infty}\left(\frac{(-1)^n n! c^n f\cos\alpha}{m_0^{n+1}}t\left(\cos\left(B\right)S_1(At_1)+\sin\left(B\right)C_1(At_1)\right)\right)\\
&+\sum_{n=0}^{\infty}\left[\frac{(-1)^n n! c^n f\sin\alpha}{(m_0-ct)^{n+1}}\left(\cos B\iint\cdots\int C_1\left(A\left(t+t_1\right)\right)\mathrm{d}t\mathrm{d}t\cdots\mathrm{d}t\right.\right.\\
&\left.\left.-\sin B\iint\cdots\int S_1\left(A\left(t+t_1\right)\right)\mathrm{d}t\mathrm{d}t\cdots\mathrm{d}t\right)\right]_0^t\\
&-\sum_{n=0}^{\infty}\left(\frac{(-1)^n n! c^n f\sin\alpha}{m_0^{n+1}}t\left(\cos\left(B\right)C_1(At_1)-\sin\left(B\right)S_1(At_1)\right)\right)\\
&-\frac{1}{2}gt^2+V_{Y0}t+Y_0,
\end{aligned}
\tag{3.89}
$$

where $C_1(\cdot)$ and $S_1(\cdot)$ are redefined as follows.

$$
C_1(t) := \int_0^t \frac{C(t)}{A}\mathrm{d}t, \tag{3.90}
$$

$$
S_1(t) := \int_0^t \frac{S(t)}{A}\mathrm{d}t. \tag{3.91}
$$

3.7.3 Numerical Test and Discussion

This subsection shows a numerical test to verify the accuracy of the approximate solution. Henceforth we use the satellite model shown in Fig. 3.12, which is based on the lunar lander model of SLIM being planned in JAXA. The satellite equips a main thruster to decelerate the translational velocity and sub-thrusters at the mounting angle $\alpha = \pi/2$ to control the satellite's attitude.

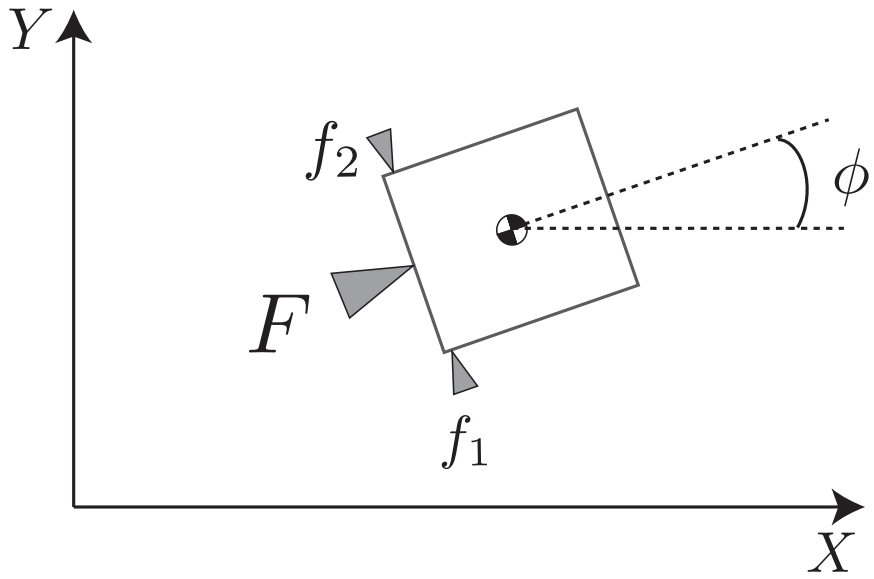

Figure 3.12: Lunar lander model.

The accuracy of the approximate solution depends on the ratio between the satellite mass and the fuel consumption. Thus, the numerical calculation is conducted for two different cases. The parameters are summarized in Table 3.4.

Figures 3.13 and 3.14 show the relative error of the translational velocity between the exact solution and the approximate solution evaluated in Eqs. (3.86) and (3.87). It is clear that the relative error becomes smaller as the degree of Fresnel integrals increases. However, because the partial integration for the Fresnel integrals requires complex calculations, the approximate solutions for $n = 0$ and $n = 1$ are used in the followings.

In the powered descending phase of the SLIM mission, the objective is to drive the satellite into a region above the target point with zero-horizontal velocity. The satellite's attitude is simultaneously controlled to a target attitude angle. Since the inertial frame can be defined arbitrarily, without loss of generality, we set the target state as $X = V_X = \dot{\phi} = 0, \phi = \pi/2$ in this discussion.

Note that the lunar lander model has a negative moment arm, that is, the thruster f_1 generates a negative directional control torque, and thus, Eq. (3.80) is

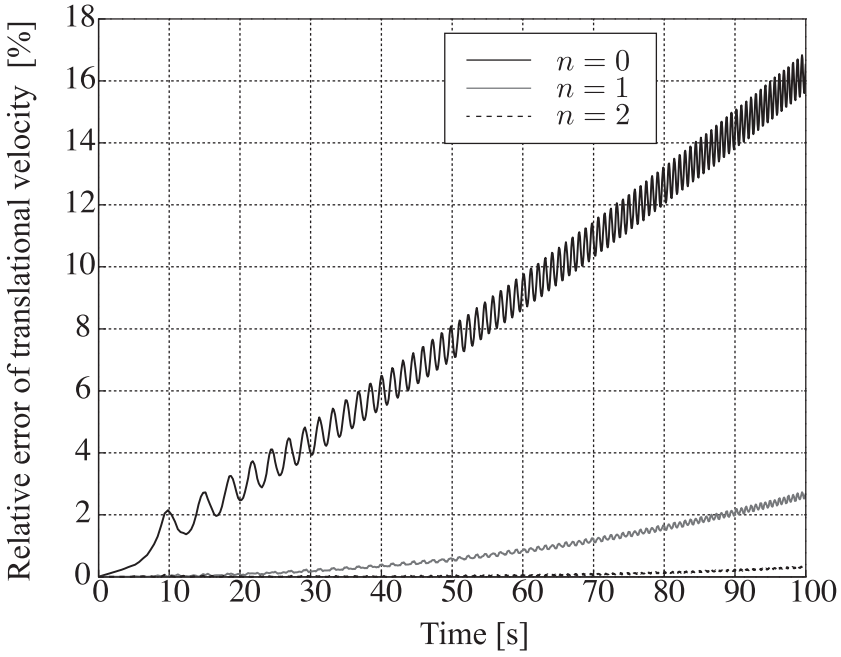

Figure 3.13: The relative error between the exact solution and the approximate solution.

Table 3.4: Satellite's parameters.

Mass m	Case1: 120.0 [kg]
	Case2: 200.0 [kg]
Moment of inertia J	100 [kgm^2]
Moment arm β	-0.5 [m]
Thruster force F, f_1, f_2	500.0, 20.0, 20.0 [N]
Fuel consumption rate c	0.16 [kg/s]

rewritten as

$$\begin{aligned}
&\frac{f\cos\alpha}{m_0 - ct}\cos\left(\frac{\beta f}{2J}t^2 + \dot{\psi}_0 t + \psi_0\right) \\
&\quad = \frac{f\cos\alpha}{m_0 - c\,(\tau - t_1)}\cos\left(-\frac{\pi}{2}A^2\tau^2 + B\right), \\
&\quad = \frac{f\cos\alpha}{m_0 - c\,(\tau - t_1)}\left(\cos\left(-\frac{\pi}{2}A^2\tau^2\right)\cos B - \sin\left(-\frac{\pi}{2}A^2\tau^2\right)\sin B\right), \\
&\quad = \frac{f\cos\alpha}{m_0 - c\,(\tau - t_1)}\left(\cos\left(\frac{\pi}{2}A^2\tau^2\right)\cos B + \sin\left(\frac{\pi}{2}A^2\tau^2\right)\sin B\right), \qquad (3.92)
\end{aligned}$$

where A is defined as shown in Eq. (3.85). The approximate solutions for $n = 1$

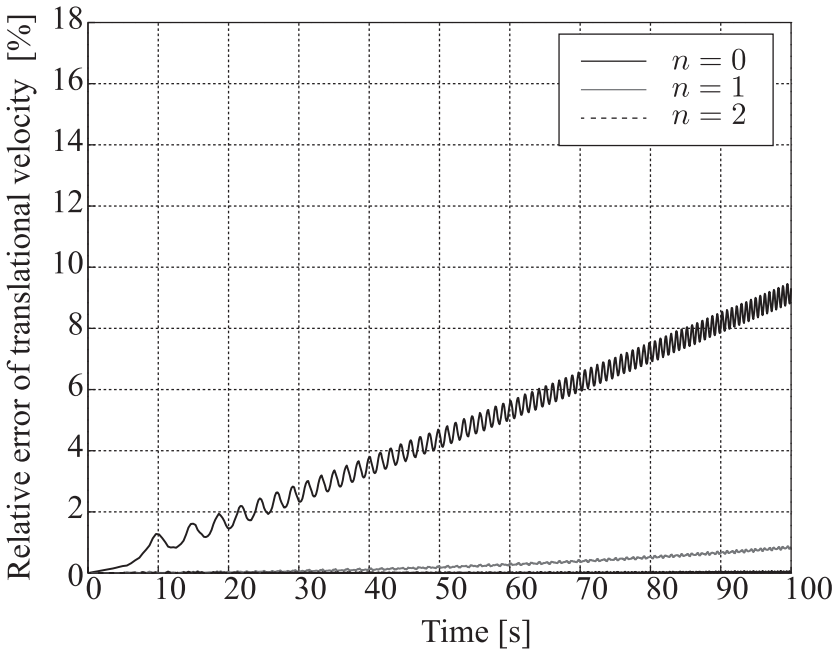

Figure 3.14: Case2: The relative error between the exact solution and the approximate solution.

are described as:

$$
\begin{aligned}
V_X = & \left[\frac{F}{m_0 - c\left(\tau - t_1\right)}\left(\cos B\frac{C\left(A\tau\right)}{A} + \sin B\frac{S\left(A\tau\right)}{A}\right)\right]_{t_1}^{t+t_1} \\
& - \left[\frac{cF}{\left(m_0 - c\left(\tau - t_1\right)\right)^2}\left(\cos B\int\frac{C\left(A\tau\right)}{A}d\tau + \sin B\int\frac{S\left(A\tau\right)}{A}d\tau\right)\right]_{t_1}^{t+t_1} \\
& - \left[\frac{f}{m_0 - c\left(\tau - t_1\right)}\left(-\cos B\frac{S\left(A\tau\right)}{A} + \sin B\frac{C\left(A\tau\right)}{A}\right)\right]_{t_1}^{t+t_1} \\
& + \left[\frac{cf}{\left(m_0 - c\left(\tau - t_1\right)\right)^2}\left(-\cos B\int\frac{S\left(A\tau\right)}{A}d\tau + \sin B\int\frac{C\left(A\tau\right)}{A}d\tau\right)\right]_{t_1}^{t+t_1} \\
& + V_{X0}, \qquad (3.93)
\end{aligned}
$$

$$
\begin{aligned}
V_Y = & \left[\frac{F}{m_0 - c\left(\tau - t_1\right)} \left(-\cos B \frac{S\left(A\tau\right)}{A} + \sin B \frac{C\left(A\tau\right)}{A} \right) \right]_{t_1}^{t+t_1} \\
& - \left[\frac{cF}{\left(m_0 - c\left(\tau - t_1\right)\right)^2} \left(-\cos B \int \frac{S\left(A\tau\right)}{A} d\tau + \sin B \int \frac{C\left(A\tau\right)}{A} d\tau \right) \right]_{t_1}^{t+t_1} \\
& - \left[\frac{f}{m_0 - c\left(\tau - t_1\right)} \left(\cos B \frac{C\left(A\tau\right)}{A} + \sin B \frac{S\left(A\tau\right)}{A} \right) \right]_{t_1}^{t+t_1} \\
& + \left[\frac{cf}{\left(m_0 - c\left(\tau - t_1\right)\right)^2} \left(\cos B \int \frac{C\left(A\tau\right)}{A} d\tau + \sin B \int \frac{S\left(A\tau\right)}{A} d\tau \right) \right]_{t_1}^{t+t_1} \\
& - gt + V_{Y0}. \qquad (3.94)
\end{aligned}
$$

3.7.4 Control Procedure

As a simple example, we consider a control maneuver consists of three steps illustrated in Fig. 3.15. First, the satellite is decelerated by the main thruster until the translational velocity becomes to a specified one (Step 1). The satellite then drifts to the position to start the attitude control maneuver (Step 2), and finally the attitude angle and the translational velocity are simultaneously controlled to the target state (Step 3).

The velocity and position time-profiles to drive the satellite to the target state can be calculated in advance using the derived approximate solution through the following procedure. Since the velocity change in Step 2 is zero, the final zero-translational velocity can be achieved in the following condition.

$$
V_{X0} + \Delta V_{X1} + \Delta V_{X3} = 0, \qquad (3.95)
$$

where ΔV_{X1} and ΔV_{X3} mean the velocity changes in Step 1 and Step 3, respectively. For simplicity, we assume that the satellite's attitude keeps an attitude angle ψ in Step 1. Thus, the analytic solutions for Step 1 are written as

$$
\begin{aligned}
\Delta V_{X1} &= \frac{F\cos\psi}{c} \log\left(m_0 - c\Delta t_1\right) - \frac{F\cos\psi}{c} \log m_0 + V_{X0}, \qquad (3.96) \\
m_0 - c\Delta t_1 &= m_0', \qquad (3.97)
\end{aligned}
$$

where m_0' denotes the satellite mass at the end of Step 1.

In Step 3, we consider a time-profile based on a bang-bang type thruster input for the attitude control. Thus, the input time is uniquely determined and is written as follows.

$$
\Delta t_3 = \sqrt{\frac{J(\psi_0 - \psi_t)}{-\beta f}}, \qquad (3.98)
$$

where ψ_0 and ψ_t denote the initial and target attitude angle in Step 3. The velocity change in Step 3 only depends on the initial angle in Step 3 and the target angle, and is shown as

$$\begin{aligned}\Delta V_{X3} = &\frac{F}{m_0' - c\Delta t_3}\left(\cos\psi_0\frac{C(A\Delta t_3)}{A} + \sin\psi_0\frac{S(A\Delta t_3)}{A}\right) + \frac{Fc}{\pi {m_0'}^2 A^2} \\ &-\frac{f}{m_0' - c\Delta t_3}\left(-\cos\psi_0\frac{S(A\Delta t_3)}{A} + \sin\psi_0\frac{C(A\Delta t_3)}{A}\right) + \frac{fc}{\pi {m_0'}^2 A^2} \\ &+\frac{F}{m_0' - c\Delta t_3}\left(\cos\psi_t\frac{C(A\Delta t_3)}{A} - \sin\psi_t\frac{S(A\Delta t_3)}{A}\right) + \frac{Fc\sin\phi_t}{\pi A^2(m_0' - 2c\Delta t_3)^2} \\ &+\frac{f}{(m_0' - c\Delta t_3)}\left(\cos\psi_t\frac{S(A\Delta t_3)}{A} + \sin\psi_t\frac{C(A\Delta t_3)}{A}\right) - \frac{fc\cos\psi_t}{\pi A^2(m_0' - 2c\Delta t_3)^2}.\end{aligned} \tag{3.99}$$

Therefore using Eqs. (3.96), (3.97), (3.98), (3.99), we can obtain the input time in Step 1 which satisfies the condition shown in Eq. (3.95).

The satellite position is also controlled by using the drift motion in Step 2. Using the approximate solution derived above, we can calculate the position change of the maneuver in Step 3. That is, the start position for Step 3 is specified and such maneuver can drive the satellite to the target position.

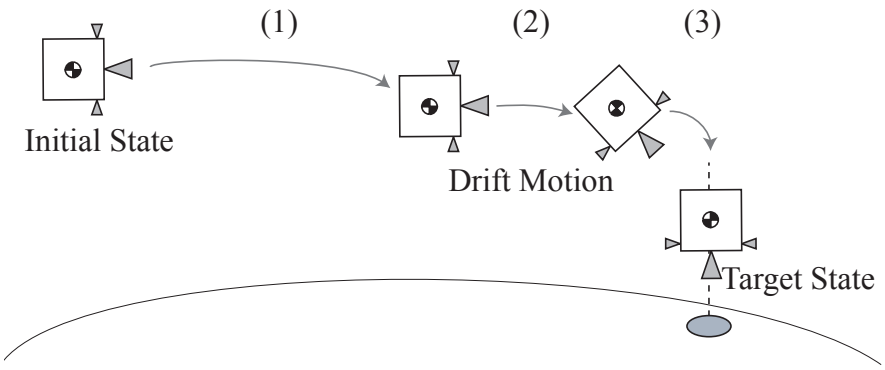

Figure 3.15: Control procedure for lunar landing mission.

3.7.5 Simulation Results

This section shows the simulation results of the control procedure for the lunar landing. The initial condition of the numerical simulation is summarized in Table 3.5. For simplicity, the moon's gravity acceleration is assumed to act in the Y direction, and the vertical region above the target position is set to be free.

Figure 3.16 shows the time history of the translational velocity along X-axis calculated by using the approximate solution for $n = 1$. The figure means that the satellite's horizontal velocity is successfully controlled to zero. The satellite's position is simultaneously controlled to the region above the target position as shown in Fig. 3.17. In the control maneuver the control thrusts described in Fig. 3.18 are applied. Figures 3.19 and 3.20 depict the time histories of the satellite's attitude and the angular rate, and they show the satellite's state is controlled to the target state.

Table 3.5: Initial condition.

Position X_0, Y_0	-388.0, 15.0[km]
Velocity V_{X0}, V_{Y0}	1500.0, 0.0[m/s]
Attitude angle ϕ_0	180.0 [deg]
Angular rate $\dot{\phi}_0$	0.0 [deg/s]
Mass m_0	200.0 [kg]

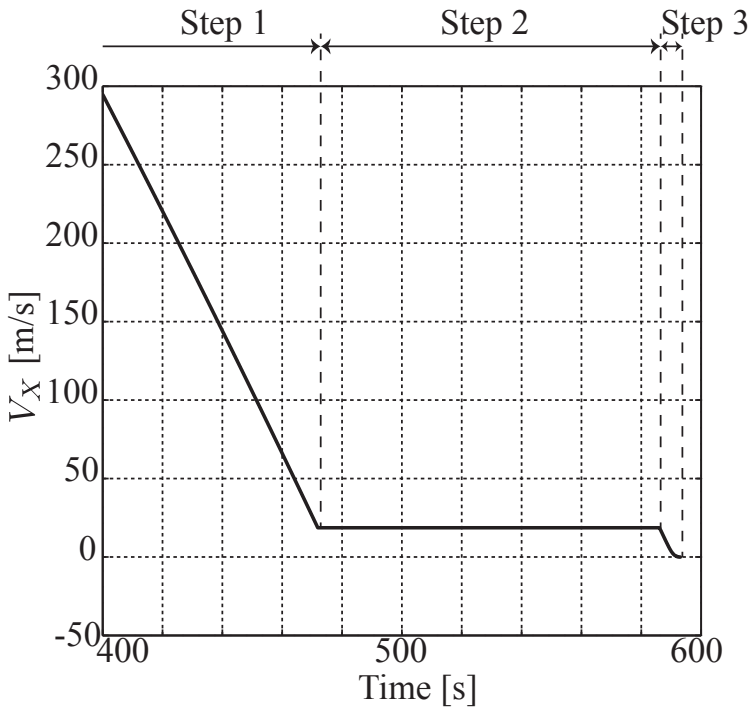

Figure 3.16: The time history of translational velocity.

Figures for the case $n = 0$ are omitted since the time-profiles are almost same as those for $n = 1$. Although applying the approximate solution for $n = 0$ can drive

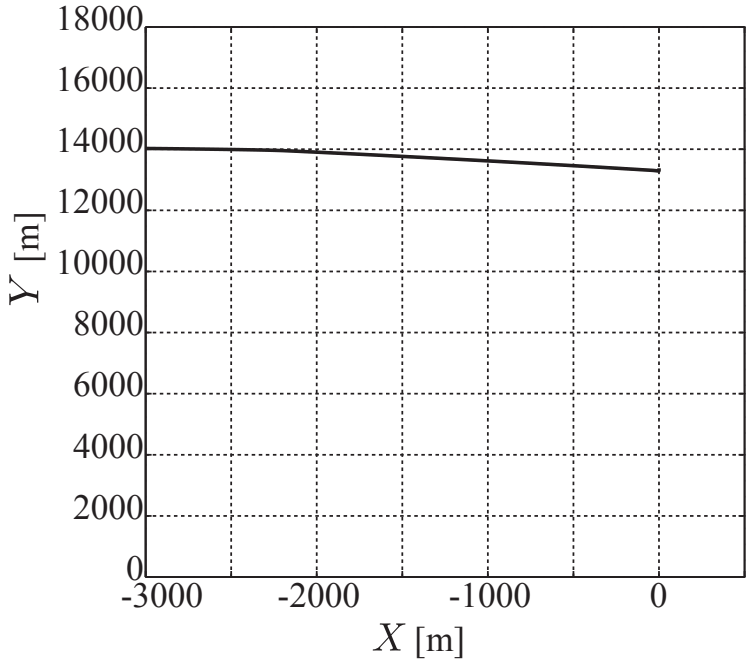

Figure 3.17: The time history of the satellite's position.

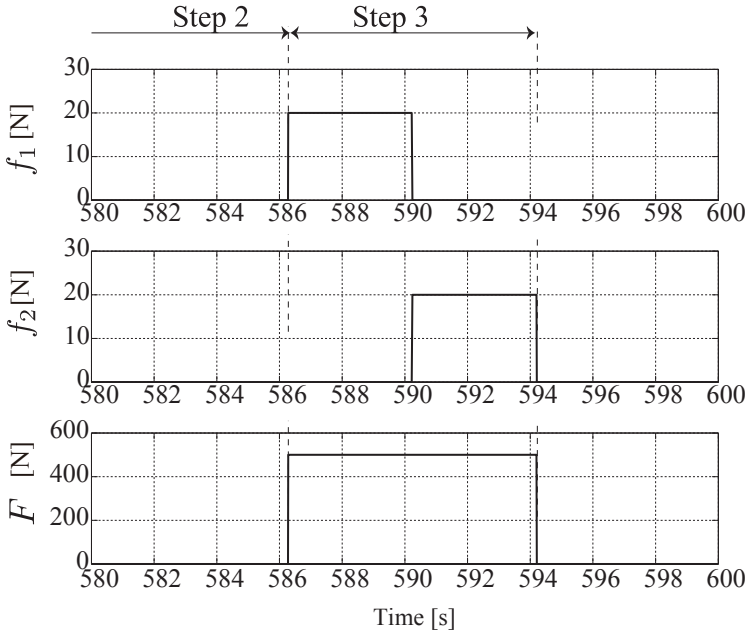

Figure 3.18: The time histories of the control thrusts.

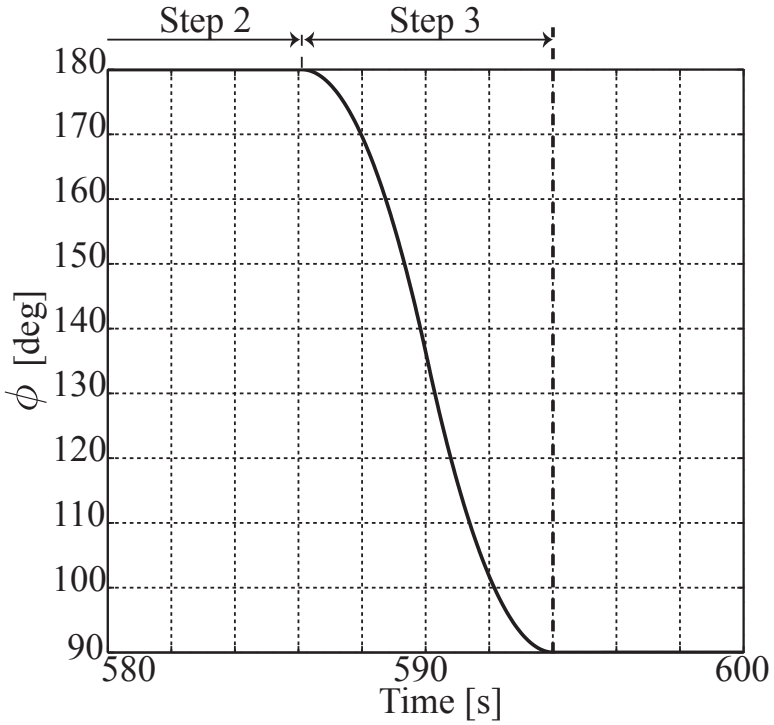

Figure 3.19: The time history of the satellite's attitude angle.

the satellite to the proximity target state, its error is larger than that of $n = 1$ as summarized in Table 3.6. Because the attitude control maneuver is conducted only once and the input time is calculated $\Delta t_3 = 3.96$[s] in this simulation, as shown in Figure 3.14, the error is quite small even when we use the approximate solution of $n = 0$. In other words, for the case when many attitude control maneuvers are conducted, larger error is expected for the approximation of $n = 0$, and thus high order approximation should be applied.

Table 3.6: Simulation Results.

Degree of Fresnel integrals	Translational velocity V_X	Position X
$n = 0$	0.04 [m/s]	1.0 [m]
$n = 1$	0.01 [m/s]	0.3 [m]

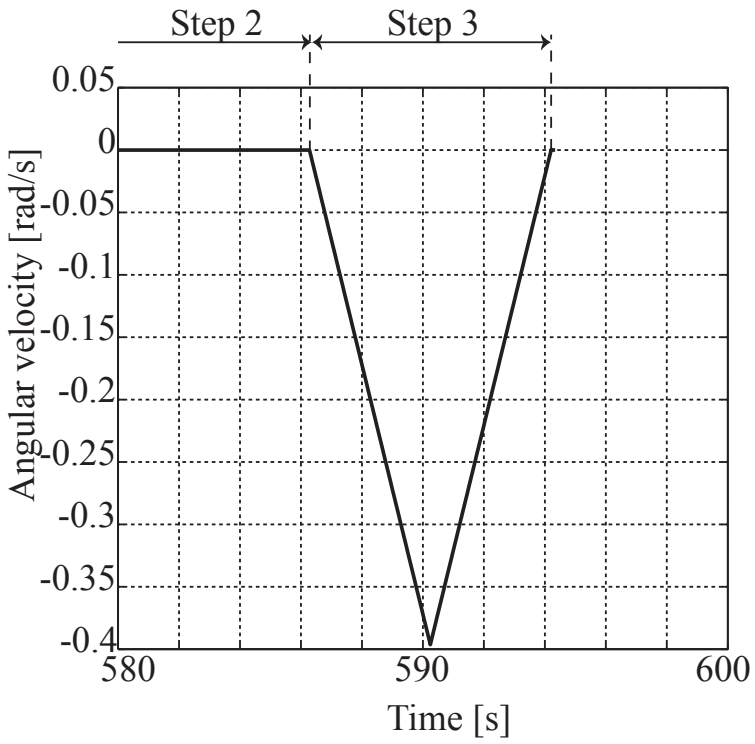

Figure 3.20: The time history of the angular velocity.

3.8 Summary of Chapter 3

This chapter has dealt with a position and attitude control of an underactuated satellite with a small number of on-off thrusters. Using the wz-parameters to represent the satellite attitude, we have shown the attitude control procedure in three maneuvers. In each maneuver, the translational motion has been controlled simultaneously, and the proper input timings and durations have been obtained with analytical solutions. Furthermore, the proposed control technique has been applied to a practical case for a lunar landing mission. For the powered descending phase of the mission, a satellite's mass change due to fuel consumption has been considered using the partial integration of Fresnel integrals. This method has enabled us to approximate the translational motion of the satellite with high accuracy. Numerical simulation results have demonstrated the effectiveness of the proposed control procedures for both the three-dimensional satellite and the lunar lander.

Chapter 4

Position and Attitude Control in Formation Flying

Chapter 4 discusses a relative position and attitude control of a satellite in formation flying. A translational motion of a follower satellite is affected with the orbital motion of a leader satellite, and thus notably differs from the one discussed in the previous chapter. Rendezvous and formation reconfiguration problems are typical control methods required for formation flying missions and have been discussed in many studies in order to minimize the fuel or energy consumption. These works, however, consider accelerations as control inputs, that is an attitude control of a satellite has not been explicitly discussed in the formation flying maneuvers. This chapter therefore deals with both a rendezvous and a reconfiguration problem explicitly considering the attitude dynamics of a satellite. In section 4.1, a fuel-efficient rendezvous approach in a circular orbit using constant thrusts is derived. The control method effectively uses a drift motion for the energy efficiency, and furthermore modal analysis analytically shows the necessary accelerations for two cases of input directions: 1) along-track thrusts, 2) radial directional thrusts. In section 4.2, an optimal reconfiguration method is shown under attitude constraints with respect to an inertial frame. To control both translational and rotational motion, a tracking method for a reference input trajectory is firstly obtained based on Lyapunov stability. The tracking method reduces the reconfiguration problem under the attitude constraints to the one under thrust directional constraints, and thus the reference input is designed to satisfy an optimal condition and the constraints on the inputs.

4.1 Fuel-Efficient Rendezvous Maneuver

This section deals with an orbital control of a follower satellite relative to a target satellite in a circular orbit under a constraint of a few thrusters. The thrusters

of the follower are fixed to its body and generate constant magnitude of forces in unilateral directions. To generate control forces in required directions, the follower attitude is also controlled using the thruster forces alone. Furthermore, the attitude control of the follower is necessary to estimate the relative position of the follower satellite from the time profile of line-of-sight (LOS). First, the controllability with constant inputs in unilateral direction is examined based on modal analysis. Then, the energy efficiency of the controllers is discussed according to the directions of control forces. Finally, some numerical simulations show the verification of the controller and compare the energy efficiency.

4.1.1 Equations of Motion

HIll's equation

The equations of motion for formation flying in a circular orbit have been studied based on the linearized equations, called the Hill's equation or Clohessy-Wiltshire equation [24]. The Hill's equation describes a relative motion of a follower satellite in a leader-fixed coordinate. In the leader-fixed frame, x-axis lies in the radial direction from the Earth, z-axis is in the direction of the orbital momentum vector of the leader, and y-axis completes a right-handed coordinate (Fig. 4.1). The equation of motion of the follower satellite is written as [52]

$$\ddot{\boldsymbol{R}} = -\frac{\mu}{((R_0+x)^2+y^2+z^2)^{\frac{3}{2}}}(\boldsymbol{R}_0+\boldsymbol{x}_{\rm pos})+\boldsymbol{u}, \tag{4.1}$$

where $\boldsymbol{x}_{\rm pos} := \left[\begin{array}{ccc} x & y & z \end{array}\right]^T$, $\boldsymbol{R}(=\boldsymbol{R}_0+\boldsymbol{x}_{\rm pos})$, $\boldsymbol{R}_0$, μ, and $\boldsymbol{u}$ are a position vector of the follower, an orbital radius of the follower, an orbital radius of the leader, the gravitational constant of the Earth, and external accelerations, respectively. Assuming that the orbital radius of the leader satellite is much larger than the distance between the leader and follower, we obtain linearized equations as

In-plane motion

$$\begin{aligned} \frac{\mathrm{d}}{\mathrm{d}t}\left[\begin{array}{c} x \\ y \\ \dot{x} \\ \dot{y} \end{array}\right] &= \left[\begin{array}{cccc} 0 & 0 & 1 & 0 \\ 0 & 0 & 0 & 1 \\ 3\Omega^2 & 0 & 0 & 2\Omega \\ 0 & 0 & -2\Omega & 0 \end{array}\right]\left[\begin{array}{c} x \\ y \\ \dot{x} \\ \dot{y} \end{array}\right] + \left[\begin{array}{cc} 0 & 0 \\ 0 & 0 \\ 1 & 0 \\ 0 & 1 \end{array}\right]\left[\begin{array}{c} u_x \\ u_y \end{array}\right] \\ &\Rightarrow \dot{\boldsymbol{x}} = A\boldsymbol{x}+B\boldsymbol{u}_{xy}. \end{aligned} \tag{4.2}$$

Out-of-plane motion

$$\frac{d}{dt}\left[\begin{array}{c} z \\ \dot{z} \end{array}\right] = \left[\begin{array}{cc} 0 & 1 \\ -\Omega^2 & 0 \end{array}\right]\left[\begin{array}{c} z \\ \dot{z} \end{array}\right] + \left[\begin{array}{c} 0 \\ u_z \end{array}\right], \tag{4.3}$$

where Ω is an orbital rate of the leader satellite and $\boldsymbol{x} := [x, y, \dot{x}, \dot{y}]^T$. These equations indicate the decoupling between the in-plane and out-of-plane motion of the follower satellite. Thus this chapter discusses the in-plane motion control in the following sections, because the out-of-plane motion is simple harmonic and the control procedure is shown in the previous study [53].

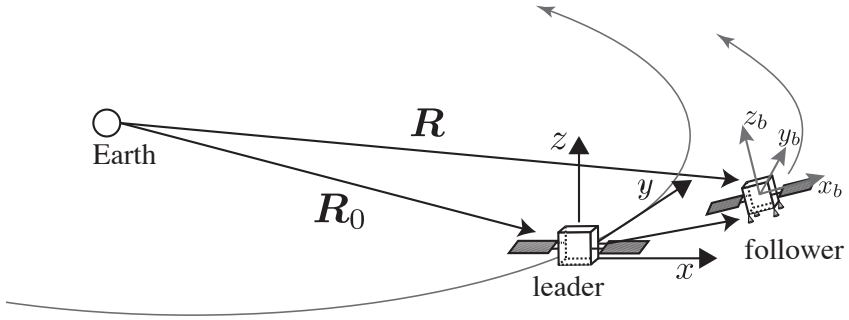

Figure 4.1: Coordinate systems in formation flying.

The analytical solutions of the Hill's equation with no external forces are obtained as follows [52]:

$$\boldsymbol{x}(t) = \begin{bmatrix} 4-3c & 0 & s/\Omega & 2(1-c)/\Omega \\ 6(s-\Omega t) & 1 & -2(1-c)/\Omega & 4s/\Omega - 3t \\ 3\Omega s & 0 & c & 2s \\ -6\Omega(1-c) & 0 & -2s & -3+4c \end{bmatrix} \boldsymbol{x}_0, \tag{4.4}$$

where the subscript "0" denotes initial states and $c := \cos\Omega t$, $s := \sin\Omega t$. The equations are further simplified as

$$\begin{aligned} x(t) &= a\cos(\Omega t + \Phi) + 2b, && (4.5)\\ y(t) &= -2a\sin(\Omega t + \Phi) - 3bt + d, && (4.6)\\ \dot{x}(t) &= -\Omega a\sin(\Omega t + \Phi), && (4.7)\\ \dot{y}(t) &= -2\Omega a\cos(\Omega t + \Phi) - 3b, && (4.8) \end{aligned}$$

where

$$\begin{aligned} a &:= \sqrt{(3x_0 + 2\dot{y}_0/\Omega)^2 + (\dot{x}_0/\Omega)^2}, && (4.9)\\ b &:= 2\Omega x_0 + \dot{y}_0, && (4.10)\\ d &:= y_0 - 2\dot{x}_0/\Omega, && (4.11)\\ \Phi &:= \arctan\left(\frac{\dot{x}_0}{\Omega(3x_0 + 2\dot{y}_0/\Omega)}\right). && (4.12) \end{aligned}$$

The parameters, a, b, d, and Φ denote the size of the relative orbit, a drift velocity, the distance of the center of the ellipse from the leader satellite, and an initial phase, respectively. Since the position of the follower satellite is written as

$$\left(\frac{x-2b}{a}\right)^2+\left(\frac{y+3bt-d}{2a}\right)^2=1, \tag{4.13}$$

the relative motion becomes an elliptic orbit when $b=0$ and furthermore, the leader-centered ellipse when $b=d=0$.

Rotational equation

The rotational equations of motion of the follower satellite with respect to the leader-fixed frame are written as follows.

$$J\dot{\boldsymbol{\omega}}+\tilde{\boldsymbol{\omega}}J\boldsymbol{\omega}=T, \tag{4.14}$$

where $\tilde{*}$ is a skew-symmetric matrix, that is

$$\tilde{\boldsymbol{\omega}}=\begin{bmatrix}0 & -\omega_z & \omega_y\\ \omega_z & 0 & -\omega_x\\ -\omega_y & \omega_x & 0\end{bmatrix}. \tag{4.15}$$

The attitude kinematics in terms of ZYX Euler angles are written as

$$\begin{bmatrix}\dot{\phi}\\ \dot{\theta}\\ \dot{\psi}\end{bmatrix}=\sec\theta\begin{bmatrix}\cos\theta & \sin\phi\sin\theta & \cos\phi\sin\theta\\ 0 & \cos\phi\cos\theta & -\sin\phi\cos\theta\\ 0 & \sin\phi & \cos\phi\end{bmatrix}\begin{bmatrix}\omega_x\\ \omega_y\\ \omega_z\end{bmatrix}-\begin{bmatrix}0\\ 0\\ \Omega\end{bmatrix} \tag{4.16}$$

The orbital rate Ω appears in the last term of the right-hand side in Eq. (4.16) due to the rotating frame.

Thruster configuration

Despite the result in Chapter 2, the minimum thruster configuration to control a satellite position and attitude with constant thrusts has not been specified because the constraint on the magnitudes of thruster forces makes the mathematical discussion hard. However, the previous works [53,54] and the controller in Chapter 3 show that the satellite position and attitude can be controlled with four thrusters placed to be parallel with respect to a principal axis of the satellite. Thus, this chapter also assumes the follower satellite equips four thrusters parallel along x_b-axis as shown in Fig. 4.2. The thrusters generate the same magnitudes of constant forces and have the same length of a moment arm about y_b- and z_b-axes.

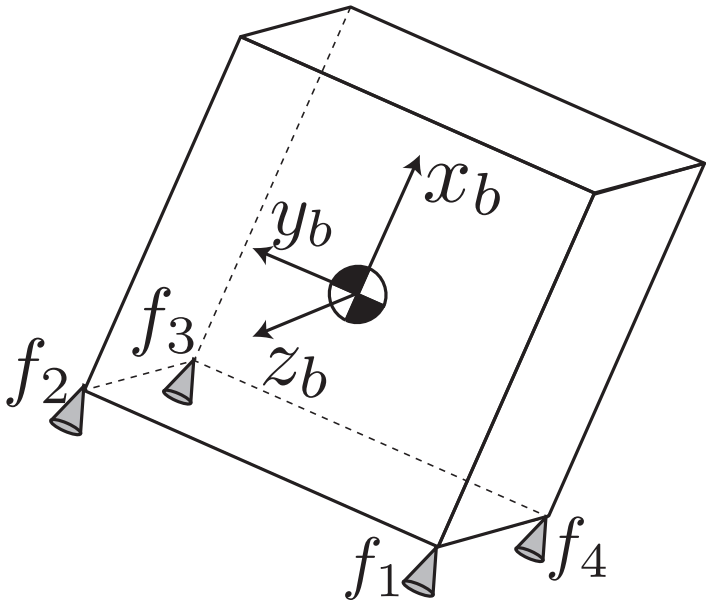

Figure 4.2: Thruster configuration.

The control thrusts generate both translational and rotational motion of the follower and is written in the leader-fixed frame as

$$\boldsymbol{u} = \frac{1}{m} R_{ib} \boldsymbol{F}_b, \tag{4.17}$$

where

$$R_{ib} = \begin{bmatrix} \cos\psi\cos\theta & -\sin\psi\cos\phi + \cos\psi\sin\theta\sin\phi & \sin\psi\sin\phi + \cos\psi\sin\theta\cos\phi \\ \sin\psi\cos\theta & \cos\psi\cos\phi + \sin\psi\sin\theta\sin\phi & -\cos\psi\sin\phi + \sin\psi\sin\theta\cos\phi \\ -\sin\theta & \cos\theta\sin\phi & \cos\theta\cos\phi \end{bmatrix}, \tag{4.18}$$

$$\boldsymbol{F}_b = \begin{bmatrix} f_1 + f_2 + f_3 + f_4 & 0 & 0 \end{bmatrix}^T. \tag{4.19}$$

The control torques generated by the thrusters are described as

$$\boldsymbol{T} = \begin{bmatrix} 0 & a_{\text{arm}}(f_1 + f_2 - f_3 - f_4) & a_{\text{arm}}(f_1 + f_4 - f_2 - f_3) \end{bmatrix}^T, \tag{4.20}$$

where a_{arm} is the moment arm of the thrusters.

4.1.2 Modal Analysis

Modal variables

The system matrix, A, for the in-plane motion of the Hill's equation has three eigenvectors and eigenvalues although the order of A is four, and thus is defective. The eigenvectors and eigenvalues are obtained as

$$\begin{bmatrix} \boldsymbol{e}_1 & \boldsymbol{e}_3 & \boldsymbol{e}_4 \end{bmatrix} = \begin{bmatrix} 0 & -1/(2\Omega) & -1/(2\Omega) \\ 1 & i/\Omega & -i/\Omega \\ 0 & i/2 & -i/2 \\ 0 & 1 & 1 \end{bmatrix}, \tag{4.21}$$

$$\lambda_1 = 0, \tag{4.22}$$

$$\lambda_3 = -i\Omega, \tag{4.23}$$

$$\lambda_4 = i\Omega, \tag{4.24}$$

where i is an imaginary number. The following calculations form two real eigenvectors.

$$\begin{aligned} \boldsymbol{e}_3' &= \Omega(\boldsymbol{e}_3 - \boldsymbol{e}_4)/i \\ &= \begin{bmatrix} 0 & 2 & \Omega & 0 \end{bmatrix}^T, \end{aligned} \tag{4.25}$$

$$\begin{aligned} \boldsymbol{e}_4' &= \Omega(\boldsymbol{e}_3 + \boldsymbol{e}_4) \\ &= \begin{bmatrix} -1 & 0 & 0 & 2\Omega \end{bmatrix}^T. \end{aligned} \tag{4.26}$$

A generalized eigenvector $\boldsymbol{e}_2$ is obtained as follows.

$$\begin{aligned} &(A - \lambda_1 I)\boldsymbol{e}_2 = \boldsymbol{e}_1 \\ &\Rightarrow \boldsymbol{e}_2 = \begin{bmatrix} -2/(3\Omega) & \alpha & 0 & 1 \end{bmatrix}^T, \end{aligned} \tag{4.27}$$

where α is an arbitrary value and henceforth the case when $\alpha = 0$ is considered for the sake of simplicity.

The variable transformation using the eigenvectors simplifies the interpretation of relative orbit control [55]. Here, modal variables are defined as

$$\begin{aligned} \boldsymbol{\xi} &= \begin{bmatrix} \xi_1 & \xi_2 & \xi_3 & \xi_4 \end{bmatrix}^T \\ &:= P\boldsymbol{x}, \end{aligned} \tag{4.28}$$

where

$$\begin{aligned} P &:= E^{-1} \\ &= \begin{bmatrix} \boldsymbol{e}_1 & \boldsymbol{e}_2 & \boldsymbol{e}_3' & \boldsymbol{e}_4' \end{bmatrix}^{-1}. \end{aligned} \tag{4.29}$$

The components of the modal variables are written as:

$$\begin{aligned}
\xi_1 &= y - 2\dot{x}/\Omega, && (4.30)\\
\xi_2 &= -3(2\Omega x + \dot{y}), && (4.31)\\
\xi_3 &= \dot{x}/\Omega, && (4.32)\\
\xi_4 &= 3x + 2\dot{y}/\Omega. && (4.33)
\end{aligned}$$

The modal variables ξ_1 and ξ_2 mean the distance between the leader and the center of the relative elliptic orbit and the drift velocity, respectively, whereas, ξ_3 and ξ_4 denote oscillatory mode. In fact, the initial values of ξ_1 and ξ_2 are equivalent to the parameters d and $-3b$ defined in Eqs.(4.11) and (4.10). The Euclidean norm of ξ_3 and ξ_4 has the same form as the parameter a shown in Eq. (4.9). The differential equations of the modal variables are described as follows:

$$\begin{aligned}
&\dot{\boldsymbol{\xi}} = PAP^{-1}\boldsymbol{\xi} + PB\boldsymbol{u}\\
&\Rightarrow \dot{\boldsymbol{\xi}} = \begin{bmatrix} 0 & 1 & 0 & 0 \\ 0 & 0 & 0 & 0 \\ 0 & 0 & 0 & \Omega \\ 0 & 0 & -\Omega & 0 \end{bmatrix} \boldsymbol{\xi} + \begin{bmatrix} -2/\Omega & 0 \\ 0 & -3 \\ 1/\Omega & 0 \\ 0 & 2/\Omega \end{bmatrix} \boldsymbol{u}, \qquad (4.34)
\end{aligned}$$

or equivalently,

$$\begin{aligned}
\dot{\xi}_1 &= \xi_2 - 2u_x/\Omega, && (4.35)\\
\dot{\xi}_2 &= -3u_y, && (4.36)\\
\dot{\xi}_3 &= \Omega\xi_4 + u_x/\Omega, && (4.37)\\
\dot{\xi}_4 &= -\Omega\xi_3 + 2u_y/\Omega. && (4.38)
\end{aligned}$$

Controllability and Energy Efficiency

The state equations of the modal variables are useful to consider the controllability and the energy efficiency even when control inputs are constrained to be constant in one direction. Moreover, only positive control forces are assumed in this section because the control thrusts are applied with a few number of thrusters. Thus, the controllability and the fuel consumption in terms of the modal variables are considered for two cases of input directions: 1) positive along-track thrusts and 2) positive radial thrusts.

Firstly, the controllability and the energy efficiency with positive along-track thrusts, i.e. $\boldsymbol{u} = [0 \quad u_y]^T$ $(u_y \geq 0)$, are examined. The modal equations show that a positive along-track input can control all modal variables to zero only when initial states satisfy some conditions. Equation (4.36) indicates the initial value of ξ_2 must be positive because it monotonically decreases with positive acceleration. Equation (4.35) then means the time derivative of ξ_1 becomes positive, and thus

the initial value of ξ_1, i.e. $\xi_{1,0}$, should be negative. On the other hand, there are no restrictions for the initial states of ξ_3 and ξ_4 because of their oscillatory motion. Thus the necessary acceleration to steer all variables to zero is uniquely determined by the initial value of ξ_2. Equation (4.36) is integrated and the analytic solution provides the minimum necessary acceleration as

$$u_{yd} = u_y \Delta t = -(\xi_2 - \xi_{2,0})/3, \tag{4.39}$$

where Δt is an input time.

Secondly, the relative motion control with positive radial thrusts is considered. For a single input $u_x(\geq 0)$, Eq. (4.36) shows the variable ξ_2 is uncontrollable, whereas the other modal variables can be controlled. The drift velocity ξ_2 thus must be controlled beforehand to a target state. The fuel consumption is uniquely determined according to the initial value of ξ_1 for the positive input. The analytical solution of Eq. (4.35) descrbies the required acceleration as

$$u_{xd} = -\Omega(\xi_1 - \xi_{1,0})/2 + n\xi_{2,0}\Delta t/2. \tag{4.40}$$

The relative orbit control with along-track thrusts is therefore more energy efficient than that with radial thrusts, because the necessary acceleration in the along-track direction is only u_{yd}. On the other hand, the relative motion control with radial thrusts requires not only u_{xd}, but also u_{yd} in total due to the uncontrollability of ξ_2. Thus, the following discussion extends the control method shown in [53] by using a drift velocity generated with along-track thrusts, and compares the fuel consumptions.

4.1.3 Conrol Method

This subsection firstly derives analytical solutions of translational and rotational motion of a satellite in x-y plane. The analytical solutions provide input timings which drive the satellite to a target state. Based on the analytic solutions, two control procedures are shown to compare the energy efficiency.

Analytical solution of modal variables

The satellite angular velocity monotonically increases or decreases because of constant inputs, and this section uses the angular rate as an independent variable instead of time. The time derivative of an arbitrary parameter β, for instance, is transformed as follows.

$$\begin{aligned} \dot{\beta} &= \frac{\mathrm{d}\beta}{\mathrm{d}t} \\ &= \frac{\mathrm{d}\beta}{\mathrm{d}\omega_z}\frac{\mathrm{d}\omega_z}{\mathrm{d}t} \\ \Rightarrow \beta' &= \gamma\dot{\beta}, \end{aligned} \tag{4.41}$$

where the prime denotes the derivative with respect to the angular rate and $\gamma := J_z/T_z$. The analytical solution for the attitude angle is obtained as

$$\begin{aligned} \psi' &= \gamma(\omega_z - \Omega) \\ &\Rightarrow \quad \psi = \frac{\gamma}{2}(\omega_z^2 - \omega_{z0}^2) - \gamma\Omega(\omega_z - \omega_{z0}) + \psi_0. \end{aligned} \tag{4.42}$$

This analytical solution includes no terms of time due to the integration along the angular velocity.

The analytical solutions of the modal equations are also obtained with integrations along the angular rate. The equation of the variable ξ_2, for instance, is rewritten as:

$$\begin{aligned} \dot{\xi}_2 &= -3u \\ &= -3F_b \sin\psi \\ \Rightarrow \xi_2' &= -3\gamma F_b \sin\psi \\ &= -3\gamma F_b \sin\left[\frac{\gamma}{2}(\omega_z^2 - \omega_{z0}^2) - \gamma\Omega(\omega_z - \omega_{z0}) + \psi_0\right] \\ &= -3\gamma F_b \sin\left[\frac{\gamma}{2}\omega_z^2 - \gamma\Omega\omega_z + \zeta_0\right], \end{aligned} \tag{4.43}$$

where

$$\zeta_0 = -\frac{\gamma}{2}\omega_{z0}^2 + \gamma\Omega\omega_{z0} + \psi_0. \tag{4.44}$$

In a similar way to Chapter 3, the analytic solution of Eq. (4.43) can be obtained with Fresnel integrals, although it cannot be integrated with fundamental functions. Using the Fresnel integrals, we derive the analytic solution as:

$$\begin{aligned} \xi_2 = &-3\frac{F_b}{m}\sqrt{\pi\gamma}\cos\chi\left[S\left(\sqrt{\frac{\gamma}{\pi}}(\omega_z - \Omega)\right) - S\left(\sqrt{\frac{\gamma}{\pi}}(\omega_{z0} - \Omega)\right)\right] \\ &- 3\frac{F_b}{m}\sqrt{\pi\gamma}\sin\chi\left[C\left(\sqrt{\frac{\gamma}{\pi}}(\omega_z - \Omega)\right) - C\left(\sqrt{\frac{\gamma}{\pi}}(\omega_{z0} - \Omega)\right)\right], \end{aligned} \tag{4.45}$$

where

$$\xi := \zeta_0 - \frac{\gamma}{2}\Omega^2. \tag{4.46}$$

The analytic solutions for the other modal variables can be obtained in the same way.

Rendezvous Maneuver

The relative motion control shown in the paper [53] is reviewed using the modal variables. In the paper, the satellite attitude is controlled so that the thrusters are

aligned to the radial direction, and then the orbit is changed without an attitude change. As discussed in the above subsection, the radial directional inputs can drive the follower to the leader only when $\xi_{2,0} = 0$. Thus the control maneuver to vanish a drift velocity is required, i.e. $\xi_2 \to 0$, in advance. After the maneuver, the orbital motion of the follower becomes elliptical orbit and the thruster direction is oriented to the radial direction as shown in Fig. 4.3.

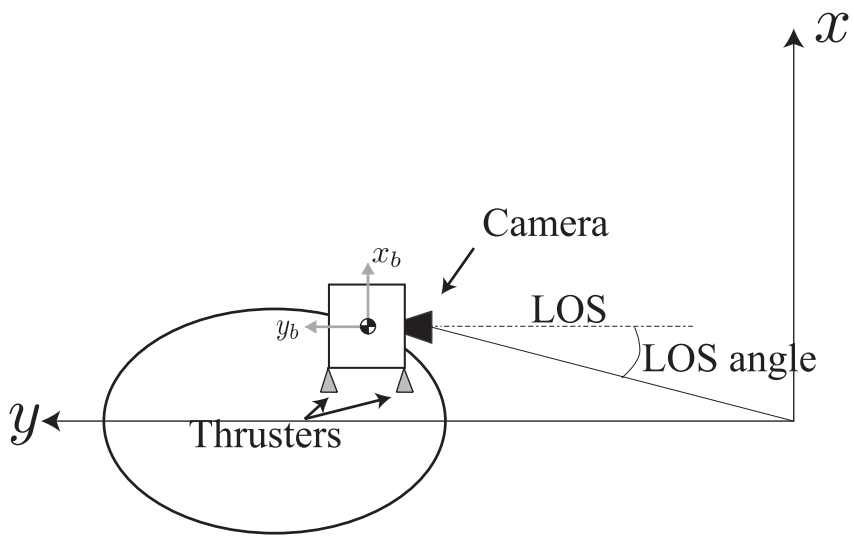

Figure 4.3: Initial relative orbit

When $\xi_{2,0} = 0$ and no along-track inputs are applied, Eqs. (4.35) and (4.36) indicate that a positive radial thrust monotonically decreases ξ_1 , and the distance from the leader can be controlled to zero. Also, to control ξ_3 and ξ_4, introduce a Lyapunov function candidate described as

$$L = \frac{1}{2}(\xi_3^2 + \xi_4^2). \tag{4.47}$$

The time derivative of Eq. (4.47) is written as follows.

$$\dot{L} = \xi_3 \frac{u_x}{\Omega}. \tag{4.48}$$

Thus the radial directional thrusts $u_x(\geq 0)$ applied when $\xi_3 < 0$ make the time derivative of the Lyapunov function negative, and consequently drive the variables ξ_3 and ξ_4 to zero. Note that the maximum LOS angle varies as the parameters L and ξ_1 decrease. The control inputs are thus applied so that the center of the relative orbit gradually approach the origin and the LOS angle keep a smaller angle than the field-of-view of the camera.

The control procedure with radial thrusts is improved by using a drift motion. As shown in the previous subsection, the control input along track direction is more fuel-efficient than the one in radial direction to control the relative motion of follower. The difference of the energy efficiency is due to the drift velocity. Since the drift motion steers the follower to the leader with no external forces, the less energy is required for the rendezvous.

The control procedure using the drift velocity consists of the following steps: (also see Fig. 4.4)

1. Attitude control and a drift velocity generation.
2. Attitude control to track the leader satellite.
3. Attenuation of the drift velocity.
4. Final maneuver without the attitude change.

In the first step, the follower changes the attitude and generates a drift velocity. For example, a negative drift velocity approaching the leader is necessary for the initial state shown in Fig. 4.3. The drift velocity is generated with positive along-track acceleration as described in Eq. (4.36) and is analytically calculated with Eq. (4.45). Then, the follower attitude is controlled to track the leader with a camera. After the approach with the drift motion, the drift velocity can be attenuated also using the analytical solution shown in Eq. (4.45). Finally, the follower satellite approaches the target satellite without attitude change.

4.1.4 Numerical Simulation

Numerical simulation results demonstrate the effectiveness of the proposed control method and the comparison of the fuel consumptions. The simulation parameters and initial condition are summarized in Table 4.1 and 4.2, respectively. The field-of-view of the camera and the orbital rate are assumed to be ± 45.0[deg] and 0.001[rad/s], equivalently $|\boldsymbol{R}_0| = 7359.5$[km].

Figures 4.5 and 4.6 show the time histories of the follower position and the LOS angle for the maneuver with radial thrusts. These figures describe the follower satellite approaches the leader satellite keeping the LOS within the field of view of the camera. In total, the thrusters are fired 62.5[s] as shown in Fig. 4.7 and the energy consumption in this maneuver, $(f_1 + f_2 + f_3 + f_4)\Delta t/m$, is equal to $-\Omega(\xi_{1d} - \xi_{1,0})/2 = 5.0$[m/s].

Figure 4.8 shows the time history of the relative position of the follower and the follower is successfully controlled to the leader using the drift motion. Figures 4.9 and 4.10 show the time histories of the LOS angle and the attitude angle of the follower in the leader-fixed frame, respectively. The follower attitude is changed to generate the drift velocity and then is controlled to the leader satellite keeping

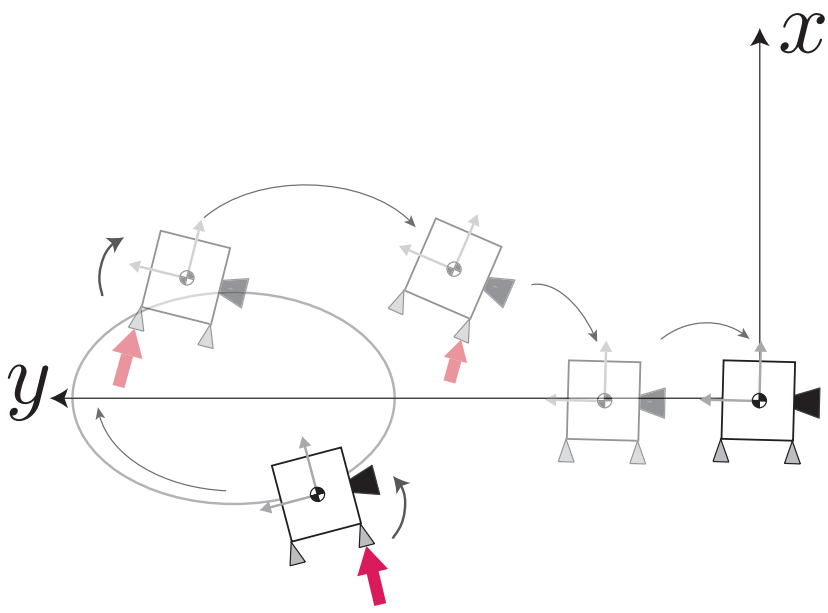

Figure 4.4: Rendezvous maneuver using a drift motion.

Table 4.1: Simulation parameters

Mass m [kg]	500.0
Thruster force $f_i (i = 1, 2, 3, 4)$[N]	10.0
Moment arm a[m]	0.5
Moment of inertia J_x, J_y, J_z [kgm^2]	300.0, 250.0, 200.0
Field of view of a camera [deg]	$\pm$45.0
Orbital rate Ω[rad/s]	0.001

the LOS angle less than the field of view of the camera. This maneuver fires the thrusters for 2.4 [m/s] as described in Fig. 4.11 and is more fuel-efficient than the result using only the radial thrusts.

Table 4.2: Initial condition

Position x_0, y_0, z_0 [m]	-1000.0, 10000.0, 0.0
Translational velocity v_{x0}, v_{y0}, v_{z0}[m/s]	0.0, 2.0, 0.0
Attitude angle ϕ_0, θ_0, ψ_0[rad]	0.0, 0.0, 0.0
Angular rate $\omega_{x0}, \omega_{y0}, \omega_{z0}$ [rad/s]	0.0, 0.0, 0.001
Modal variables $\xi_{1,0}, \xi_{2,0}, \xi_{3,0}, \xi_{4,0}$	10000.0, 0.0, 0.0, 1000.0

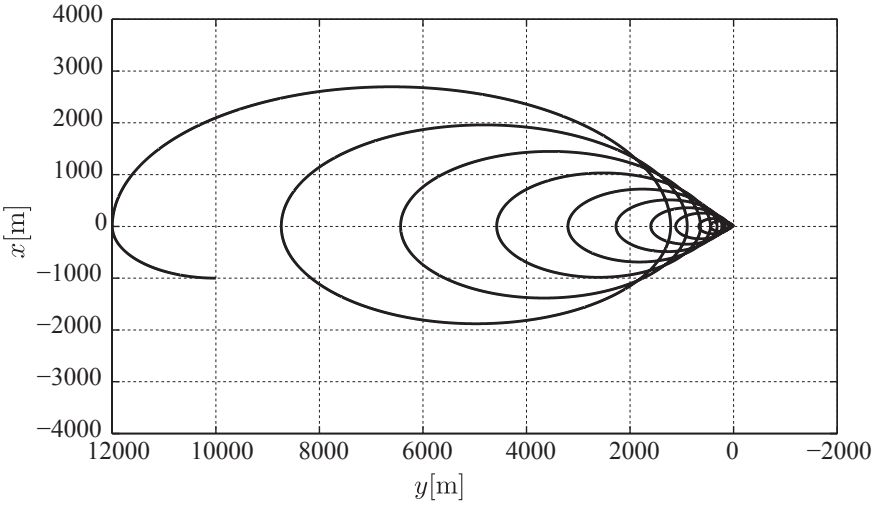

Figure 4.5: The time history of follower position for the maneuver without attitude change.

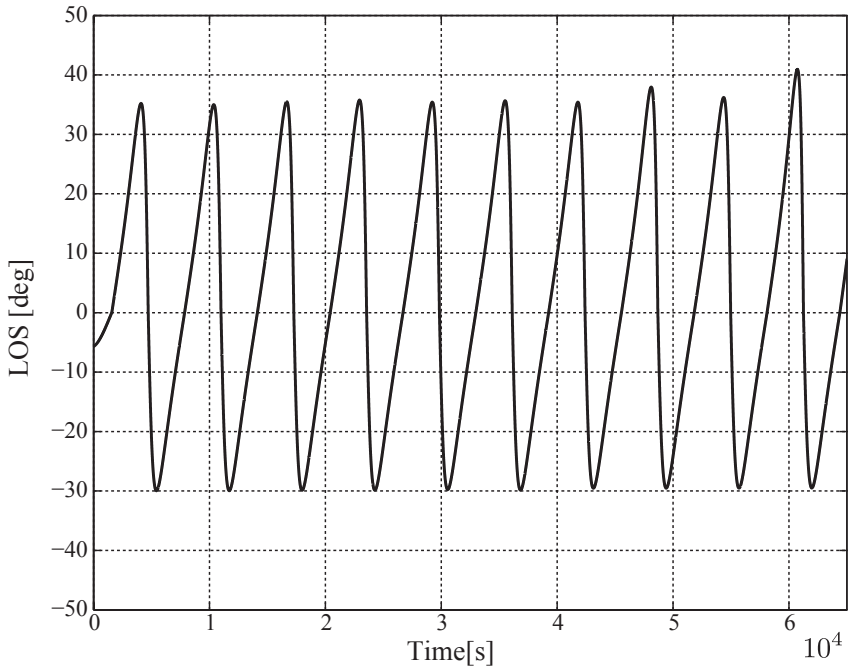

Figure 4.6: The time history of LOS angle for the maneuver without attitude change.

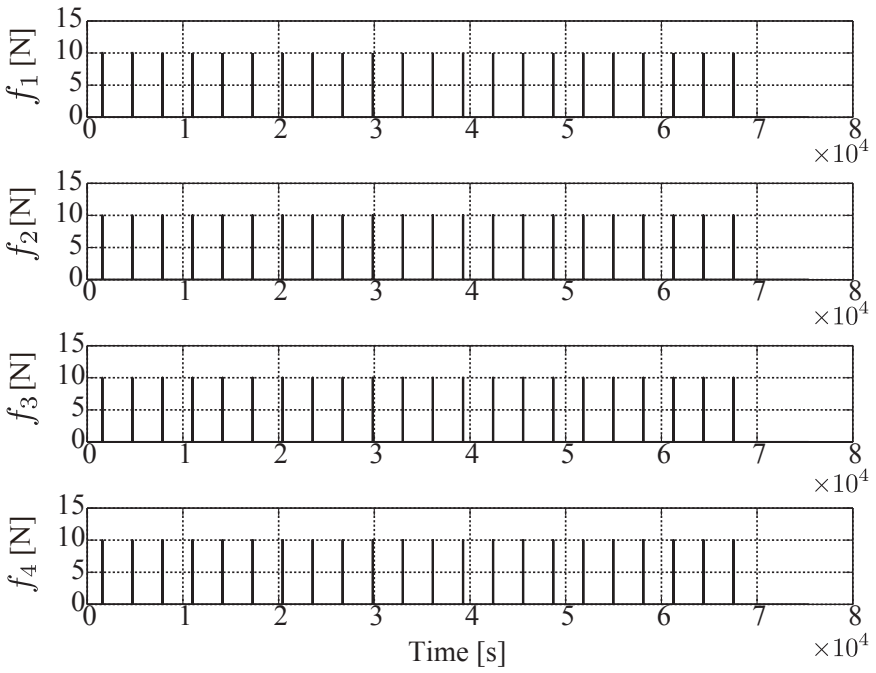

Figure 4.7: The time histories of control thrusts for the maneuver without attitude change.

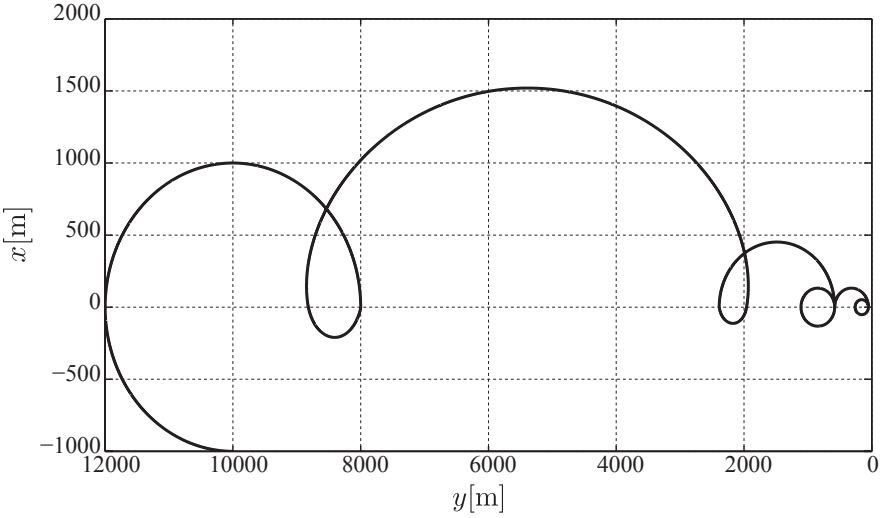

Figure 4.8: The time history of follower position for the proposed maneuver.

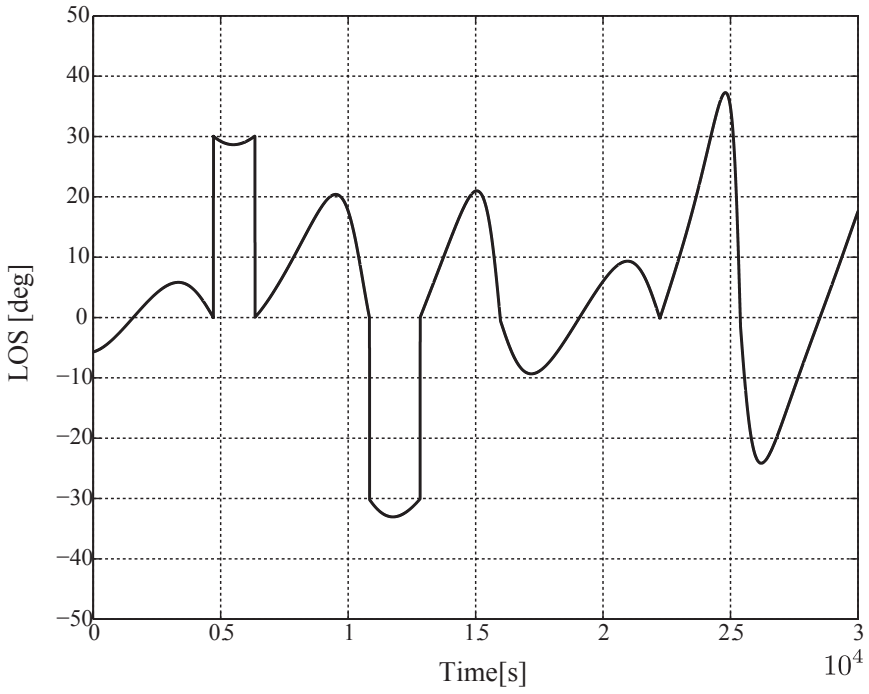

Figure 4.9: The time history of LOS angle for the proposed maneuver.

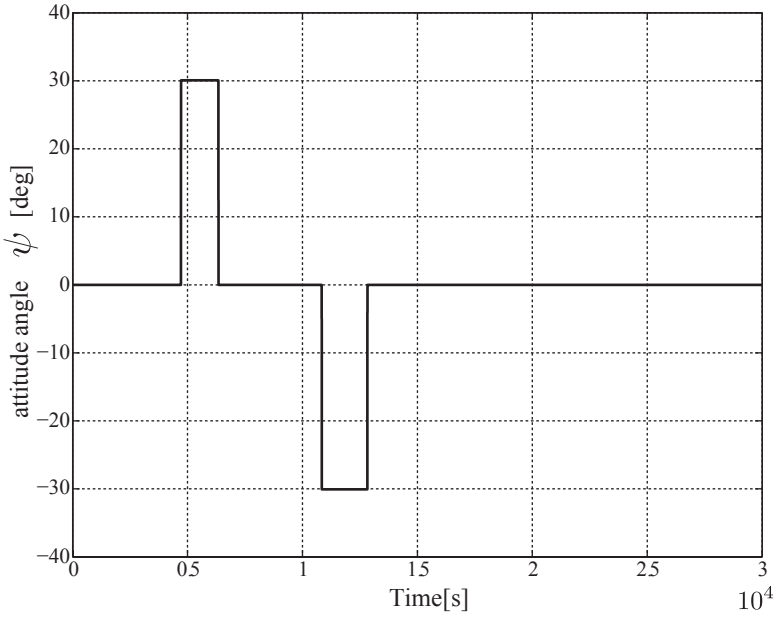

Figure 4.10: The time history of attitude angle of follower for the proposed maneuver.

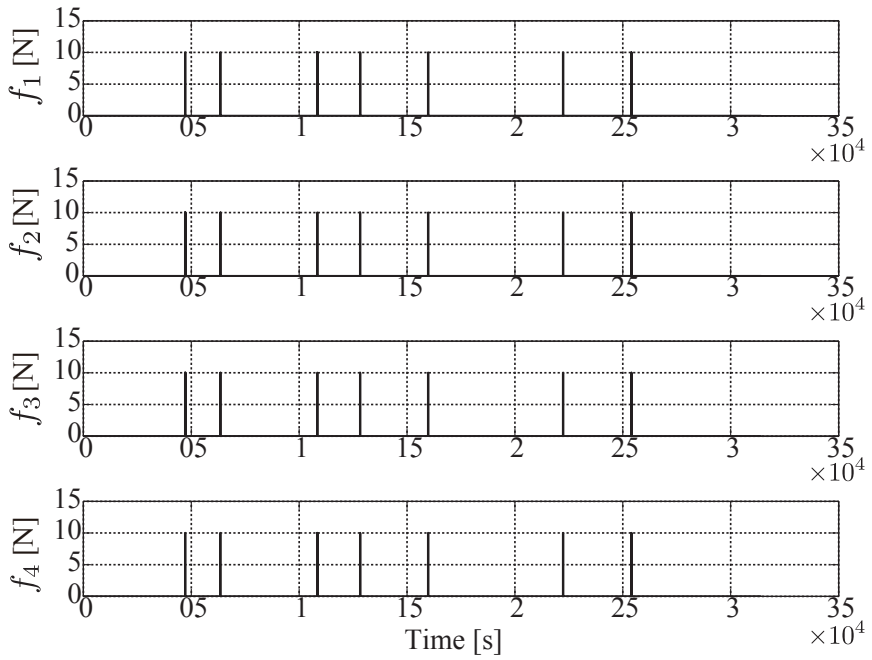

Figure 4.11: The time histories of control thrusts for the proposed maneuver.

4.1.5 Summary of Section 4.1

This section has dealt with a fuel-efficient rendezvous maneuver of a follower satellite with a small number of thrusters. The modal analysis and its variable transformation have provided the interpretation of controllability with positive constant inputs in one direction: an along-track thrust can control all modal variables, whereas a radial directional thrust requires a preliminary control maneuver to vanish a drift term in advance. The difference of the energy consumption and the proper input timings have been derived in terms of the modal variables, and consequently a fuel-efficient maneuver using a drift motion has been shown. Numerical simulation results compared the energy efficiency and verified the effectiveness of the control procedure.

4.2 Optimal Formation Reconfiguration Under Attitude Constraints

An optimal reconfiguration control by the use of a small number of thrusters is addressed under attitude constraints. The satellite attitude angle during the in-plane reconfiguration maneuver is restricted within a certain bound from a specified direction in an inertial frame. Such constraint arises from some requirements: electric power generation with fixed solar array panels, observation or communication with ground-based stations. In a similar assumption to the previous section, the satellite is assumed to have a few number thrusters; for in-plane formation maneuver the number of thrusters is set to two, whereas the magnitudes of the thruster forces are variable. The purpose of this section is to derive an optimal controller to reconfigure the formation between two satellites with a few number of thrusters considering the attitude constraints. To this end, a control method to track reference inputs is firstly derived, and then the reference input design and the condition to satisfy the attitude constraint are discussed. Numerical simulation results show that the designed reconfiguration method is effective for keeping the satellite attitude angle within a specified bound.

4.2.1 Modal Equation

This section redefines state variables and modal variables to make consistent with the proposed method discussed later. The state variables for in-plane motion are redefined as $\boldsymbol{x} = \begin{bmatrix} \Omega x & \dot{x} & \Omega y & \dot{y} \end{bmatrix}^T$. The resulting analytical solution of the Hill's

equation with no external forces is obtained as follows.

$$\begin{aligned} \boldsymbol{x}_h(t) &= \begin{bmatrix} 4-3c & s & 0 & 2(1-c) \\ 3s & c & 0 & 2s \\ 6(s-\Omega t) & -2(1-c) & 1 & 4s-3t \\ -6(1-c) & -2s & 0 & -3+4c \end{bmatrix} \boldsymbol{x}_0 \\ &\Rightarrow \quad \boldsymbol{x}_h(t) = \Phi(t)\boldsymbol{x}_0, \end{aligned} \tag{4.49}$$

where $\boldsymbol{x}_h(t_f)$ and $\Phi(t)$ denote a homogeneous solution and the state transition matrix, respectively. The modal variables are modified and redefined as

$$\xi_1 = -3\Omega x - 2\dot{y}, \tag{4.50}$$
$$\xi_2 = \dot{x}, \tag{4.51}$$
$$\xi_3 = 2\dot{x} - \Omega y, \tag{4.52}$$
$$\xi_4 = 2\Omega^2 x + \Omega\dot{y}. \tag{4.53}$$

Note that the above modal variables are shuffled from the one defined in Eq. (4.28), and the variables ξ_1 and ξ_2 denote an oscillatory mode, whereas ξ_3 and ξ_4 mean the distance between the leader and the center of relative orbit and a drift velocity, respectively. The state transition matrix is also transformed with the modal variables as follows [31].

$$\Phi_\xi = \begin{bmatrix} \cos(\Omega t) & \sin(\Omega t) & 0 & 0 \\ -\sin(\Omega t) & \cos(\Omega t) & 0 & 0 \\ 0 & 0 & 1 & 3\Omega t \\ 0 & 0 & 0 & 1 \end{bmatrix}. \tag{4.54}$$

4.2.2 Rotational Equation and Thruster Configuration

The rotational equation of a follower in x-y plane is expressed with a single spin motion as,

$$\dot{\psi} = \omega_z - \Omega, \tag{4.55}$$
$$J_z\dot{\omega}_z = T_z, \tag{4.56}$$

where T_z and J_z are external torque and the moment of inertia around z_b-axis, respectively.

In this section, the follower satellite is assumed to equip two thrusters to control the position and attitude and, without loss of generality, the x_b-axis in body-fixed frame corresponds with the thrust direction as shown in Fig. 4.12. The thrusters can generate variable magnitudes of thrust forces whose directions are restricted in positive direction due to thruster mechanisms. Thus the in-plane forces shown in Eq. (4.2) are written as follows.

$$\boldsymbol{u}_{xy} = \frac{1}{m} R(\psi)\boldsymbol{F}_b, \tag{4.57}$$

where $\boldsymbol{F}_b = [f_1 + f_2 \quad 0]^T (f_1, f_2 \geq 0)$ is redefined as the in-plane forces in the body-fixed frame, and $R(\cdot)$ denotes a two-dimensional rotational matrix, that is,

$$R(\psi) = \begin{bmatrix} \cos\psi & \sin\psi \\ -\sin\psi & \cos\psi \end{bmatrix}. \tag{4.58}$$

The control torques, on the other hand, is written as

$$T_z = f_1 a_{\mathrm{arm1}} + f_2 a_{\mathrm{arm2}}, \tag{4.59}$$

where a_{arm1} and a_{arm2} are the moment arms of the thrusters which take a negative value when the thrusters generate a clockwise directional control torque. Consequently the following relation is used to distribute the required control acceleration and torque into two thrusters.

$$\begin{bmatrix} f_1 \\ f_2 \end{bmatrix} = \begin{bmatrix} 1 & 1 \\ a_{\mathrm{arm1}} & a_{\mathrm{arm2}} \end{bmatrix}^{-1} \begin{bmatrix} m\sqrt{u_x^2 + u_y^2} \\ T_z \end{bmatrix}. \tag{4.60}$$

Although the inverse matrix in the right-hand side of Eq. (4.60) becomes singular when the thrusters generate control torques in the same direction, the condition indicates that the system becomes uncontrollable.

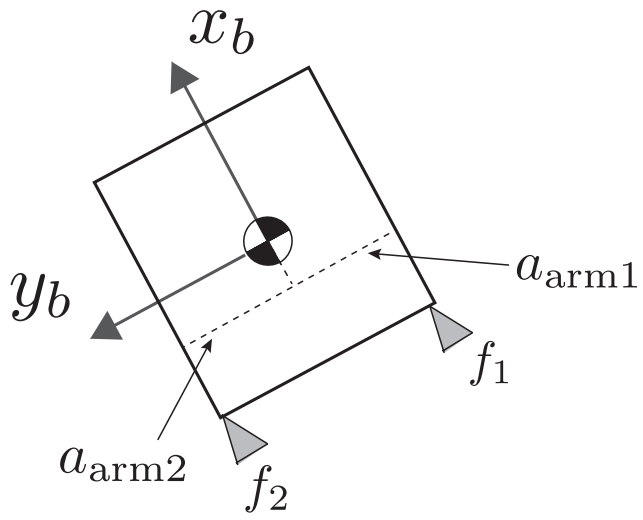

Figure 4.12: Thruster configuration.

4.2.3 Control Method

As shown in Fig. 4.13, we assume that the attitude constraint of the follower is less than a specified angle ψ_{bound} from X-axis in the inertial coordinates and the desired attitude angle, e.g. a normal vector of a solar array panel or an antenna, is expressed with ψ_{offset} in the body-fixed frame. The attitude constraint is written as

$$|\theta(t) + \psi(t) + \psi_{\text{offset}}| \leq \psi_{\text{bound}}, \tag{4.61}$$

where $\theta(t)$ is a true anomaly of the leader satellite. In the reconfiguration maneuver, the size of the relative orbit is controlled to a desired one, and thus the reconfiguration problem in terms of the modal variables is described as $(\xi_{1,0}, \xi_{2,0}, \xi_{3,0}, \xi_{4,0}) \rightarrow (\xi_{1d}, \xi_{2d}, \xi_{3,0}, \xi_{4,0})$.

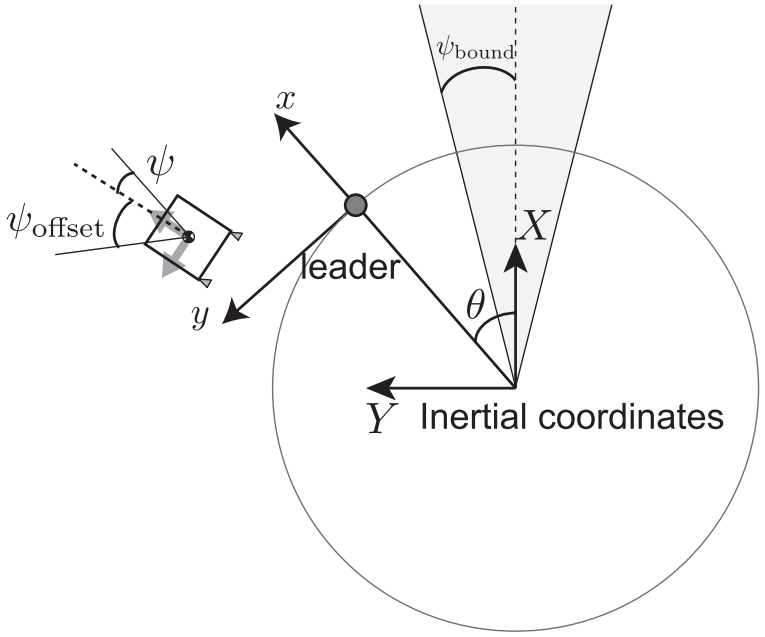

Figure 4.13: Attitude constraints in inertial frame

Reference Input Tracking

A control method to track reference accelerations is firstly derived. Since the follower equips a few thrusters, the satellite's attitude must be controlled so that the thrust direction is oriented along the reference acceleration vector. To this

end, the following Lyapunov function candidate is considered.

$$L = \frac{1}{2}(\psi - \psi_d)^2 + \frac{1}{2}(\dot{\psi} - \dot{\psi}_d)^2, \tag{4.62}$$

where $\psi_d := \arctan(u_{yd}(t)/u_{xd}(t))$ represents the angle of the reference acceleration vector. The time derivative of Eq. (4.62) is calculated as

$$\begin{aligned} \dot{L} &= (\dot{\psi} - \dot{\psi}_d)(\ddot{\psi} - \ddot{\psi}_d + \psi - \psi_d) \\ &= (\dot{\psi} - \dot{\psi}_d)(T_z/J_z - \ddot{\psi}_d + \psi - \psi_d). \end{aligned} \tag{4.63}$$

Thus, the following controller is proposed.

$$T_z/J_z = \ddot{\psi}_d - \psi + \psi_d - K_\psi(\dot{\psi} - \dot{\psi}_d), \tag{4.64}$$

where K_ψ is a positive constant gain. Substituting the control input into Eq. (4.63), we obtain the time derivative of the Lyapunov function as

$$\dot{L} = -K_\psi(\dot{\psi} - \dot{\psi}_d)^2 \leq 0. \tag{4.65}$$

The control torque shown in Eq. (4.64) thus drives the follower attitude to track the reference acceleration. This indicates that the reconfiguration problem under the attitude constraint is equivalent to the one under the directional constraint of the reference acceleration. Note that the reference inputs, u_{xd} and u_{yd} , must be at least two times differentiable due to the term $\ddot{\psi}_d$. If the reference inputs, for instance, include a feedback term of a velocity $\dot{x}$, the term $\ddot{\psi}_d$ requires the time derivative of an acceleration $\dddot{x}$ for the feedback. Such term is difficult to estimate and thus the reference tracking method disables an application of a full-state feedback.

Optimal Reconfiguration Controller

The optimal controller for the reference inputs under the directional constraint is discussed based on the method shown in [30]. The advantages of using the controller in [30] are: 1) the optimal input is infinitely differentiable because of the function of time; 2) the condition to satisfy the attitude constraint can be obtained from an analogy with an elliptical equation. The control method in [30] is here briefly followed.

The optimal controller is designed to minimize the energy consumption regarding accelerations as control inputs. The cost function is defined for a reconfiguration maneuver with a fixed time t_f as

$$J = \int_0^{t_f} (u_x^2 + u_y^2)\mathrm{d}t. \tag{4.66}$$

The control inputs are expressed with the Fourier series.

$$u_x = \frac{a_{x0}}{2} + \sum_{n=1}^{\infty} \left(a_{xn} \cos\left(n\Omega_f t\right) + b_{xn} \sin\left(n\Omega_f t\right) \right), \tag{4.67}$$

$$u_y = \frac{a_{y0}}{2} + \sum_{n=1}^{\infty} \left(a_{yn} \cos\left(n\Omega_f t\right) + b_{yn} \sin\left(n\Omega_f t\right) \right), \tag{4.68}$$

where $\Omega_f = 2\pi/t_f$, and a_{j0}, a_{jn}, and b_{jn} ($j = x, y$) are the Fourier coefficients. The cost function is rewritten in terms of the Fourier coefficients using the Parseval's theorem as follows.

$$J = \frac{t_f}{2} \left(\frac{a_{x0}^2}{2} + \sum_{n=1}^{\infty} (a_{xn}^2 + b_{xn}^2) \right) + \frac{t_f}{2} \left(\frac{a_{y0}^2}{2} + \sum_{n=1}^{\infty} (a_{yn}^2 + b_{yn}^2) \right). \tag{4.69}$$

Thus the optimal control problem is equivalent to finding the Fourier coefficients which minimize the cost function, and the Fourier coefficients are related to the boundary condition and the Lagrange multipliers.

The analytical solution of Hill's equation with control inputs are described as

$$\begin{aligned} \boldsymbol{x}(t_f) &= \boldsymbol{x}_h(t_f) + \boldsymbol{x}_p(t_f) \\ &= \Phi \boldsymbol{x}_0 + \boldsymbol{x}_p(t_f), \end{aligned} \tag{4.70}$$

where $\boldsymbol{x}_p(t_f)$ means a particular solution. The particular solution term is further rewritten as a matrix form:

$$\begin{aligned} \boldsymbol{x}_p(t_f) &= \begin{bmatrix} 2 & -2 & 0 & 0 \\ 0 & 0 & 2 & 0 \\ -3\Omega t_f & 0 & 4 & 3 \\ -3 & 4 & 0 & 0 \end{bmatrix} \begin{bmatrix} I_2 \\ I_3 \\ I_4 \\ I_5 \end{bmatrix} \\ &\Rightarrow \boldsymbol{x}_p(t_f) = B_p \boldsymbol{I}, \end{aligned} \tag{4.71}$$

where

$$I_2 = \int_0^{t_f} u_y(\tau) \mathrm{d}\tau, \tag{4.72}$$

$$I_3 = \int_0^{t_f} u_y(\tau) \cos\left[\Omega(t_f - \tau)\right] \mathrm{d}\tau - \frac{1}{2} \int_0^{t_f} u_x(\tau) \sin\left[\Omega(t_f - \tau)\right] \mathrm{d}\tau, \tag{4.73}$$

$$I_4 = \int_0^{t_f} u_y(\tau) \sin\left[\Omega(t_f - \tau)\right] \mathrm{d}\tau + \frac{1}{2} \int_0^{t_f} u_x(\tau) \cos\left[\Omega(t_f - \tau)\right] \mathrm{d}\tau, \tag{4.74}$$

$$I_5 = \Omega \int_0^{t_f} u_y(\tau) \tau \mathrm{d}\tau - \frac{2}{3} \int_0^{t_f} u_x(\tau) \mathrm{d}\tau. \tag{4.75}$$

The integral terms describe the constraints between a desired state and the homogeneous solution as

$$\begin{aligned}\begin{bmatrix} I_2 \\ I_3 \\ I_4 \\ I_5 \end{bmatrix} &= B_p^{-1}\left(x(t_f) - x_h(t_f)\right) \\ &= \begin{bmatrix} 2 & 0 & 0 & 1 \\ 3/2 & 0 & 0 & 1 \\ 0 & 1/2 & 0 & 0 \\ 2\beta & -2/3 & 1/3 & \beta \end{bmatrix} \begin{bmatrix} \Omega\left(x(t_f) - x_h(t_f)\right) \\ \dot{x}(t_f) - \dot{x}_h(t_f) \\ \Omega\left(y(t_f) - y_h(t_f)\right) \\ \dot{y}(t_f) - \dot{y}_h(t_f) \end{bmatrix}. \end{aligned} \tag{4.76}$$

The constraints of the boundary states are transformed with the modal variables and rewritten as follows.

$$\boldsymbol{I}_\xi = B_p^{-1} P^{-1}(\boldsymbol{\xi} - \boldsymbol{\xi}_h). \tag{4.77}$$

The permutation of the components of $\boldsymbol{I}_\xi$ yields $\boldsymbol{I}'_\xi = [I_{\xi 3} \quad I_{\xi 4} \quad I_{\xi 5} \quad I_{\xi 2}]^T$ and this constraint is further transformed to form a new constraint vector $\boldsymbol{K}$ as

$$\boldsymbol{K} = \begin{bmatrix} \cos\frac{\beta}{2} & \sin\frac{\beta}{2} & 0 & 0 \\ -\sin\frac{\beta}{2} & \cos\frac{\beta}{2} & 0 & 0 \\ 0 & 0 & -\frac{2}{\beta} & 1 \\ 0 & 0 & 0 & 1 \end{bmatrix} \boldsymbol{I}'_\xi, \tag{4.78}$$

where $\boldsymbol{K} = \begin{bmatrix} K_3 \sin(\beta/2) & K_4 \sin(\beta/2) & K_5 & K_2 \end{bmatrix}^T$ and $\beta = \Omega t_f$. The transformed constraint $\boldsymbol{K}$ provides the simple relationship with the Lagrange multipliers as shown in [30]. The optimal inputs for a fixed time reconfiguration are described as follows.

$$u_x(t) = \frac{2}{3}T_1 + \frac{\Lambda}{2}\sin\left(\Omega t - \Theta\right), \tag{4.79}$$

$$u_y(t) = T_0 - T_1 \Omega t + \Lambda \cos\left(\Omega t - \Theta\right), \tag{4.80}$$

where T_0, T_1, Λ, and Θ are constants described with the Lagrange multipliers.

Conditions on Attitude Constraints

The conditions to satisfy the attitude constraint are obtained from an analogy between an elliptical equation and the optimal controller. The optimal controller shown in Eqs. (4.79) and (4.80) have similar forms to a general elliptical equation, that is,

$$\frac{(x - c_x)^2}{a_{\text{ellipse}}^2} + \frac{(y - c_y)^2}{b_{\text{ellipse}}^2} = 1. \tag{4.81}$$

This analogy means that the time history of the optimal input is similarly described as an ellipse when no divergence terms appear. Thus, the input trajectory is predicted to be an ellipse when $T_1 = 0$ and furthermore an origin-centered ellipse when $T_0 = T_1 = 0$. Since the leader satellite is orbiting in a circular orbit, the desired attitude angle represented in the leader-fixed frame monotonically decreases at the rate of Ω. The analogy is therefore useful to design the input trajectory satisfying the attitude constraint.

The conditions to make an input trajectory an ellipse, i.e. $T_1 = 0$ is obtained with the relation between an initial state and a target state. Since the boundary states of ξ_3 and ξ_4 are $\xi_{3,0} = \xi_{3h}(t_f)$ and $\xi_{4,0} = \xi_{4h}(t_f)$, the integral constraints are simplified to $K_2 = K_5 = 0$ from Eqs. (4.77) and (4.78). Also, the cost function is further minimized when $\theta = \beta/2$ [31]. These boundary states indicate that the condition, $T_1 = 0$, is satisfied when $K_4 = 0$. Thus, using Eqs. (4.77) and (4.78), we obtain the boundary constraint as follows.

$$(\xi_1(t_f) - \xi_{1h}(t_f)) \tan\frac{\beta}{2} + (\xi_2(t_f) - \xi_{2h}(t_f)) = 0. \tag{4.82}$$

The modal variables are here rewritten with polar coordinates as

$$\xi_{1f} = a_f \cos\gamma_f, \tag{4.83}$$
$$\xi_{2f} = a_f \sin\gamma_f, \tag{4.84}$$

where the notation (t_f) is dropped off for the sake of simplicity and instead the subscript "f" denotes the state when $t = t_f$. Similarly, using the state transition matrix of the modal variables in Eq. (4.54), we obtain

$$\xi_{1h} = a_0 \cos\gamma_0 \cos\beta + a_0 \sin\gamma_0 \sin\beta, \tag{4.85}$$
$$\xi_{2h} = -a_0 \cos\gamma_0 \sin\beta + a_0 \sin\gamma_0 \cos\beta. \tag{4.86}$$

Substitution of Eqs. (4.83), (4.84), (4.85), and (4.86) into Eq. (4.82) yields

$$a_f \left\{ \tan\left(\frac{\beta}{2}\right) \cos\gamma_f + \sin\gamma_f \right\} - a_0 \left\{ \sin(\gamma_0 - \beta) + \tan\left(\frac{\beta}{2}\right) \cos(\gamma_0 - \beta) \right\} = 0. \tag{4.87}$$

Since the parameters a_0 and a_f are nonzero and determined by the initial and the final states, the following conditions are obtained:

$$\tan\frac{\beta}{2} \cos\gamma_f + \sin\gamma_f = 0, \tag{4.88}$$
$$\sin(\gamma_0 - \beta) + \tan\frac{\beta}{2} \cos(\gamma_0 - \beta) = 0. \tag{4.89}$$

These equations hold when the following boundary states are satisfied for the reconfiguration maneuver with a fixed time $\beta(=\Omega t_f)$.

$$\frac{y_0}{2x_0} = \tan\frac{\beta}{2}, \tag{4.90}$$

$$\frac{y_f}{2x_f} = -\tan\frac{\beta}{2}. \tag{4.91}$$

The initial and the final states satisfying Eqs. (4.90) and (4.91) therefore make $T_1 = 0$, and the optimal input trajectory becomes an ellipse.

4.2.4 Numerical Simulation

Numerical simulation demonstrates the effectiveness of a reconfiguration maneuver under the attitude constraints. The satellite mass, the moment of inertia, and the moment arm of thrusters are set as $m = 200.0$[kg], $J_z = 60.0$[kgm^2], and $(\beta_1, \beta_2) = (0.5, -0.5)$[m]. The leader satellite is assumed to be orbiting in a circular orbit at 6.313×10^{-4}[rad/s]. The follower is controlled to the target orbit from the initial semimajor axis 4000[m] to the target one 2000[m]. The parameters for the attitude constraint are considered as $\psi_{\text{offset}} = 0$[deg] and $\psi_{\text{bound}} = 45$[deg].

Figure 4.14 describes the reconfiguration trajectory of the follower satellite and shows the follower is successfully controlled to the target orbit. Figures 4.15 and 4.16 show the time histories of the attitude angle with respect to the inertial frame and the trajectory of inputs, respectively. The input trajectory describes an ellipse and thus the attitude angle of the follower is kept less than the specified bound during the maneuver.

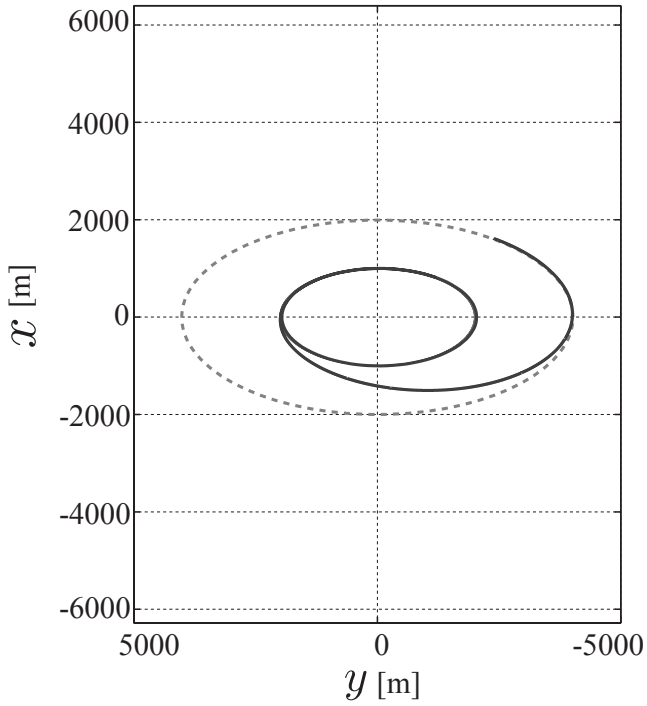

Figure 4.14: Reconfiguration trajectory of the follower.

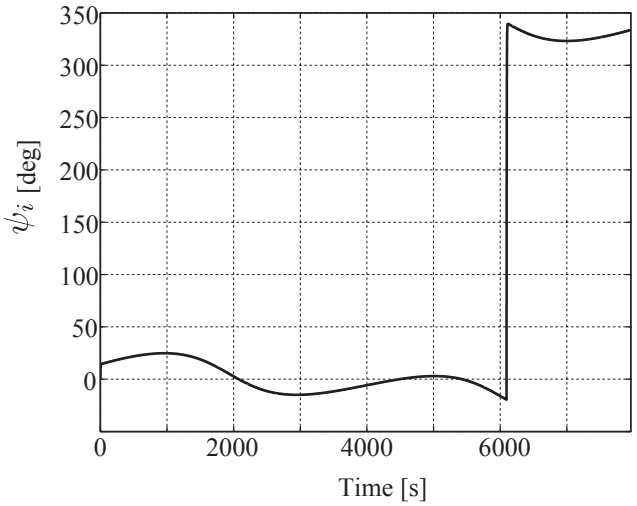

Figure 4.15: The time history of the attitude angle in inertial frame

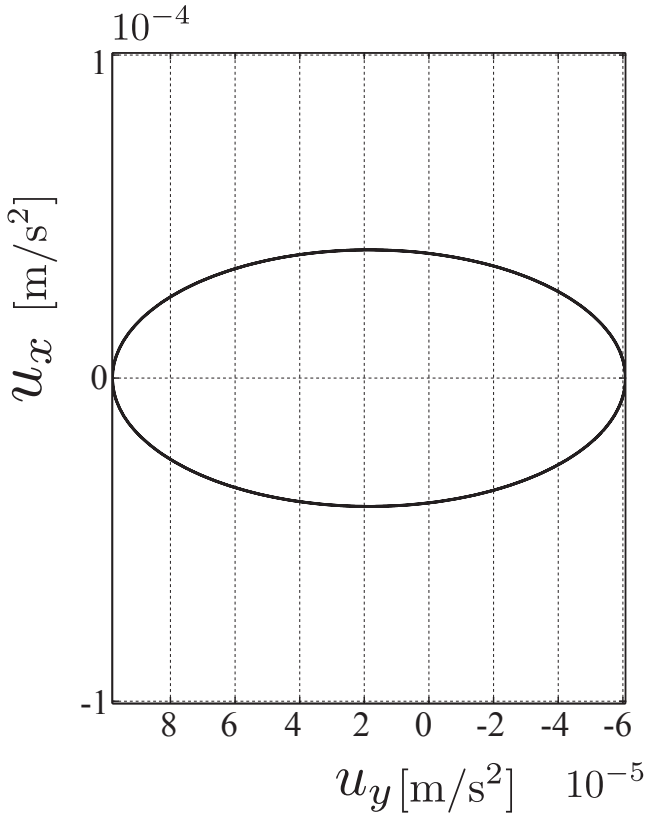

Figure 4.16: The input trajectory

4.2.5 Summary of Section 4.2

This section has dealt with an optimal reconfiguration problem in a circular orbit using a few number of thrusters under attitude constraints. Firstly, the attitude tracking method to follow a reference orbit has been derived based on Lyapunov stability. The tracking controller has reduced the reconfiguration problem under the attitude constraint to the one under the thrust directional constraint. Thus, using the analogy between the optimal controller with the Fourier series and an elliptical equation, we show the conditions to keep the attitude angle less than a specified bound. Numerical simulation demonstrates the verification of the proposed method.

Chapter 5

Conclusions

This dissertation has discussed a position and attitude control of a satellite using a small number of thrusters. By the use of less number of inputs than state variables enables control of a satellite even when some actuators have failed, and consequently such controller contributes to extend mission lifetime of the satellite. The difficulties of an underactuated system with thrusters stem from not only less inputs than the number of state variables, but also input constraints due to thruster mechanisms. That is, thruster forces must be positive and in practice, the magnitude of the thrusts are constant. To tackle this challenging problems, this dissertation has proposed control procedures based on analytical solutions for a free-floating satellite in three-dimension as well as a formation flying control of a satellite.

Chapter 2 has dealt with a three dimensional attitude control of an underactuated satellite using thrusters. The minimum necessary number of thrusters has been discussed based on the controllability of nonholonomic systems and unilateral constraints. The results have shown that three thrusters allocated parallel to a satellite body or four thrusters for nonparallel configuration are necessary to control the satellite attitude. This necessary number of thrusters is less than the one shown in previous works due to the consideration of nonholonomic control. Also, the graphical method for the thruster configuration has provided a proper thruster configuration to use less thruster forces. Based on the thruster configuration, a nonholonomic controller has been derived which is applicable to satellites regardless of the moment of inertia ratios. Numerical simulations verified the proposed control law and compared the necessary thrusts for the attitude control with different thruster configurations.

In Chapter 3, a position and attitude control procedure for a free-floating satellite with four thrusters has been derived. In addition to the unilateral constraints on control thrusts, the magnitudes of the thruster forces have been assumed to be constant. To deal with these input constraints, analytical solutions using Fresnel integrals have been obtained, and the analytical solutions have allowed us to de-

termine proper input timings and durations. Furthermore, the proposed control technique with Fresnel integrals have been extended to discuss a practical problem for a lunar landing mission. It has been shown that the proposed method can be applied to approximate the satellite motion with high accuracy even when the mass change of a satellite is considered.

Chapter 4 has discussed a position and attitude control for formation flying of a satellite. In this chapter, the attitude control of the satellite has been explicitly considered as well as the position control with a few thrusters, and it has enabled us to design a controller to track a leader satellite with a camera and to satisfy attitude constraints during a maneuver. For a rendezvous-docking problem, we have shown a fuel-efficient maneuver actively changing a satellite attitude. The attitude change is useful not only to track a leader satellite with an optical sensor, but also to generate a drift velocity. Since the drift motion steers the follower to the leader without external forces, the control maneuver requires less thruster forces than the one without the drift motion. Also, an optimal reconfiguration method under attitude constraints has been proposed based on an input tracking method. The tracking controller have indicated the attitude constraint in an inertial frame is equivalently considered as input directional constraints in the leader-fixed frame, and thus an optimal input trajectory has been designed to satisfy the constraints during the maneuver.

The underactuated controllers in this paper have been obtained for a free-floating spacecraft as well as a satellite in formation flying. Though the control methods based on analytical solutions allow us to design desired trajectories and control inputs in advance, the open-loop controllers may suffer from some disturbances and uncertainties, e.g. solar radiation pressure, perturbations due to the Earth's oblateness, and modeling errors. In practice, missions and controllers need to handle with those disturbances, and the proposed methods and studies would provide basic solutions to incorporate the real circumstances. One of the further developments thus are considered to make a feedback and robust controller to accommodate the disturbances. Also the proposed method for formation flying would be extended to one in an elliptical orbit under disturbances.

References

[1] Takahide Mizuno, Katsuhiko Tsuno, Eisuke Okumura, and Michio Nakayama. LIDAR for Asteroid Explore Hayabusa: Development and on Board Evaluation. *Journal of the Japan Society for Aeronautical and Space Sciences*, Vol. 54, pp. 514–521, 2006.

[2] Roger W Brockett. Asymptotic stability and feedback stabilization. *Differential Geometric Control Theory*, pp. 181–191, 1983.

[3] H G Tanner and K J Kyriakopoulos. Discontinuous backstepping for stabilization of nonholonomic mobile robots. In *Robotics and Automation, 2002. Proceedings. ICRA '02. IEEE International Conference on*, pp. 3948–3953, 2002.

[4] W. Lin, R. Pongvuthithum, and C. Qian. Control of high-order nonholonomic systems in power chained form using discontinuous feedback. *IEEE Transactions on Automatic Control*, Vol. 47, No. 1, pp. 108–115, 2002.

[5] R.M. Murray and S.S. Sastry. Nonholonomic motion planning: Steering using sinusoids. *IEEE Transactions on Automatic Control*, Vol. 38, No. 5, pp. 700–716, 1993.

[6] G. Oriolo and Y. Nakamura. Control of mechanical systems with second-order nonholonomic constraints: Underactuated manipulators. *Decision and Control, 1991., Proceedings of the 30th IEEE Conference on*, pp. 2398–2403 vol. 3, 1991.

[7] A. De Luca, R. Mattone, and G. Oriolo. Stabilization of an underactuated planar 2R manipulator. *International Journal of Robust and Nonlinear Control*, Vol. 10, No. 4, pp. 181–198, 2000.

[8] Reza Olfati-Saber. Nonlinear control and reduction of underactuated systems with symmetry. III. Input coupling case. In *Decision and Control*, pp. 3778–3783. IEEE, 2001.

[9] P. Crouch. Spacecraft attitude control and stabilization: Applications of geometric control theory to rigid body models. *IEEE Transactions on Automatic Control*, Vol. 29, No. 4, pp. 321–331, 1984.

[10] Christopher I Byrnes and Alberto Isidori. On the attitude stabilization of rigid spacecraft. *Automatica*, Vol. 27, No. 1, pp. 87–95, 1991.

[11] K YAMADA and S YOSHIKAWA. Spacecraft Attitude Control Using Two Reaction Wheels. *Transactions of the Society of Instrument and Control Engineers*, Vol. 34, No. 1, pp. 34–40, 1998.

[12] H. Krishnan, M. Reyhanoglu, and H. McClamroch. Attitude stabilization of a rigid spacecraft using two control torques: A nonlinear control approach based on the spacecraft attitude dynamics. *Automatica*, Vol. 30, No. 6, pp. 1023–1027, 1994.

[13] P. Morin and C. Samson. Time-varying exponential stabilization of a rigid spacecraft with two control torques. *IEEE Transactions on Automatic Control*, Vol. 42, No. 4, pp. 528–534, 1997.

[14] F. Terui, N Sako, K Yoshihara, T Yamamoto, and S Nakasuka. Visual Feedback Attitude Control of a Bias Momentum Micro Satellite Using Two Wheels. In *5th International Conference on Spacecraft Formation Flying Missions and Technologies*, pp. 81–88, 2002.

[15] Fuyuto Terui, Shinichi Kimura, Yasufumi Nagai, Hiroshi Yamamoto, Keisuke Yoshihara, Toru Yamamoto, and Shinichi Nakasuka. Moon Tracking Attitude Control Experiment of a Bias Momentum Micro Satellite". MU.-LabSat". *Transactions of the Japan Society for Aeronautical and Space Sciences*, Vol. 48, No. 159, pp. 28–33, 2005.

[16] Nadjim M. Horri and Phil Palmer. Practical Implementation of Attitude-Control Algorithms for an Underactuated Satellite. *Journal of Guidance, Control, and Dynamics*, Vol. 35, No. 1, pp. 40–50, 2012.

[17] Fuyuto Terui. Position and attitude control of a spacecraft by sliding mode control. In *American Control Conference*, pp. 217–221. IEEE, 1998.

[18] Kei Senda, Yoshisada Murotsu, Akira Nagaoka, and Akira Mitsuya. Position/Attitude Control for a Ground Testbed Simulating a Space Robot. *Journal of the Robotics Society of Japan*, Vol. 16, No. 6, pp. 824–831, 1998.

[19] Fabio Curti, Marcello Romano, and Riccardo Bevilacqua. Lyapunov-Based Thrusters' Selection for Spacecraft Control: Analysis and Experimentation. *Journal of Guidance, Control, and Dynamics*, Vol. 33, No. 4, pp. 1143–1160, July 2010.

[20] H.J. Sussmann. A general theorem on local controllability. *SIAM Journal on Control and Optimization*, Vol. 25, p. 158, 1987.

[21] B Goodwine and J Burdick. Controllability with unilateral control inputs. In *Decision and Control, 1996., Proceedings of the 35th IEEE*, pp. 3394–3399, 1996.

[22] K.M. Lynch. Controllability of a planar body with unilateral thrusters. *IEEE Transactions on Automatic Control*, Vol. 44, No. 6, pp. 1206–1211, 1999.

[23] Gerhard Krieger, Alberto Moreira, Hauke Fiedler, Irena Hajnsek, Marian Werner, Marwan Younis, and Manfred Zink. TanDEM-X: A satellite formation for high-resolution SAR interferometry. *Geoscience and Remote Sensing, IEEE Transactions on*, Vol. 45, No. 11, pp. 3317–3341, 2007.

[24] W H Clohessy and R S Wiltshire. Terminal Guidance System for Satellite Rendezvous. *Journal of the Aerospace Sciences*, Vol. 27, No. 9, pp. 653–658, January 1960.

[25] Tschauner J and Hempel P. Rendezvous zu Einemin in Elliptischer Bahn Umlaufenden Ziel. *Astronautica Acta*, Vol. 11, No. 2, pp. 104–109, June 1965.

[26] TE Carter. State transition matrices for terminal rendezvous studies: Brief survey and new example. In *Journal of Guidance Control and Dynamics*, pp. 148–155. Eastern Connecticut State Univ, Dept Math & Comp Sci, Willimantic, CT 06226 USA, 1998.

[27] K Yamanaka and F Ankersen. New state transition matrix for relative motion on an arbitrary elliptical orbit. *Journal of Guidance, Control, and Dynamics*, Vol. 25, No. 1, pp. 60–66, 2002.

[28] T Carter and J. Brient. Fuel-optimal rendezvous for linearized equations of motion. *Journal of Guidance Control Dynamics*, Vol. 15, No. 6, pp. 1411–1416, 1992.

[29] Motoyuki Shibata and Akira Ichikawa. Orbital Rendezvous and Flyaround Based on Null Controllability with Vanishing Energy. *Journal of Guidance, Control, and Dynamics*, Vol. 30, No. 4, pp. 934–945, July 2007.

[30] P Palmer. Optimal relocation of satellites flying in near-circular-orbit formations. *Journal of Guidance, Control, and Dynamics*, Vol. 29, No. 3, pp. 519–526, 2006.

[31] Phil Palmer. Reachability and Optimal Phasing for Reconfiguration in Near-Circular Orbit Formations. *Journal of Guidance, Control, and Dynamics*, Vol. 30, No. 5, pp. 1542–1546, September 2007.

[32] Hancheol Cho, Sang-Young Park, Sung-Moon Yoo, and Kyu-Hong Choi. Analytical solution to optimal relocation of satellite formation flying in arbitrary elliptic orbits. *Aerospace Science and Technology*, pp. 1–16, January 2012.

[33] Jing Li and Xiao-Ning XI. Fuel-Optimal Low-Thrust Reconfiguration of Formation- Flying Satellites via Homotopic Approach. *Journal of Guidance, Control, and Dynamics*, Vol. 35, No. 6, pp. 1709–1717, November 2012.

[34] H. Shen and R. Tsiotras. Time-optimal control of axisymmetric rigid spacecraft using two controls. *Journal of Guidance, Control, and Dynamics*, Vol. 22, pp. 682–694, 1999.

[35] Shihua Li and Yu-Ping Tian. Exponential stabilization of the attitude of a rigid spacecraft with two controls. In *American Control Conference, 2002. Proceedings of the 2002*, pp. 797–802, 2002.

[36] P. Tsiotras and A. Schleicher. Detumbling and partial attitude stabilization of a rigid spacecraft under actuator failure. *AIAA Guidance, Navigation and Control Conference*, 2000.

[37] V CoverstoneCarroll. Detumbling and reorienting underactuated rigid spacecraft. *Journal of Guidance, Control, and Dynamics*, Vol. 19, No. 3, pp. 708–710, 1996.

[38] Marcel J Sidi. *Spacecraft dynamics and control: a practical engineering approach*, Vol. 7. Cambridge university press, 2000.

[39] P A Servidia and RS Sanchez Pena. Thruster design for position/attitude control of spacecraft. *IEEE Transactions on Aerospace and Electronic Systems*, Vol. 38, No. 4, pp. 1172–1180, 2002.

[40] P A Servidia and R.S. Sanchez Pena. Practical stabilization in attitude thruster control. *IEEE Transactions on Aerospace and Electronic Systems*, Vol. 41, No. 2, pp. 584–598, 2005.

[41] P A Servidia and R S Pena. Spacecraft thruster control allocation problems. *IEEE Transactions on Automatic Control*, Vol. 50, No. 2, pp. 245–249, February 2005.

[42] P. Tsiotras, M Corless, and J.M. Longuski. A novel approach to the attitude control of axisymmetric spacecraft. *Automatica*, Vol. 31, No. 8, pp. 1099–1112, 1995.

[43] M. Aicardi, G. Cannata, and G. Casalino. Attitude feedback control: Unconstrained and nonholonomic constrained cases. *Journal of Guidance, Control, and Dynamics*, Vol. 23, No. 4, pp. 657–664, 2000.

[44] CG Broyden. A simple algebraic proof of Farkas's lemma and related theorems. *Optimization methods and software*, Vol. 8, No. 3-4, pp. 185–199, 1998.

[45] P. Tsiotras and J.M. Longuski. A new parameterization of the attitude kinematics. *Journal of the Astronautical Sciences*, Vol. 43, No. 3, pp. 243–262, 1995.

[46] P. Tsiotras and V. Doumtchenko. Control of spacecraft subject to actuator failures- State-of-the-art and open problems. *Journal of the Astronautical Sciences*, Vol. 48, No. 2, pp. 337–358, 2000.

[47] M.D. Shuster. A Survey of Attitude Representations. *The Journal of the Astronautical Sciences*, Vol. 41, No. 4, pp. 439–517, 1993.

[48] Yasuhiro Yoshimura, Takashi Matsuno, and Shinji Hokamoto. 3-D Attitude Control of an Underactuated Satellite with Constant Inputs. In *The 28th International Symposium on Space Technology and Science*, Okinawa, April 2011.

[49] Hirohisa Kojima. Stabilization of Angular Velocity of Asymmetrical Rigid Body Using Two Constant Torques. *Journal of Guidance, Control, and Dynamics*, Vol. 30, No. 4, pp. 1163–1168, July 2007.

[50] Livneh Rafael and Wie Bong. New results for an asymmetric rigid body with constant body-fixed torques. *Journal of Guidance, Control, and Dynamics*, Vol. 20, No. 5, pp. 873–881, January 1997.

[51] K.D. Mielenz. Computation of Fresnel integrals. *JOURNAL OF RESEARCH-NATIONAL INSTITUTE OF STANDARDS AND TECHNOLOGY*, Vol. 102, pp. 363–366, 1997.

[52] Bong Wie. *Space vehicle dynamics and control*. Aiaa, 1998.

[53] Shunsuke TSUGE and Shinji Hokamoto. Relative Attitude and Orbital Control with a Fewer Thrusters for Rendezvous-Docking. In *Asia-Pacific International Symposium on Aerospace Technology*, pp. 1–6, November 2012.

[54] Y Yoshimura, T Matsuno, and S Hokamoto. Position and Attitude Control of an Underactuated Satellite with Constant Thrust. In *AIAA Guidance, Navigation and Control Conference*, August 2011.

[55] Mauricio Guelman, Klaus Schilling, and Danna Linn Barnett. Formation flight line of sight guidance. *Acta Astronautica*, Vol. 71, pp. 163–169, January 2012.

Acknowledgements

I would like to express the deepest appreciation to Prof. Shinji Hokamoto, who has been my advisor since 2008. The six years of advice and educations have significantly helped and motivated my research. Also thanks to all members of the laboratory and my friends for their cooperations, insightful comments and suggestions.

Finally, I would like to offer my special thanks to my parents for their support and encouragement.